

## **Distribution Agreement**

In presenting this thesis or dissertation as a partial fulfillment of the requirements for an advanced degree from Emory University, I hereby grant to Emory University and its agents the non-exclusive license to archive, make accessible, and display my thesis or dissertation in whole or in part in all forms of media, now or hereafter known, including display on the world wide web. I understand that I may select some access restrictions as part of the online submission of this thesis or dissertation. I retain all ownership rights to the copyright of the thesis or dissertation. I also retain the right to use in future works (such as articles or books) all or part of this thesis or dissertation.

Signature:

---

Gregory James Karahalios

---

Date

The Stabilization of Reactive Copper Complexes Using 1,4,7-Triazacyclononane

Derivatives

By

Gregory J. Karahalios  
Master of Science

Chemistry

---

Christopher Scarborough, Ph.D.  
Advisor

---

Simon Blakey, Ph.D.  
Committee Member

---

Cora MacBeth, Ph.D.  
Committee Member

---

Frank McDonald, Ph.D.  
Committee Member

Accepted:

---

Lisa A. Tedesco, Ph.D.  
Dean of the James T. Laney School of Graduate Studies

---

Date

The Stabilization of Reactive Copper Complexes Using 1,4,7-Triazacyclononane  
Derivatives

By

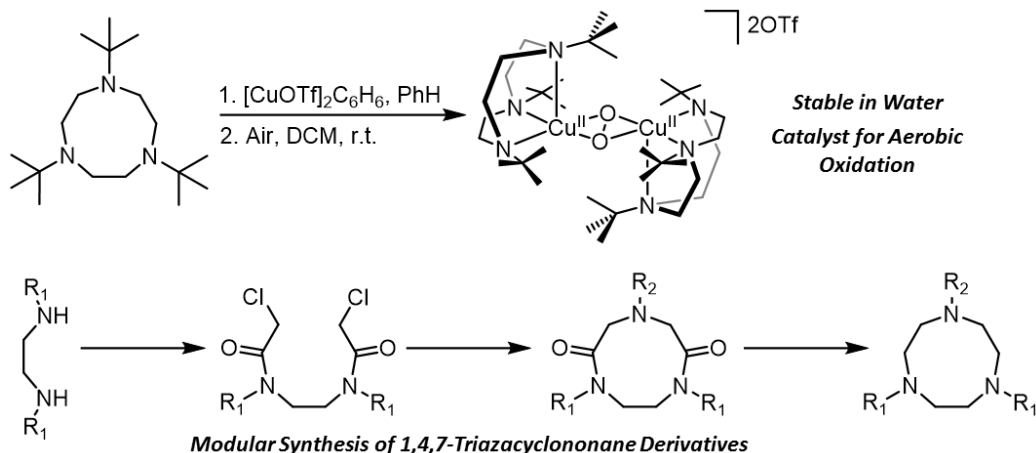
Gregory J. Karahalis

B.A., Boston University, 2011

Advisor: Christopher Scarborough, Ph.D.

An abstract of a thesis submitted to the Faculty of the  
James T. Laney School of Graduate Studies of Emory University  
in partial fulfillment of the requirements for the degree of  
Master of Science  
in Chemistry  
2016

## Abstract



Copper dioxygen complexes are the subject of immense study due to their role in a wide array of enzymatic processes, from dioxygen transport to O-atom insertion into both aromatic and aliphatic C-H bonds. However, due to the highly reactive nature of many copper dioxygen systems, study outside of proteins significantly departs from the aqueous solvent and ambient temperatures in which enzymes operate, often requiring low temperatures and organic solvents to avoid complex decay. This report describes a method using the oxidatively robust ligand, 1,4,7-tri-*tert*-butyl-1,4,7-triazacyclononane (*t*Bu<sub>3</sub>tacn), to support a copper complex capable of forming a copper dioxygen adduct under ambient conditions. The complex is well-characterized as a dinuclear copper  $\mu$ - $\eta^2$ : $\eta^2$ -peroxo complex, with support for this structure deriving from x-ray crystallography, electronic absorption spectroscopy, and resonance Raman spectroscopy. The dioxygen complex displays a room temperature half-life of 9.6 days in water with dibasic sodium phosphate, representing the highest solution stability outside of a protein. The dioxygen complex is capable of catalytic aerobic reactivity with 3,5-di-*tert*-butylcatechol, 2,4-di-*tert*-butylphenol, and benzoin, but is incapable of phenol oxidation in aqueous conditions. Therefore, to expand the study of reactive copper complexes, the synthesis of derivatives of 1,4,7-triazacyclononane is detailed, including modification of the synthesis of *t*Bu<sub>3</sub>tacn.

The Stabilization of Reactive Copper Complexes Using 1,4,7-Triazacyclononane  
Derivatives

By

Gregory J. Karahalis

B.A., Boston University, 2011

Advisor: Christopher Scarborough, Ph.D.

A thesis submitted to the Faculty of the  
James T. Laney School of Graduate Studies of Emory University  
in partial fulfillment of the requirements for the degree of  
Master of Science  
in Chemistry  
2016

## **Acknowledgements**

I would like to thank Dr. Christopher C. Scarborough, the principal investigator for whom I have worked for the past several years. His experience and knowledge in the fields of organic and inorganic chemistry have been valuable throughout the course of my work as a graduate student in his laboratory. He has played a significant role in my development as a chemist. I thank him for his guidance and supervision, and for the opportunities he has presented to me.

I would like to thank my committee members – Dr. Simon Blakey, Dr. Cora MacBeth, and Dr. Frank McDonald – for their support throughout my graduate career. Their feedback has always been highly valuable. The variety of chemical expertise found among them has helped me deal with the demanding and multifaceted challenges of scientific research. Their perspectives have enhanced my views of chemistry, and for that I am grateful.

I would especially like to thank again Dr. Cora MacBeth. Despite her own extremely busy schedule, she has always gone out of her way to help me overcome obstacles in research. Her knowledge of inorganic chemistry is astounding, and her passion for chemistry is contagious. I have always been able to trust her advice and counsel. She has been a true academic role model.

I would like to thank the members of the Scarborough lab, particularly Tom Pickel and Christian Wallen. As sources of immediate counsel, in the lab and in the office, they have been essential to my development as a chemist. Their feedback during group meetings has enhanced my critical thinking skills and my ability to communicate science.

I would like to thank Jason Bothwell and Christian Wallen for taking the time to provide edits to my thesis. I know they both have busy schedules, so their advice is much appreciated. The quality of the thesis would not be the same without their input.

I would like to thank my friends, in Atlanta and abroad. My best friend at home, Mary McBride, has always been there to support me. My best friend from my undergraduate lab, Dr. Laura Furst, has been a friend and role model, as well as a source of advice throughout my graduate career. My best friends in the South, Jack Trieu and Jason Bothwell, have seen all the good times and the bad, and they have stuck with me all the way. They are some of the most brilliant people I have ever met, and they inspire me daily.

I would like to thank my family for their support throughout this academic endeavor. My mother, my step-mothers, my brother, my sister, and my step-sisters have always been there when I have needed them most. It has been a long journey; there have been trials and substantial loss. But, by facing them together, we have made it through. I could never have made it as far without them.

I would also like to thank my boyfriend, Bradford Smith. He has dealt with my highly demanding schedule and the effects my stress. He has listened to my seemingly endless odes to chemistry with more attention than any of my students. His love and unwavering support have kept me sane over the past year and brought me through some tough times. He has earned my respect, and he inspires me to be a better person. I have never been happier than I am now with him, and I know I have nothing to fear when I am by his side.

## Table of Contents

I. Introduction .....	1
A. Modeling Copper Dioxygen Chemistry in Metalloenzymes .....	1
B. Investigation of the Synthesis of 1,4,7-Triazacyclononane Derivatives .....	11
II. Results and Discussion.....	14
A. Synthesis and Characterization of a Copper Dioxygen Complex .....	14
B. Reactivity of Copper Dioxygen Complexes .....	22
C. Modification of the Synthesis of 1,4,7-Tri- <i>tert</i> -butyl-1,4,7- triazacyclononane .....	32
D. Exploring Modularity in the Synthesis of Derivatives of 1,4,7- Triazacyclononane.....	37
III. Conclusions .....	45
IV. Future Directions .....	46
A. Synthesis and Utility of Tethered Tacn Derivatives .....	46
B. Ambient Electrochemical and Chemical Reduction of Peroxo Complexes Toward the Active Site of Particulate Methane Monooxygenase .....	47
C. Investigation of Steric Modularity of Tacn on Copper Dioxygen Cluster Formation, Stability, and Reactivity .....	54
D. Stabilization of a Mononuclear Copper Nitrene .....	61
V. Supplementary Information .....	68
A. General Considerations .....	68
B. Experimental Procedures .....	69
C. Resonance Raman Spectra.....	89
D. UV-Vis Spectra.....	92
E. NMR Spectra .....	101
VI. References.....	122



## List of Figures

1. Metalloenzyme Reactivity .....	2
2. Common Dinuclear Copper Dioxygen Complexes and Supporting Ligands .....	3
3. Comparison of a Copper Zeolite to pMMO .....	6
4. Percent Buried Volume Plot .....	12
5. Space-filling Model of Complex <b>1</b> .....	15
6. Crystal Structures of Complexes <b>2</b> and <b>3</b> .....	17
7. UV-Vis Spectrum of <b>3</b> with Molecular Orbital Diagram .....	18
8. Resonance Raman of <b>3</b> with Comparison to Other [Cu <sub>2</sub> O <sub>2</sub> ] <sup>2+</sup> Complexes .....	20
9. Decomposition of <b>3</b> by Resonance Raman Measured with 514.5 nm Laser .....	22
10. Decomposition of <b>3</b> by Resonance Raman Measured with 632.8 nm Laser .....	23
11. Tyrosinase Mechanism and Space-Filling Model of Complex <b>3</b> .....	24
12. Comparison of Copper Semiquinonate Structures .....	27
13. Mass Spectrometry of Tacn <sub>2</sub> (dien) and Tacn <sub>3</sub> (tren).....	40
14. Reactivity of <sup>R</sup> <b>6</b> .....	42
15. Previous Models of Biological Clusters .....	46
16. Cyclic Voltammetry of <b>3</b> in DMF .....	48
17. Cyclic Voltammetry of <b>3</b> Showing pH Dependence in Water.....	49
18. Assembly of Copper Complexes with Superoxide.....	50
19. Increasing Steric Strain on a Copper Dioxygen Core .....	55
20. UV-Vis and Resonance Raman Spectra of Complex <b>13</b> .....	56
21. UV-Vis Spectra of Complex <b>14</b> .....	58
22. UV-Vis Spectra of Aerobic Reaction of Copper Supported by <sup>Ad</sup> <b>8</b> <sub>Ad</sub> .....	60
23. Crystal Structures of Complexes <b>15</b> and <b>16</b> .....	61
24. Crystal Structure of Complex <b>17</b> .....	61
25. Introduction to Copper Nitrene Complexes .....	62
26. UV-Vis Spectra of Decomposition of <sup>H</sup> <b>18</b> .....	64

27. UV-Vis, EPR, and Crystal Data on <sup>Me</sup> <b>19</b> .....	65
S1. Resonance Raman Spectral Fits for Complex <b>3</b> .....	90
S2. Comparison of UV-Vis Spectra of <b>3</b> in Different Solvents .....	92
S3. UV-Vis Spectrum of the Product of Decomposition of <b>3</b> in Methanol.....	93
S4. Decomposition of <b>3</b> in Water with NaH <sub>2</sub> PO <sub>4</sub> Under N <sub>2</sub> .....	94
S5. Decomposition of <b>3</b> in Water with Na <sub>2</sub> HPO <sub>4</sub> Under N <sub>2</sub> .....	95
S6. Decomposition of <b>3</b> in Acetonitrile Under N <sub>2</sub> .....	96
S7. Decomposition of <b>3</b> in Methanol Under N <sub>2</sub> .....	97
S8. Decomposition of <b>3</b> in Methanol Under O <sub>2</sub> .....	98
S9. Decomposition of <b>3</b> in Methanol Under O <sub>2</sub> with Benzoin .....	99
S10. Decomposition of <b>3</b> in Methanol Under O <sub>2</sub> with 2,4-Di- <i>tert</i> -butylphenol.....	100
S11. Conversion of Benzoin at 50 °C by <b>3</b> .....	101
S12. Decomposition of <b>3</b> to <b>1</b> in Acetonitrile.....	102
S13. Decomposition of <b>3</b> in Methanol.....	103
S14. Extraction of Ligand from Decomposition of <b>3</b> in Methanol.....	104
S15. Representative <sup>1</sup> H NMR Spectra of Copper Complexes at the End of Various Aerobic Reactions with Complex <b>3</b> .....	105
S16. <sup>1</sup> H NMR Spectrum of <b>2</b> in <i>d</i> -Chloroform .....	106
S17. <sup>1</sup> H NMR Spectrum of <b>3</b> in <i>d</i> <sub>4</sub> -Methanol.....	107
S18. <sup>19</sup> F NMR Spectra of <b>2</b> and <b>3</b> in <i>d</i> <sub>4</sub> -Methanol .....	108
S19. <sup>1</sup> H NMR Spectrum Showing Paramagnetic Species During Reaction of Complex <b>3</b> with 3,5-Di- <i>tert</i> -butylcatechol .....	108
S20. <sup>1</sup> H NMR Spectrum Showing Product of Reaction of Complex <b>2</b> with Trimethylamine N-Oxide .....	109
S21. NMR Spectra of <sup>Me</sup> <b>6</b> .....	110
S22. <sup>1</sup> H NMR Spectra of <sup>Me</sup> <b>6</b> at Room Temperature and 85 °C .....	111
S23. NMR Spectra of <sup>Bn</sup> <b>6</b> .....	112
S24. <sup>1</sup> H NMR Spectra of <sup>Bn</sup> <b>6</b> at Room Temperature and 85 °C .....	113
S25. NMR Spectra of <sup>iPr</sup> <b>6</b> .....	114

S26. $^1\text{H}$ NMR Spectra of $^{\text{iPr}}\mathbf{6}$ at Room Temperature and $85\text{ }^\circ\text{C}$ .....	115
S27. NOE NMR Spectrum of $^{\text{Me}}\mathbf{6}$ .....	116
S28. NOE NMR Spectrum of $^{\text{Bn}}\mathbf{6}$ .....	116
S29. NOE NMR Spectrum of $^{\text{iPr}}\mathbf{6}$ .....	117
S30. NOE NMR Spectrum of $^{\text{tBu}}\mathbf{6}$ .....	118
S31. $^1\text{H}$ NMR Spectra Showing Formation of <b>10</b> and <b>11</b> .....	118
S32. $^1\text{H}$ NMR Spectra for Analysis of Reaction Between <b>2</b> , <b>20</b> , and Dihydroanthracene .....	119
S33. $^1\text{H}$ NMR Spectra for Analysis of Reaction Between <b>2</b> , <b>20</b> , and Dihydroanthracene with $\text{Sc}(\text{OTf})_3$ Additive.....	119
S34. $^1\text{H}$ NMR Spectra for Analysis of Reaction Between <b>21</b> , <b>20</b> , and Dihydroanthracene .....	120
S35. $^1\text{H}$ NMR Spectra for Analysis of Reaction Between <b>21</b> , <b>20</b> , and Dihydroanthracene with $\text{Sc}(\text{OTf})_3$ Additive.....	120
S36. $^1\text{H}$ NMR Spectra for Analysis of Reaction Between <b>20</b> , and Dihydroanthracene ..	121
S37. $^1\text{H}$ NMR Spectra for Analysis of Reaction Between <b>20</b> , and Dihydroanthracene with $\text{Sc}(\text{OTf})_3$ Additive .....	121

## List of Schemes

1. Decomposition of a $[\text{Cu}_2\text{O}_2]^{2+}$ Complex Supported by $i\text{Pr}_3\text{tacn}$ .....	8
2. Syntheses of Tacn, $i\text{Pr}_3\text{tacn}$ , $\text{Me}_3\text{tacn}$ , and $\text{Me}_2\text{Pytacn}$ .....	9
3. Syntheses of Asymmetric and $\text{C}_2$ -Symmetric Tacn Derivatives.....	10
4. Applications of Cyclization-Reduction Strategy Applied to Macrocycles, $\text{Me}_2\text{Bntacn}$ , and $t\text{Bu}_3\text{tacn}$ .....	11
5. Synthetic Modularity Exploited for $t\text{Bu}_2\text{Bntacn}$ -dione and $t\text{Bu}_4\text{dtne}$ Toward the Formation of Dinuclear Copper Complexes.....	13
6. Synthesis of <b>2</b> and <b>3</b> (OTf) <sub>2</sub> .....	17
7. A General Synthesis of Substituted Tacn Derivatives.....	33
8. Unoptimized Chloroacetylation Reaction.....	33
9. Optimized Synthesis of $t\text{Bu}_3\text{tacn}$ ( $t\text{Bu}_3\mathbf{8}$ ).....	37
10. Single vs. Double Amination: Competition Experiment.....	41
11. Synthesis of $i\text{Pr}_3\text{tacn}$ ( $i\text{Pr}_3\mathbf{8}$ ).....	44
12. Hypothetical Photophysical Generation of $[\text{Cu}_2\text{O}_2]^+$ Core.....	52
13. Hypothetical Formation of $[\text{Cu}_2\text{O}_2\text{H}]^{2+}$ Through the Use of Inter- and Intramolecular H-Atom Donors.....	53
14. Reaction of Complex <b>2</b> with Trimethylamine N-oxide.....	54
15. Synthesis and Decomposition of Copper Nitrene Adducts.....	64

## List of Tables

1. Catalytic Aerobic Oxidation of 3,5-Di-tert-butylcatechol.....	25
2. Catalytic Aerobic Oxidation of 2,4-Di-tert-butylphenol .....	29
3. Catalytic Aerobic Oxidation of Benzoin .....	30
4. Solution Half-Life of <b>3</b> .....	31
5. Aerobic Oxidation of Benzyl Alcohol .....	32
6. Scope of Amine Cyclization Toward <sup>tBu</sup> <b>7</b> <sub>R</sub> .....	38
7. Estimated Percent Rotamer Population in Solution .....	43
8. Dihydroanthracene Reactivity with Copper and Nitrene Source .....	66

## List of Abbreviations

1D	one-dimensional
Ad	1-adamantyl
ATRP	atom transfer radical polymerization
Bn	benzyl
C <sub>3</sub>	three-fold symmetric axis
cm <sup>-1</sup>	wavenumbers
DBED	N,N'-di- <i>tert</i> -butylethylenediamine
DCM	dichloromethane
dien	diethylenetriamine
DME	1,2-dimethoxyethane
DMF	N,N-dimethylformamide
en	ethylenediamine
ESI	electrospray ionization
FeMo-co	iron-molybdenum cofactor
GC	gas chromatography
h	hours
<sup>i</sup> Pr	isopropyl
IR	infrared
KIE	kinetic isotope effect
λ <sub>max</sub>	wavelength of maximum absorption
M	molar
Me	methyl
MeCN	acetonitrile
MeOH	methanol
mmol	millimole
mol	mole
mol%	mole percent

MS	mass spectrometry
$\mu\text{mol}$	micromole
nacnac	$\beta$ -diketiminate
NMR	nuclear magnetic resonance
NOE	nuclear Overhauser effect
NSI	nanospray ionization
OTf	trifluoromethanesulfonate
Ph	phenyl
pMMO	particulate methane monooxygenase
ppm	parts per million
Py	picolyl
rR	resonance Raman
S <sub>N</sub> 2	substitution nucleophilic bimolecular
tacn	1,4,7-triazacyclononane
THF	tetrahydrofuran
TLC	thin-layer chromatography
tren	tris(2-aminoethyl)amine
triflate	trifluoromethanesulfonate
<sup>t</sup> Bu	<i>tert</i> -butyl
TMCD	N,N,N',N'-tetramethylcyclohexane-1,2-diamine
tmpa	tris(2-methylpyridyl)amine
Tp	tris(pyrazolyl)borate
UV-Vis	ultraviolet-visible
vs	versus
Å	Angstroms





## I. Introduction

### A. *Modeling Copper Dioxygen Chemistry in Metalloenzymes*

Nature utilizes a wide variety of earth-abundant metals to accomplish a plethora of chemical reactions through metalloenzymes, yet copper metalloenzymes stand out for their chemical versatility. Copper centers in metalloenzymes have been shown to mediate electron transfer reactions, such as with blue copper proteins;<sup>1</sup> copper enzymes are involved in denitrification, such as with nitrite reductase and nitrous oxide reductase;<sup>2-3</sup> and copper in metalloenzymes are frequently used to bind, and often activate, dioxygen, such as with hemocyanin, tyrosinase, and particulate methane monooxygenase.<sup>4</sup> Copper's potential for reactivity along with its abundance in the earth's crust, with 548-950 million metric tons of estimated reserves,<sup>5</sup> makes it an attractive target for chemical investigations. Studying the characteristics and reactivity profile of copper, both inside and outside of protein coordination, not only yields insight into protein mechanisms, but directs the design and implementation of well-defined copper complexes for use in cost-effective methods of performing organic transformations.<sup>6</sup> This dual purpose provides an overarching motivation for the research described herein.

Of particular interest among copper-containing metalloenzymes are those that react with dioxygen. This should come as no surprise: from the perspective of green, or environmentally friendly, chemistry, "molecular oxygen or air is the ideal oxidant."<sup>7</sup> Furthermore, oxygen-reactive copper enzymes are competent to catalyze a range of processes (Figure 1). Mononuclear copper enzymes can use oxygen to turn over after substrate oxidation, such as with galactose oxidase,<sup>8</sup> or they can perform functionalization with weak C—H bonds, such as with peptidylglycine  $\alpha$ -hydroxylating monooxygenase.<sup>9-</sup>

<sup>10</sup> Dinuclear copper enzymes can generate bridging peroxo complexes capable of electrophilic aromatic substitution with phenolic residues, such as with tyrosinase.<sup>11</sup> One dinuclear copper enzyme, particulate methane monooxygenase, is known to selectively oxidize the unactivated C—H bond of methane to form methanol in a poorly-understood mechanism that involves dioxygen uptake.<sup>12-14</sup> Additionally, dinuclear copper enzymes can reversibly bind dioxygen to act as a carrier of the gas, as occurs with hemocyanin.<sup>15</sup> In all cases, the activity of the copper metalloenzymes shows potential for industrial application.

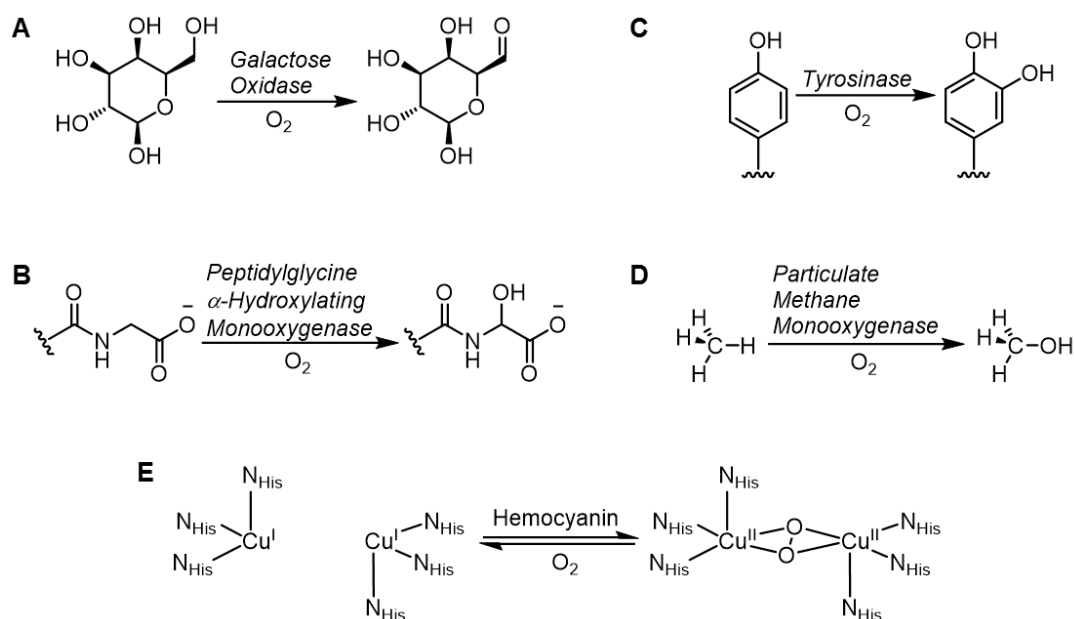


**Figure 1** Examples of copper metalloenzyme reactivity: (A) galactose oxidase; (B) peptidylglycine  $\alpha$ -hydroxylating monooxygenase; (C) tyrosinase; (D) particulate methane monooxygenase; (E) hemocyanin.

Indeed, much work has been performed on the generation of model complexes displaying biomimetic reactivity.<sup>16</sup> In enzymes, copper-peroxo complexes are commonly formed through copper bound to histidine ligands;<sup>4</sup> therefore, model complexes of copper metalloenzymes generally employ nitrogen donors. Many ligands have been utilized for this process, most commonly derivatives of ethylenediamine (en),  $\beta$ -diketiminato (nacnac),

1,4,7-triazacyclononane (tacn), tris(pyrazolyl)borate (Tp), and tris(2-pyridylmethyl)amine (tmpa) (Figure 2A).<sup>17</sup> During the course of studies on copper dioxygen complexes, bridging dinuclear copper complexes have usually been observed as three isomers:  $\mu$ -1,2-peroxo,  $\mu$ - $\eta^2$ : $\eta^2$ -peroxo, and bis( $\mu$ -oxo) (Figure 2B). Furthermore, the isomers are known to equilibrate between one another,<sup>11, 18-31</sup> with effects from solvent,<sup>20, 22, 27-28</sup> steric bulk,<sup>25, 31</sup> temperature,<sup>20, 22</sup> concentration,<sup>32</sup> electronics,<sup>23-24, 28</sup> and counterion<sup>20, 22, 29</sup> shown to shift the equilibrium between isomers.

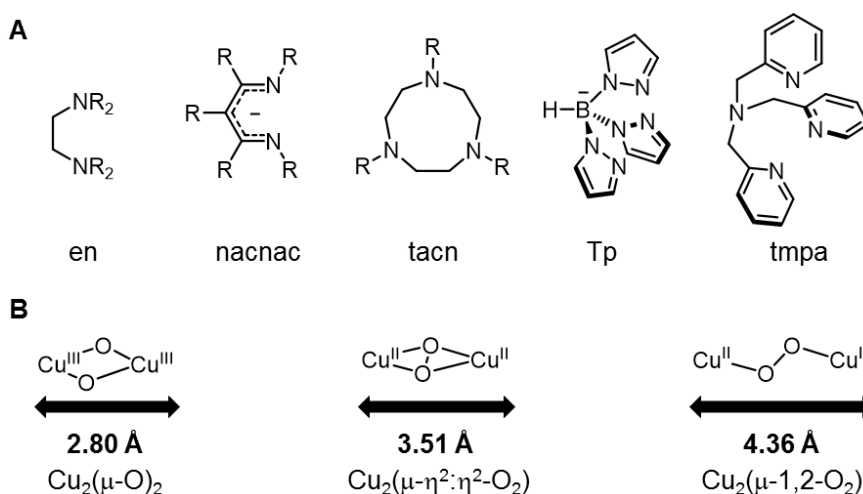


**Figure 2** (A) Common ligands used for generating copper dioxygen model complexes (from left to right): ethylenediamine (en),  $\beta$ -diketiminato (nacnac), 1,4,7-triazacyclononane (tacn), tris(pyrazolyl)borate (Tp), tris(2-methylpyridyl)amine (tmpa). (B) The three common [Cu<sub>2</sub>O<sub>2</sub>]<sup>2+</sup> isomers along with the average Cu—Cu distance for each.

Of note in the dinuclear-copper-catalyzed aerobic processes, such as oxygen transport, electrophilic aromatic substitution, and selective functionalization of unactivated sp<sup>3</sup> C—H bonds, is the involvement of a single common dioxygen adduct: the  $\mu$ - $\eta^2$ : $\eta^2$ -peroxo, also known as the side-on peroxo. Indeed, at the current state of understanding of aerobic copper metalloenzymes, only the mononuclear end-on superoxide and dinuclear side-on peroxide species have been observed and implicated in direct substrate reactivity (multicopper oxidases simply reduce dioxygen from electrons obtained separately).<sup>4</sup>

Hemocyanin reactivity has since been shown in model complexes with nitrogen donors, with reversible dioxygen complexation observed through modulating pressure and temperature.<sup>33-37</sup> Tyrosinase reactivity has also been shown outside of proteins, with nitrogen-donor model complexes displaying electrophilic aromatic substitution with a variety of substituted phenols.<sup>11, 38-42</sup> Oxygenation of  $sp^3$  C-H bonds has been achieved in the presence of amine-supported side-on peroxo complexes in solution; however this reactivity is often attributed to a bis( $\mu$ -oxo) form, as it occurs when an equilibrium between the two forms is clearly present.<sup>32, 43</sup>

However, though amine-based ligands have not led to a dicopper side-on peroxo capable of strong  $sp^3$  C—H oxygenation, zeolites impregnated with copper, such as Cu-ZSM-5 and Cu-MOR, have been shown to form dinuclear side-on peroxo complexes which, at elevated temperatures, perform conversion of methane to methanol. Initial studies on the reactivity of  $N_2O$  and NO with Cu-ZSM-5 have led to the observation of a  $Cu_2O_2$  species, initially assumed to be a bis( $\mu$ -oxo) isomer.<sup>44-46</sup> This has led to the discovery that the oxidized copper in Cu-ZSM-5 and in copper mordenites could oxidize methane to methanol selectively at elevated temperatures.<sup>47-48</sup> Careful spectroscopic work with this system has led to the reassignment of the initial oxidized intermediate to a side-on peroxo,<sup>49</sup> much like the initial oxidized intermediate observed with biological methane oxidation in particulate methane monooxygenase (pMMO).<sup>50</sup> Finally, vibrational spectroscopy, particularly resonance Raman, has suggested that the side-on peroxo species at elevated temperatures is converted to a  $[Cu_2O]^{2+}$  active species for methane oxidation.<sup>51-</sup>  
<sup>54</sup> This example highlights the importance of the side-on dicopper peroxo species as an intermediate toward an active species for selective conversion of methane to methanol.

Unfortunately, despite advancements in zeolites, there are many drawbacks to these systems.<sup>48, 52</sup> The initial copper peroxo requires pretreatment by heating to elevated temperatures, ideally 450 °C, to generate the active species for methane oxidation. Then, the atmosphere is flushed with helium and then with 5% methane in nitrogen gas, requiring less than 10 ppm water content. Then the system is heated again to 100-200 °C to react with methane. The methanol produced is absorbed onto the zeolite, requiring extraction for each phase. The maximum methanol yield of the system is 10  $\mu\text{mol/g}$ . In order for the system to be catalytic, the oxygenation and activation process must be repeated.

The zeolite systems contrast starkly with biological methane oxidation catalyzed by pMMO, both in structure (Figure 3A) and reactivity (Figure 3B). Unlike the O-bound copper in zeolites, copper in pMMO has an N-bound coordination environment.<sup>55</sup> The copper zeolite systems require elevated temperatures to react with methane, whereas the copper in pMMO reacts catalytically with methane at 45 °C.<sup>55-56</sup> Unlike the water-sensitive copper zeolite system, pMMO is necessarily exposed to aqueous biological media; the presence of O—H bonds near the core may even be important for site reactivity, as the active site is even positioned near a tyrosine residue.<sup>57</sup> The dicopper center is also near another monocopper site, which may be capable of reducing the dicopper center to generate an active species, as has been supported by calculations.<sup>58</sup> The superior reactivity and drastically different characteristics of copper oxidation of methane in pMMO compared to oxidation in zeolites suggest that the active forms for methane oxidation may be different.

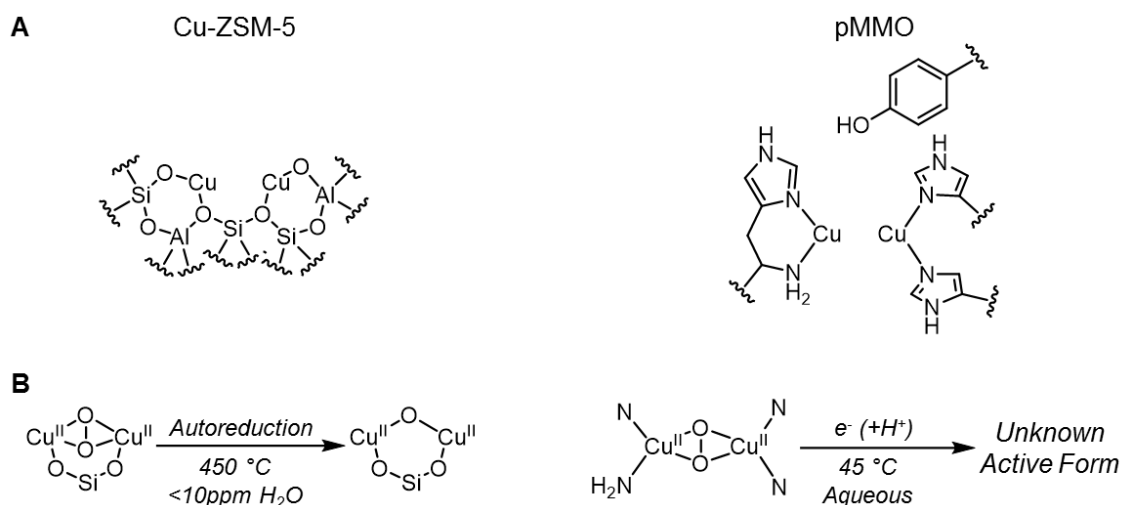


**Figure 3** Comparisons between the dicopper sites of Cu-ZSM-5 and pMMO. (A) Structure of anaerobic dicopper site. (B) Conditions for generating methane-reactive form.

Though the work over the past few decades on copper dioxygen complexes has been enlightening, there is still much to be done. Although dicopper side-on peroxo complexes have been generated that can persist in solution at room temperature on the hour time-scale,<sup>34, 36, 59</sup> none have been investigated under the aqueous conditions relevant to biological systems. Furthermore, only one experiment on electrochemistry has been performed,<sup>33</sup> in an organic solvent at  $-80\text{ }^\circ\text{C}$ , showing an irreversible one-electron reduction of the system. As electrochemistry in ambient aqueous media may be directly relevant to biological methane oxidation, aqueous stability of a copper dioxygen complex would be essential for a model complex.

To address the remaining questions for dicopper side-on peroxo complexes, a stable ligand must be designed to support this isomer of the complex. Besides one noteworthy example involving the self-assembly of copper with imidazole ligands,<sup>41</sup> copper dioxygen complexes have been supported by multidentate ligands.<sup>17</sup> As copper(II) complexes prefer a coordination number of five, a dicopper(II) side-on peroxo would be best supported by a three-coordinate ligand. Unfortunately, a three-coordinate ligand also supports a bis( $\mu$ -

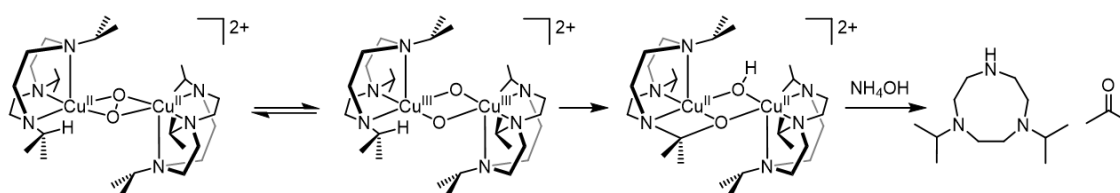
oxo) isomer. However, the average Cu—Cu distance for a side-on peroxo complex is 3.51 Å, while that value contracts to an average of 2.80 Å for a bis( $\mu$ -oxo) complex (Figure 2B). This 0.71 Å difference in Cu—Cu distance means that increasing the steric bulk of a ligand near the copper center biases the complex to a side-on peroxo isomer.<sup>17</sup> For example, the first dicopper side-on peroxo complex to be characterized by x-ray diffraction has copper bound to the tridentate ligand tris(pyrazolyl)borate bearing isopropyl substituents,<sup>60</sup> satisfying both the coordination number and steric preferences of the side-on peroxo isomer.

Among the polydentate N-donor ligands, three-coordinate 1,4,7-triazacyclononane (tacn) has been shown to support copper dioxygen complexes. Tacn ligands can bear a variety of substituents on the three amine positions, allowing for careful selection of a steric environment for copper. Furthermore, unlike tris(pyrazolyl)borate ligands, which bear a negative charge and lead to neutral dicopper side-on peroxo complexes, the tacn ligand is neutral and leads to dicationic dicopper peroxo complexes. This quality allows for further control of complex solubility through careful selection of a counteranion. Therefore, tacn derivatives are ideal candidates to form and study dicopper side-on peroxo complexes in a variety of solvents, potentially including water.

Unfortunately, copper-dioxygen complexes supported by tacn derivatives decompose intramolecularly under ambient conditions, precluding more relevant biological comparisons between the characteristics and reactivity of the complexes generated. The decay occurs through oxygen-atom insertion into weak  $\alpha$ -amino C—H bonds found on alkyl substituents of tacn, likely through the dominant or equilibrium presence of a bis( $\mu$ -oxo) core. For example, allowing the dicopper dioxygen complexes of

1,4,7-tribenzyl-1,4,7-triazacyclononane ( $\text{Bn}_3\text{tacn}$ ) and 1,4,7-triisopropyl-1,4,7-triazacyclononane ( ${}^i\text{Pr}_3\text{tacn}$ ) to warm to room temperature leads to N-dealkylation in each case along with the detection of benzaldehyde and acetone, respectively (Scheme 1).<sup>43</sup> A Hammett analysis following the decomposition of aryl-substituted  $\text{Bn}_3\text{tacn}$  derivatives leads to a  $\rho$  value of  $-0.80$ ; the low magnitude, implicating a lack of significant charge buildup, suggests a radical or concerted mechanism, reminiscent of H-atom abstraction/radical rebound processes found with heme-iron oxo complexes.<sup>43</sup> The kinetic isotope effects (KIEs) observed for the deuterated versions of the aforementioned ligands at  $-40\text{ }^\circ\text{C}$  are high (40 for  $\text{Bn}_3\text{tacn}$ ; 26 for  ${}^i\text{Pr}_3\text{tacn}$ ), which, taken along with the large negative entropy of activation for the complexes ( $-79\text{ J K}^{-1}\text{ mol}^{-1}$  for  $\text{Bn}_3\text{tacn}$ ;  $-36\text{ J K}^{-1}\text{ mol}^{-1}$  for  ${}^i\text{Pr}_3\text{tacn}$ )<sup>32</sup> and support from theoretical work,<sup>61</sup> suggest that the rate-limiting C-H activation step involves a tunneling contribution (a KIE of 12 is the semiclassical limit). However, the use of a tacn ligand with amine donors bearing tertiary alkyl substituents may avoid ligand decomposition problems, as these substituents would lack homolytically weak  $\alpha$ -amino C—H bonds accessibly close to the active core of a supported dicopper dioxygen complex.

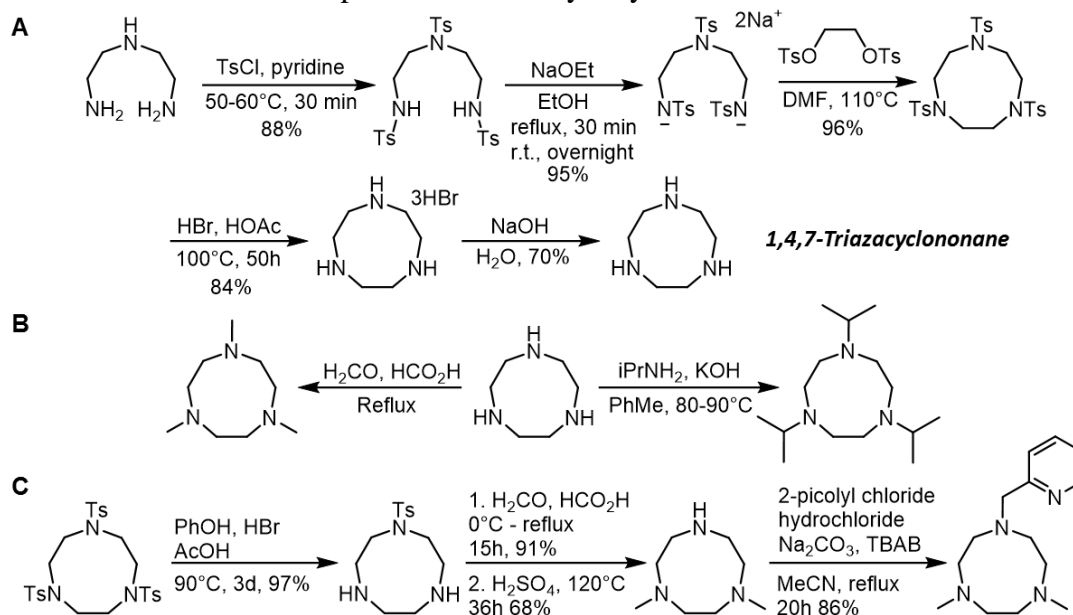
**Scheme 1. Decomposition of a  $[\text{Cu}_2\text{O}_2]^{2+}$  Complex Supported by  ${}^i\text{Pr}_3\text{tacn}$**



The lack of a rapid solution to ambient stability of tacn-supported copper dioxygen complexes owes to the synthetic inaccessibility of tacn ligands bearing tertiary alkyl substituents. The standard synthesis of substituted tacn derivatives requires either



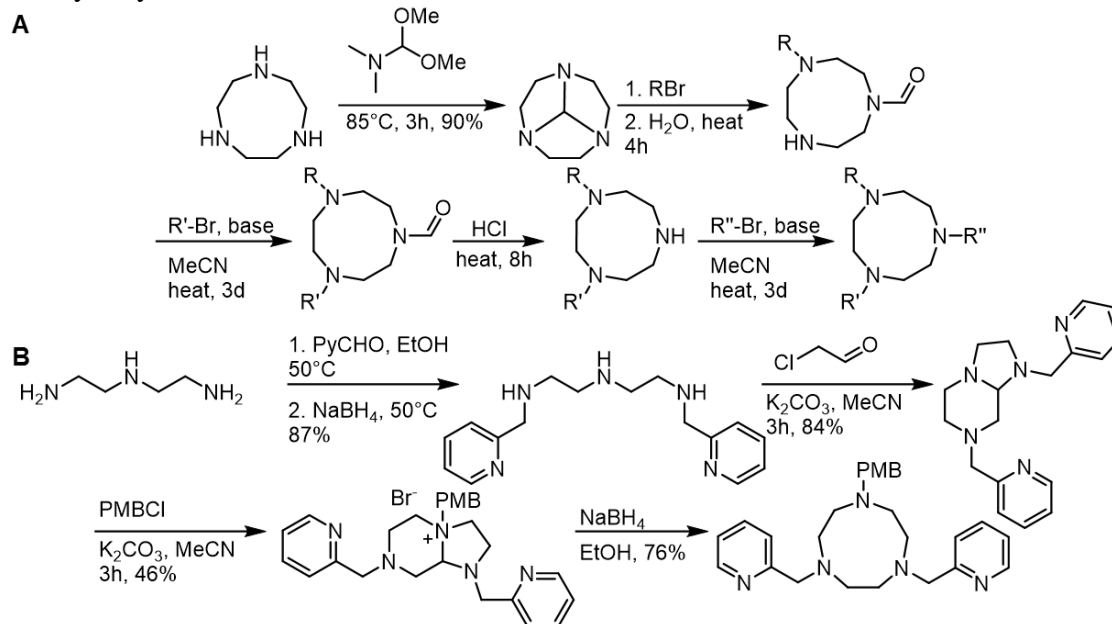
condensation-reduction procedures or  $S_N2$  reactions on unsubstituted tacn, which itself requires a week of synthesis (Scheme 2A and 2B).<sup>62-65</sup> In either case, a secondary alkyl group is the largest substituent that can be incorporated. Furthermore, the classic synthesis of tacn derivatives lacking  $C_3$  symmetry requires selective protection and deprotection of the amines with toluenesulfonyl groups (Scheme 2C).<sup>65</sup> There have been a few examples of modern updates in the synthesis of tacn derivatives, utilizing intermediates such as triazatricyclo[5.4.1.0]decane,<sup>66-67</sup> and a bicyclic amina<sup>68-70</sup> toward fully asymmetric tacn N-substitution and tacn C- or N-substitution, respectively (Scheme 3A and 3B). However, the aforementioned cases still utilize unsubstituted tacn or an intermediate in its synthesis and do not address the incorporation of tertiary alkyl substituents.



**Scheme 2.** Syntheses of (A) Tacn, (B)  $i\text{Pr}_3\text{tacn}$ ,  $\text{Me}_3\text{tacn}$ , and (C)  $\text{Me}_2\text{Pytacn}$

Most syntheses of tacn derivatives were built around the strategy of triazacyclononane ring synthesis followed by substitution, making N-substitution of tertiary alkyl groups unfeasible. However, one general synthesis of azamacrocycles developed by Bradshaw and Izatt involved building the macrocycle around pre-alkylated amines (Scheme 4A).<sup>71</sup> This process was subsequently utilized for the formation of tacn

ligands,<sup>72-73</sup> though no derivatives were formed that were otherwise inaccessible through previous syntheses (Scheme 4B). In theory, this method of building the triazacyclononane ring around pre-alkylated amines had potential for the synthesis of tacn derivatives with tertiary alkyl substituents.

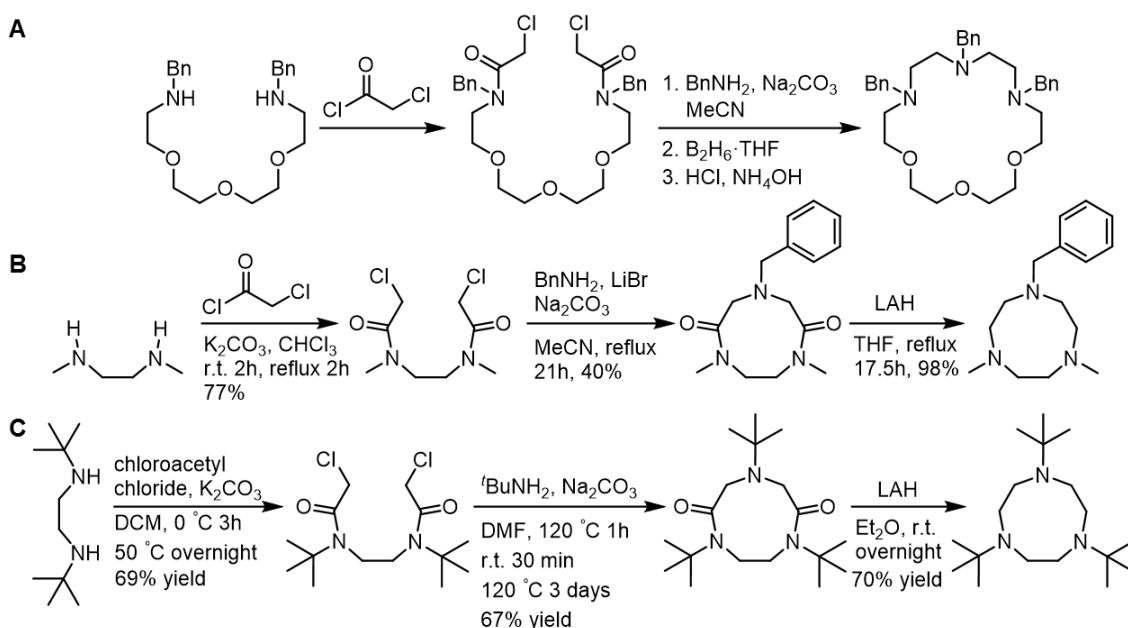


**Scheme 3.** Syntheses of (A) Asymmetric and (B)  $C_2$ -Symmetric Tacn Derivatives

Indeed, recently, the Scarborough group successfully applied Bradshaw and Izatt's process toward the first syntheses of 1,4,7-tri-*tert*-butyl-1,4,7-triazacyclononane ( $t\text{Bu}_3\text{tacn}$ ) and 1,4,7-triadamantyl-1,4,7-triazacyclononane ( $\text{Ad}_3\text{tacn}$ ) (Scheme 4C).<sup>74</sup> Preliminary coordination chemistry discussed in the study showed that the steric influence of the tertiary alkyl substituents had a pronounced effect on the coordination environment of first-row transition metals. With the exception of chromium, the transition metals studied showed a maximum coordination number of four when bound to  $t\text{Bu}_3\text{tacn}$  or  $\text{Ad}_3\text{tacn}$ , likely due to the steric bulk provided by the amine substituents of the ligand. The steric environment around the metal was measured using percent buried-volume ( $\%V_B$ ) calculations, which measured the percent of space occupied by ligand atoms a certain

distance away from a bound metal center; a higher %  $V_B$  indicated that there was less space available at a given distance from the metal (Figure 4).<sup>75</sup> Comparing four-coordinate copper complexes bound to 1,4,7-trimethyl-1,4,7-triazacyclononane ( $\text{Me}_3\text{tacn}$ ),  ${}^i\text{Pr}_3\text{tacn}$ ,  ${}^t\text{Bu}_3\text{tacn}$ , and  $\text{Ad}_3\text{tacn}$ , the percent buried volumes within the range 2-3 Å were significantly greater for  ${}^t\text{Bu}_3\text{tacn}$  and  $\text{Ad}_3\text{tacn}$  than the others, corresponding to an increased steric environment within the second coordination sphere of the bound metal.

**Scheme 4.** Applications of Cyclization-Reduction Strategy Applied to (A) Macrocycles, (B)  $\text{Me}_2\text{Bntacn}$ , and (C)  ${}^t\text{Bu}_3\text{tacn}$



#### *B. Investigation of the Synthesis of 1,4,7-Triazacyclononane Derivatives*

During the investigations of this new tacn synthesis, the second step, a cyclization reaction, was found to be potentially modular. Following the modularity found in the literature with the cyclization of the bis(chloroacetamide) of  $N,N'$ -dimethylethylenediamine around norbornenylmethylamine<sup>72</sup> and benzylamine,<sup>73</sup> the cyclization reactions of the bis(chloroacetamide) of  $N,N'$ -di-*tert*-butylethylenediamine were attempted around benzylamine, ethylenediamine, and propylenediamine. In all cases, the cyclization reaction occurred (Scheme 5A and 5B).<sup>A</sup> Furthermore, for the cyclizations

involving ethylenediamine and propylenediamine, it was found that cyclization would occur around a single amine, leading to the formation of bis(tacn) ligands bridged by two- and three-carbon units, respectively. The bis(tacn) ligands bearing tertiary alkyl substituents were shown to promote binucleation, generating dioxygen-reactive bis(copper) complexes.

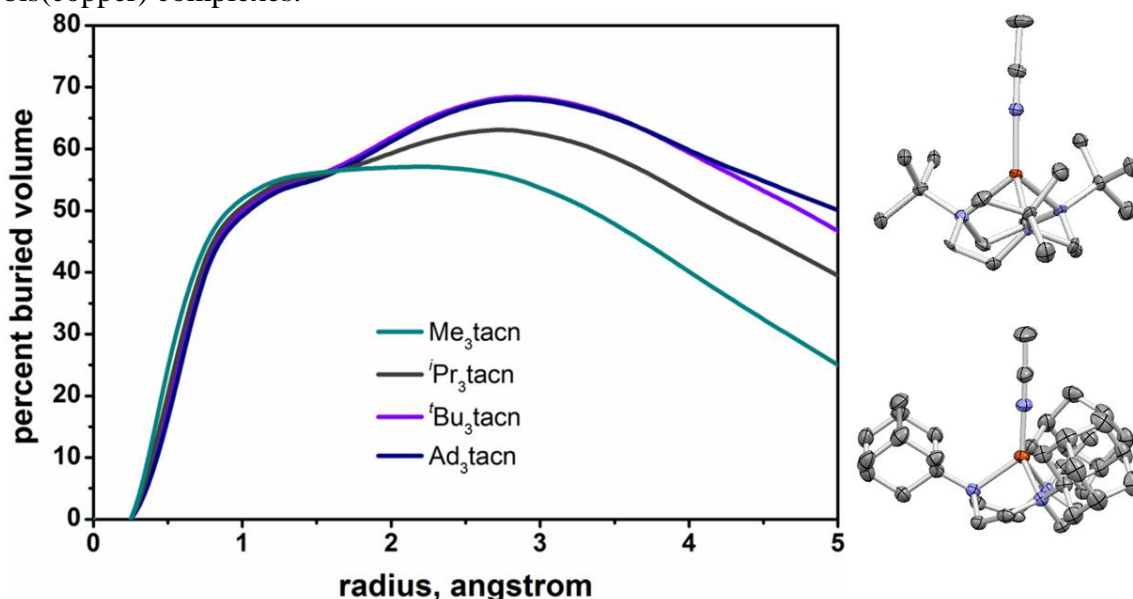
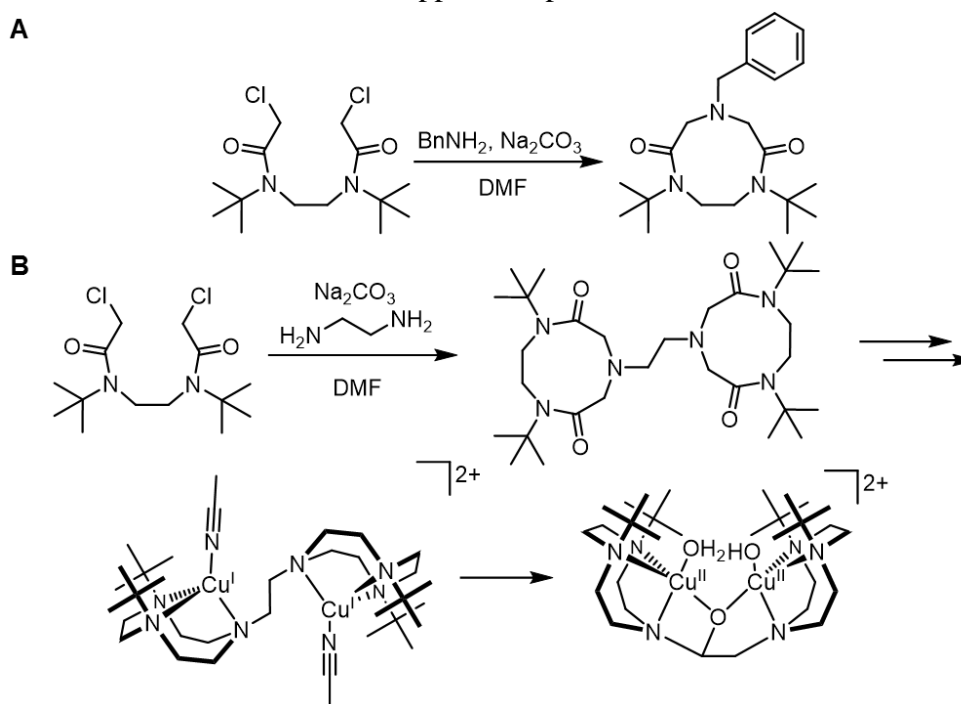


**Figure 4** Percent buried volume (%V<sub>B</sub>) plot for substituted tacn derivatives (taken from reference 74) next to crystal structures of [*t*Bu<sub>3</sub>tacnCuMeCN]<sup>+</sup> (top right) and [Ad<sub>3</sub>tacnCuMeCN]<sup>+</sup> (bottom right) (H atoms and counteranions removed for clarity).

The modularity of the synthesis has use beyond copper chemistry, as triazacyclononane derivatives have been used with a variety of metals both to address fundamental coordination chemistry and to solve industrially relevant problems. A variety of oxo complexes have been generated from tacn scaffolds, such as an iron oxo complex of 1,4-dimethyl-7-(bis(2-pyridyl)methyl)-1,4,7-triazacyclononane (<sup>Me</sup>Py<sub>2</sub>CHtacn) shown to perform water oxidation,<sup>76</sup> an iron(V) oxo complex of 1,4-dimethyl-7-(2-picolyl)-1,4,7-triazacyclononane (Me<sub>2</sub>Pytacn) capable of C-H oxidation and alkene epoxidation/dihydroxylation,<sup>77</sup> and a manganese(IV) oxo complex of Me<sub>2</sub>Pytacn capable of benzylic C-H oxidation.<sup>78</sup> Nickel complexes of Me<sub>2</sub>Pytacn have been shown to perform

alkane C—H chlorination with hypochlorite, albeit in low turnover numbers.<sup>79</sup> In a more industrially relevant example, iron(II) complexes of tacn derivatives, such as Me<sub>3</sub>tacn and 1,4,7-tricyclopentyl-1,4,7-triazacyclononane ((cyclopentyl)<sub>3</sub>tacn), have been shown to perform atom transfer radical polymerization (ATRP) reactions with a variety of alkenes.<sup>80-</sup>  
<sup>83</sup> Furthermore, bridging manganese bis(μ-oxo) complexes of Me<sub>3</sub>tacn and 1,2-bis(N,N'-dimethyl-1,4,7-triaza-1-cyclononyl)ethane (Me<sub>4</sub>dtne) have been studied as effective bleaching catalysts for detergents.<sup>84</sup> A modular synthesis of tacn may provide a platform towards improvements in each of these areas.

**Scheme 5.** Synthetic Modularity Exploited for (A) <sup>t</sup>Bu<sub>2</sub>Bntacn-dione and (B) <sup>t</sup>Bu<sub>4</sub>dtne Toward the Formation of Dinuclear Copper Complexes



*Vide infra*, I describe my efforts, both with synthetic modification and optimization of processes toward triazacyclononane derivatives and the utility of certain triazacyclononanes toward the support of copper for dioxygen reactivity.

## II. Results and Discussion

### A. *Synthesis and Characterization of a Copper Dioxygen Complex*

Often, dioxygen reactivity with a tacn-supported copper(I) complex had been found with the acetonitrile complex,  $[\text{tacnCuMeCN}]^+$ , through exposure of a solution to dioxygen. Following this precedent, the acetonitrile complex of  ${}^t\text{Bu}_3\text{tacn}$ ,  $[\text{}^t\text{Bu}_3\text{tacnCuMeCN}]\text{PF}_6$  (**1**), was prepared first by a colleague, Dr. Arumugam Thangavel. However, when Dr. Thangavel exposed a solution of **1** to air at room temperature, no immediate reaction was observed. The solution only slowly changed from the colorless **1** to a light green over the course of a few hours at room temperature.

The exact reason for this poor reactivity is unknown, however a hypothesis can be derived from buried volume calculations (Figure 4) and the results described in the first study of  ${}^t\text{Bu}_3\text{tacn}$ . In order to react with dioxygen in air, copper(I) must be able perform electron transfer with dioxygen. This electron transfer can occur either through an outer-sphere mechanism, depending mainly on the distance between and strength of the redox couple,<sup>85</sup> or an inner-sphere mechanism, in which dioxygen binds to the metal to initiate electron transfer. The sterically bulky  ${}^t\text{Bu}_3\text{tacn}$  ligand leads to a high buried volume near a copper metal center, and the axial position is already held and blocked by an acetonitrile ligand (Figure 5). Indeed, all the complexes of  ${}^t\text{Bu}_3\text{tacn}$  in the initial coordination chemistry study have a maximum coordination number of four except for the Jahn-Teller active chromium(II) complex. The copper center of **1** is essentially blocked from further coordination, making an inner-sphere mechanism of dioxygen activation difficult. Furthermore, acetonitrile acts as a good  $\pi$  acceptor for reducing metals such as copper(I), attenuating the reducing capabilities of the metal.<sup>86</sup> By lowering the strength of the

copper(I)-dioxygen redox couple and blocking approach of dioxygen to copper, acetonitrile may make outer-sphere electron transfer sluggish. Also, the copper-acetonitrile interaction strengthens due to backbonding; heating **1** under vacuum does not lead to acetonitrile dissociation.

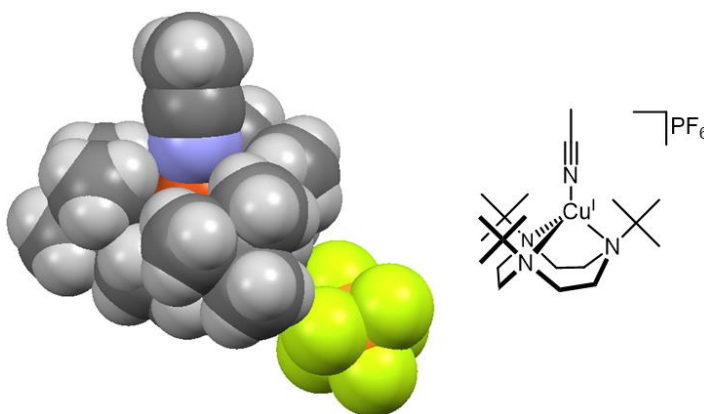


**Figure 5.** Space-filling model of the crystal structure of  $[\text{tBu}_3\text{tacnCuMeCN}]\text{PF}_6$  (**1**), displayed next to the corresponding skeletal structure for clarity, showing poor accessibility of copper (space filling model: dark orange = copper; light orange = phosphorus; lime green = fluorine; blue = nitrogen; dark grey = carbon; light grey = hydrogen).

Therefore, a different copper(I) complex of  $\text{tBu}_3\text{tacn}$  had to be selected to generate the desired dioxygen complex. An axial ligand had to be chosen that would not attenuate electron density at the copper(I) center, as acetonitrile had. Furthermore, an active complex likely required a weakly coordinating axial ligand, preferably dissociating in solution to expose the axial site of copper. This would allow the oxygen to approach the copper center to bind and react, events necessary for the formation of the desired copper dioxygen complex.

Given the conditions hypothesized to be useful for the generation of a reactive copper complex, the copper(I) trifluoromethanesulfonate dimer on benzene was chosen as the source of copper. This copper salt had been shown in the literature to form copper(I) trifluoromethanesulfonate complexes of other ligands through displacement of the bound

benzene.<sup>87-88</sup> The trifluoromethanesulfonate donor was hypothesized to be weak enough to dissociate in solution, allowing dioxygen reactivity.

Unfortunately, the commercially-obtained material was technical grade (approximately 90% pure), and the material was obtained as a brown powder instead of the characteristic white solid.<sup>89</sup> In the first preparation of the copper(I) trifluoromethanesulfonate benzene complex, it was noted that the product had crystallized out of the reaction solvent, benzene, upon cooling from reflux. Therefore, the commercially-obtained impure copper salt was purified further by heating the salt in benzene to 80 °C, filtering the hot solution over celite, and removing solvent from the filtrate *in vacuo*. This generated a white solid, in agreement with the description of the salt in the literature.

The purified copper(I) salt was found to react with <sup>t</sup>Bu<sub>3</sub>tacn in benzene under air-free conditions to produce <sup>t</sup>Bu<sub>3</sub>tacnCuOTf (**2**) (Scheme 6).<sup>90</sup> Crystals of **2** were obtained from benzene, and x-ray diffraction revealed a four-coordinate structure (Figure 6A). The data showed disorder in the ethyl bridges of the ligand macrocycle between two different twisted conformations. The <sup>1</sup>H NMR spectrum of the diamagnetic complex showed desymmetrization of the same bridge protons of the ligand upon coordination to copper(I), consistent with a similar twisted conformation in solution. We then sought to determine whether **2** in solution would generate a dioxygen complex when exposed to air.

Indeed, upon exposure of a colorless solution of **2** in dichloromethane to air, the solution flushed dark brown. Slow evaporation of the solution overnight under ambient conditions led to the formation of brown-black crystals, which could then be collected by filtration and washed with chloroform to obtain the dioxygen complex, [(<sup>t</sup>Bu<sub>3</sub>tacnCu)<sub>2</sub>(μ-



$\eta^2:\eta^2\text{-O}_2$ ](OTf)<sub>2</sub> (**3**(OTf)<sub>2</sub>) (Scheme 6). X-ray diffraction of crystals of **3**(OTf)<sub>2</sub> showed dominant formation of the side-on peroxo isomer in the solid state (Figure 6B). The crystal thus represented the first dicopper side-on peroxo crystal grown under ambient conditions; all other crystals were grown at or below  $-30\text{ }^\circ\text{C}$ .<sup>34, 36-37, 60, 91-92</sup> The complex was found to be diamagnetic, as exemplified by its <sup>1</sup>H NMR spectrum in *d*<sub>4</sub>-methanol. A similar <sup>1</sup>H NMR splitting pattern of the protons of the ligand ethyl bridge were found in **3** as in **2**, suggesting this may be indicative of copper complexes of <sup>1</sup>Bu<sub>3</sub>tacn. Furthermore, <sup>19</sup>F NMR showed trifluoromethanesulfonate resonances in **2** and **3**(OTf)<sub>2</sub> were equivalent, suggesting that the triflate anion in **2** was not bound to copper in solution (Figure S18). It was noted that the color of solid **2** was never observed to change when exposed to air, consistent with the requirement of an open axial coordination site for dioxygen reactivity.

**Scheme 6.** Synthesis of **2** and **3**(OTf)<sub>2</sub>

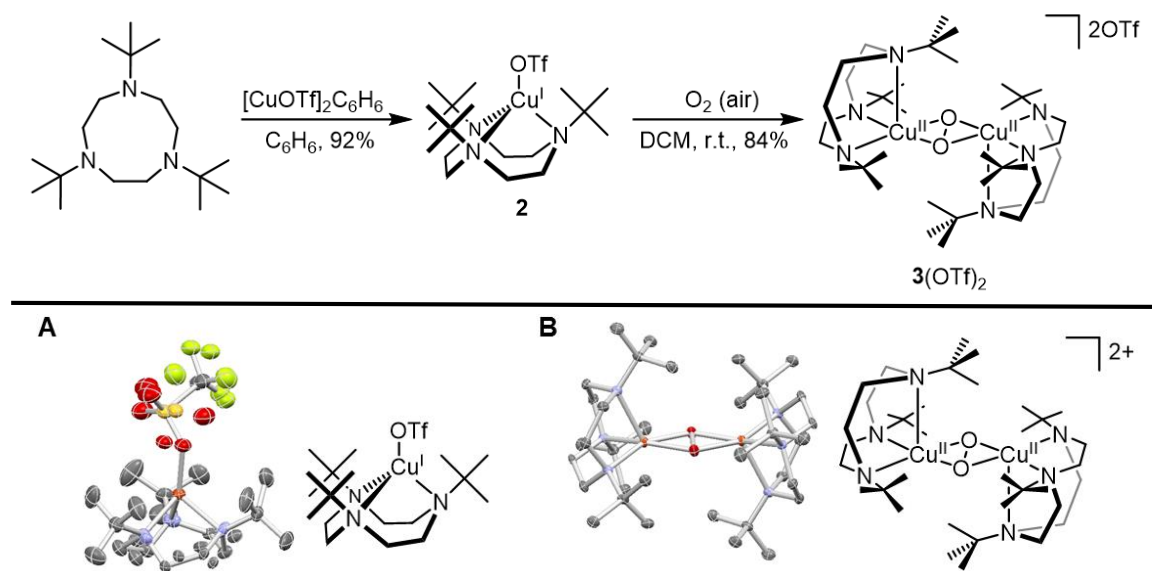


**Figure 6.** Crystal and skeletal structures of (A) **2** (disorder included) and (B) **3**(OTf)<sub>2</sub>.

Analysis of **3**(OTf)<sub>2</sub> in methanol by electronic absorption spectroscopy (UV-Vis) was indicative of the presence of the same isomer in solution as was found with its crystal structure, with no observable bis(μ-oxo) or μ-1,2-peroxo detected (Figure 7A). Side-on peroxo complexes had been shown to exhibit two characteristic absorptions in the UV-Vis region after 300 nm, corresponding to peroxo-to-copper charge-transfer transitions: the  $\pi_{\sigma}^* \rightarrow d_{xy}$  and the  $\pi_{\nu}^* \rightarrow d_{xy}$  (Figure 7B).<sup>17</sup> For previous examples of side-on peroxo complexes, the  $\pi_{\sigma}^* \rightarrow d_{xy}$  band exhibited a  $\lambda_{\max}$  in the 332-380 nm (30,100 – 26,300 cm<sup>-1</sup>) range, while the UV-Vis spectrum of **3**(OTf)<sub>2</sub> in methanol gave a  $\pi_{\sigma}^* \rightarrow d_{xy}$  transition at 400 nm (25,000 cm<sup>-1</sup>). Previous studies had suggested that a decrease in energy was attributed to some combination of a decrease in electron density at copper (from diminished ligand donor strength or increased bond length) and Cu—O bonding.<sup>17, 37</sup> Indeed, comparison of the Cu—N bond lengths from the crystal structures of [Pr<sub>3</sub>tacnCuMeCN]BPh<sub>4</sub> (2.112-2.150 Å) and **1** (2.134-2.165 Å) showed a slight bond elongation for **1**.<sup>74, 91</sup>

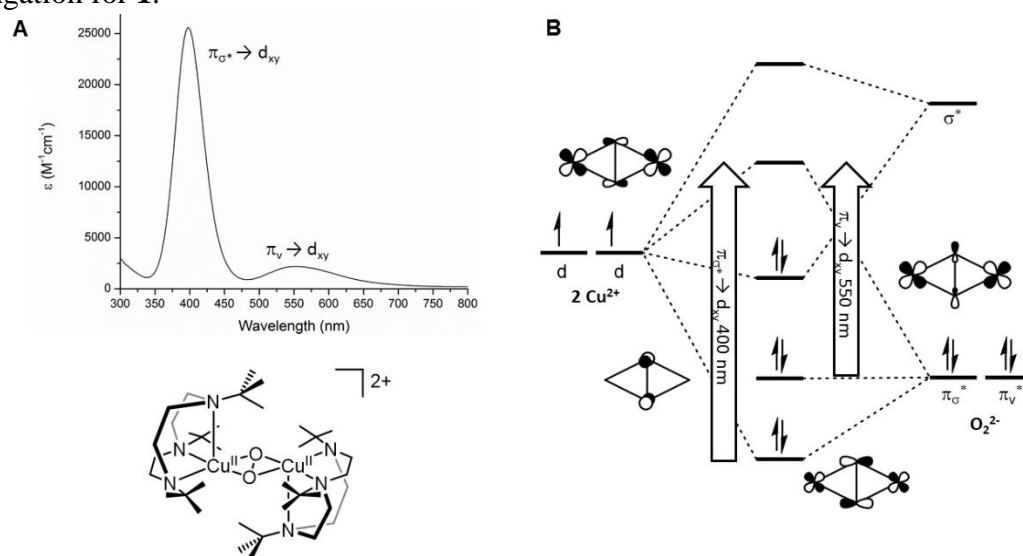


**Figure 7** (A) UV-Vis spectrum of **3** in water, with each visible absorption labeled to the corresponding charge transfer transition. (B) Qualitative frontier molecular orbital diagram mixing copper (left) and peroxide (right) (adapted from Reference 15), labeled with the transitions corresponding to the visible absorptions in (A).

Confirmation of the side-on peroxo isomer in solution came from resonance Raman (rR) spectroscopy measured at 514.5 nm (Figure 8A). The resonance observed, assigned to the O—O stretching frequency, was 773.1 cm<sup>-1</sup> in methanol. To confirm the assignment of this frequency to an O—O stretching band, complex **2** in dichloromethane (DCM) was carefully exposed to <sup>18</sup>O<sub>2</sub> in the absence of <sup>16</sup>O<sub>2</sub>, giving a stretching frequency of 728.83 cm<sup>-1</sup>, a shift consistent with involvement of both oxygen atoms. The rR spectra clearly corroborated the assignment of the complex in solution to the side-on peroxo (Figure 8B), as the isotope-sensitive frequency was far outside the range for bis(μ-oxo) (580 – 653 cm<sup>-1</sup>) (Figure 8C) and μ-1,2-peroxo (812 – 847 cm<sup>-1</sup>) (Figure 8D) isomers.<sup>17</sup> However, a resonance of 773.1 cm<sup>-1</sup> was higher than that of any other side-on peroxo dicopper complex observed (713 – 765 cm<sup>-1</sup>); this result suggested that the O—O bond was the strongest of any side-on peroxo complex measured. This was hypothesized to be in part due to a decreased backbonding from the copper d<sub>xy</sub> orbitals into the O—O σ\*, likely a result of a lack of physical overlap between the orbitals: presumably, the tertiary alkyl substituents on the supporting ligand of **3** did not allow the copper species to approach the peroxide anion as closely as other ancillary ligands. Taken with the relatively low energy of the πσ\*→d<sub>xy</sub> in the UV-Vis spectrum, it became clear that the bulk of the tacn substituents had a strong effect on the O—O bond strength observed for **3**. In fact, [(<sup>i</sup>Pr<sub>3</sub>tacnCu)<sub>2</sub>(μ-η<sup>2</sup>:η<sup>2</sup>-O<sub>2</sub>)]<sup>2+</sup> exhibited a rR frequency of 713 cm<sup>-1</sup>, the weakest O—O bond observed for a side-on peroxo; the small substituent variation from isopropyl to *tert*-butyl led to the dioxygen complex, **3**, with the strongest O—O bond reported for this isomer, at the opposite end of the spectrum.

As the copper complex **3** was a dication, solubility of **3** was explored with various anions. From these studies, **3**(OTf)<sub>2</sub> was found to be soluble in methanol, acetonitrile, acetone, N,N'-dimethylformamide (DMF), and dimethylsulfoxide (DMSO) and somewhat soluble in dichloromethane (DCM). To test solubility with other counteranions, **3**(OTf)<sub>2</sub> was stirred in a solvent with a salt bearing the counteranion to initiate anion metathesis. Solubility in ethereal solvents, such as 1,2-dimethoxyethane (DME), tetrahydrofuran (THF), and 1,4-dioxane, was increased marginally using the hexafluorophosphate anion, PF<sub>6</sub><sup>-</sup>, and extensively using the hexafluoroantimonate anion, SbF<sub>6</sub><sup>-</sup>. Furthermore, solubility in water could be obtained through metathesis with fluoride, chloride, bromide, iodide, and phosphate anion sources such as NaH<sub>2</sub>PO<sub>4</sub> and Na<sub>2</sub>HPO<sub>4</sub>. It should be noted that **3** also appeared to become soluble in water in the presence of the borohydride anion, BH<sub>4</sub><sup>-</sup>, but began decomposing within seconds after dissolution.

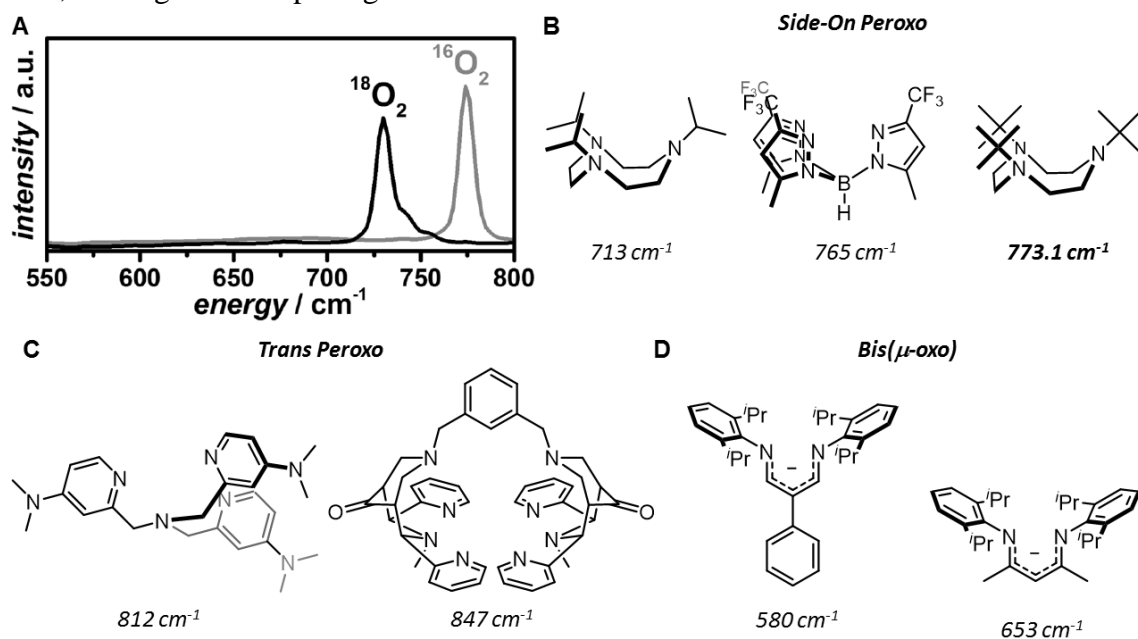


**Figure 8.** (A) Methanolic resonance Raman spectra of **3**(OTf)<sub>2</sub> made from <sup>16</sup>O<sub>2</sub> and <sup>18</sup>O<sub>2</sub> (514.5 nm excitation wavelength). (B) Ligands supporting dicopper μ-η<sup>2</sup>:η<sup>2</sup>-peroxo complexes with the lowest (left) and highest (middle) energy O—O stretching frequencies previously reported, with reference to **3** (right). (C) Ligands supporting dicopper μ-1,2-peroxo complexes with the lowest (left) and highest (right) energy O—O stretching frequencies. (D) Ligands supporting dicopper bis(μ-oxo) complexes with the lowest (left) and highest (right) energy Cu<sub>2</sub>O<sub>2</sub> core breathing mode frequencies.

As ambient solution stability was a major goal of using tacn bearing tertiary alkyl substituents to support copper dioxygen complexes, solution half-life measurements of **3** were obtained via UV-Vis. In degassed acetonitrile, **3**(OTf)<sub>2</sub> exhibited a half-life of 2.524 hours; the complex broke down into the trifluoromethanesulfonate salt of **1** as confirmed by <sup>1</sup>H NMR and UV-Vis spectroscopy, suggesting a mechanism of dioxygen displacement. In degassed methanol, **3**(OTf)<sub>2</sub> displayed a significantly longer half-life of 14.25 hours; crystallization of the decomposed solution led to the isolation of **2**, suggesting that **3** may be competent for aerobic oxidation catalysis in methanol. With this in mind, the half-life of **3**(OTf)<sub>2</sub> in methanol sparged with dioxygen was evaluated; a half-life of 13.05 hours was obtained, suggesting that **3**(OTf)<sub>2</sub> persisted long enough in methanol to sustain catalysis with dioxygen as the stoichiometric oxidant. Then, the aqueous stability of **3** was tested using phosphates as the counteranion. To simultaneously address the role of acidity on stability, the half-life of **3** was measured with sodium phosphate in dibasic (Na<sub>2</sub>HPO<sub>4</sub>) and monobasic (NaH<sub>2</sub>PO<sub>4</sub>) forms. The resulting half-life data suggested that **3** was more stable under basic conditions: the half-life times in Na<sub>2</sub>HPO<sub>4</sub> and NaH<sub>2</sub>PO<sub>4</sub> were 9.6 days and 6.7 days, respectively. It is noteworthy that the largest solution half-life for a dicopper side-on peroxo outside of a protein was 25.5 hours, making this complex the most stable side-on peroxo ever reported.<sup>34</sup> These results were particularly significant, as the conditions were analogous to the aqueous phosphate buffer solutions used in biological systems. It should be noted that, though **3**(OTf)<sub>2</sub> decomposed slowly in a variety of solvents, the ligand was found to be intact upon demetallation with ammonium hydroxide (Figure S14 for example in methanol).

Decomposition of  $3(\text{OTf})_2$  in methanol was also followed by resonance Raman spectroscopy. With 514.5 nm excitation, the O—O band of  $3(\text{OTf})_3$  was shown to disappear during decomposition, while a feature at  $524\text{ cm}^{-1}$  and its overtone appeared (Figure 9). The same feature appeared upon irradiation of the complex at 632.8 nm excitation (Figure 10). Though the species was never structurally characterized, the  $524\text{ cm}^{-1}$  feature was consistent with a Cu—N or Cu—O stretching frequency.

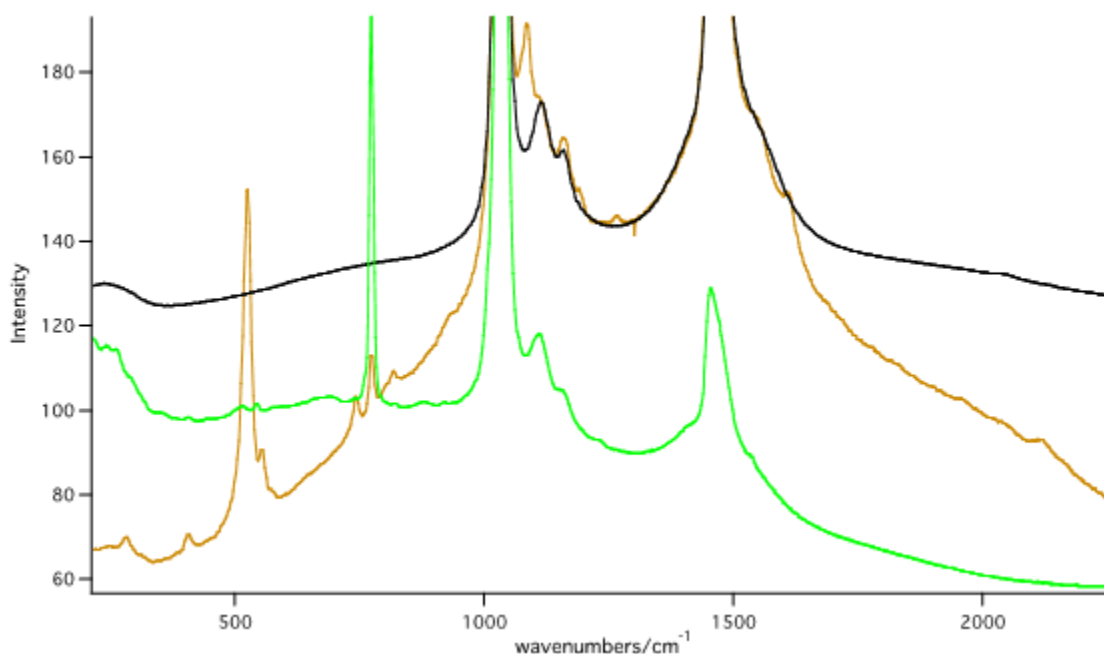


**Figure 9.** Raman spectrum of solution of **3** in MeOH after incubation in the dark for 4 days. Acquired using 514.5 nm excitation. Shown with spectrum of **3** and MeOH for comparison. Black line represents background methanol solution; green line represents initial solution of complex **3**; gold line represents the same solution after 4 days of decomposition.

### *B. Reactivity of a Copper Dioxygen Complex*

Given the impressive aqueous stability of **3** and the direct relevance of aqueous reactivity to biological systems, the ability of **3** to perform oxidation catalysis in water was assessed. Electrophilic aromatic substitution reactivity was targeted with phenols in water, as side-on peroxy complexes had been shown to perform these reactions even at low temperatures outside of proteins in organic media.<sup>38-42, 93-94</sup> Unfortunately, no reaction was

observed with phenol in water, showing complete retention of starting material when followed by  $^1\text{H}$  NMR in  $\text{D}_2\text{O}$ . In the hopes that deprotonation of the phenol to the phenolate may activate the substrate to electrophilic attack, the reaction was tested using sodium phenolate and then with a mixture of phenol and triethylamine. Under all ambient conditions, no reaction was observed with **3**, leading only to observation of unreacted starting material by  $^1\text{H}$  NMR. Even at  $50\text{ }^\circ\text{C}$ , no conversion of phenol was observed, with or without a triethylamine additive.

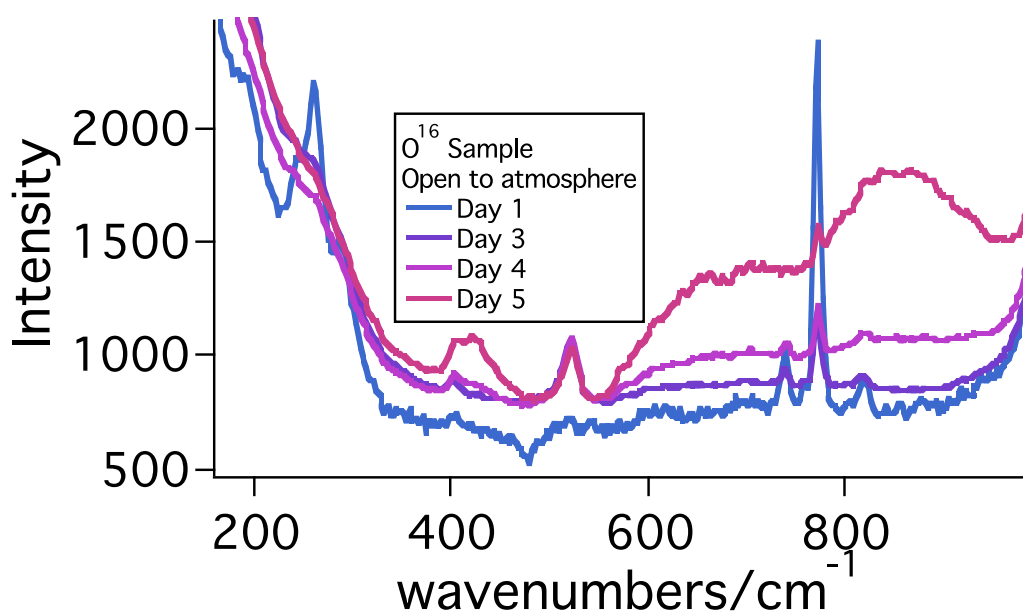


**Figure 10.** Breakdown of **3** probed by 632.8 nm excitation. New species formation evident from peak at  $524\text{ cm}^{-1}$ .

As  $\mathbf{3}(\text{OTf})_2$  at least partially regenerated **2** in methanol and maintained a relatively long half-life in methanol even under pure dioxygen atmosphere, the catalytic competency of  $\mathbf{3}(\text{OTf})_2$  in methanol was evaluated. However, as with the aqueous reactions, no ambient reactivity was observed with phenol, with or without triethylamine. The same systems were tested at  $50\text{ }^\circ\text{C}$ , yielding the same unreacted starting materials with both systems. Furthermore,  $\mathbf{3}(\text{OTf})_2$  was found to be unreactive toward catechol, a more electron-rich substrate which normally oxidizes slowly in air.

The lack of reactivity seemed initially surprising, as there are many examples of side-on peroxo complexes performing tyrosinase reactivity outside of proteins at low temperatures<sup>38-42, 93-94</sup> and even a few at room temperature in organic media.<sup>42, 95</sup> However, this may be in line with the prevailing mechanism of tyrosinase reactivity with side-on peroxo complexes (Figure 11A).<sup>15</sup> The mechanism requires phenolate to bind to one of the copper sites in order to begin substrate oxidation. Additionally, a recent study suggests that the binding of phenolate may induce formation of a bis( $\mu$ -oxo) to react with the phenolate.<sup>11</sup> The same bulky substituents protecting the ligand from degradation and enforcing a side-on peroxo isomer for the dicopper core may prevent substrate binding. This possibility becomes especially convincing when a space-filling model of the complex is observed; the copper core is barely visible through the *tert*-butyl substituents (Figure 11B). Furthermore, as splitting the O—O bond of dioxygen seems necessary for tyrosinase reactivity, the reaction would be unlikely; a bis( $\mu$ -oxo) would require the Cu—Cu distance to contract significantly, so the steric clash of the bulky *tert*-butyl substituents would likely make the barrier to the intermediate unreasonable.

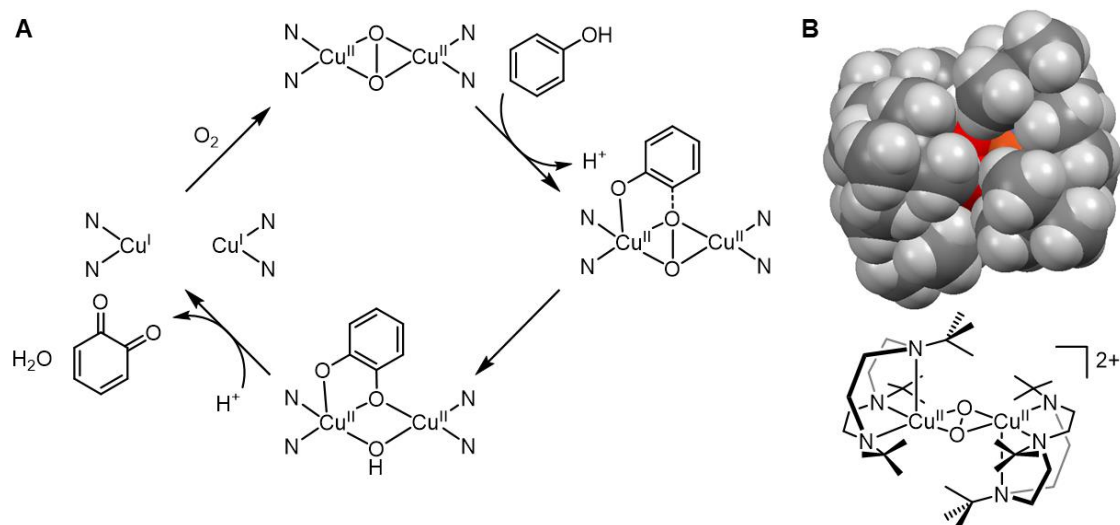


**Figure 11** (A) Proposed tyrosinase mechanism (reproduced from Reference 15). (B) Spacefilling model of **3** (top) with representative skeletal structure (bottom) shown for clarity (H atoms from crystal structure assumed).



In an attempt to probe whether oxidation was possible with a more electron-rich catechol, 3,5-di-*tert*-butylcatechol was chosen as a substrate. With 21 mol% loading in *d*<sub>4</sub>-methanol, **3**(OTf)<sub>2</sub> was found by <sup>1</sup>H NMR to react catalytically with 3,5-di-*tert*-butylcatechol to form 3,5-di-*tert*-butyl-*o*-quinone in 91% yield at room temperature in 24 hours (Table 1). In an attempt to increase the reaction rate, the reactions were attempted at 50 °C and 65 °C, generating 3,5-di-*tert*-butyl-*o*-quinone in 73% (four hours, 23 mol% **3**(OTf)<sub>2</sub>) and 71% (two hours, 19 mol% **3**(OTf)<sub>2</sub>) respectively. Although the reactions at elevated temperatures resulted in lower product yields, no starting 3,5-di-*tert*-butylcatechol was observed by NMR.

**Table 1. Catalytic Aerobic Oxidation of 3,5-Di-*tert*-butylcatechol**

Catalyst Loading (mol%)	Temperature (°C)	Yield (%)	Time (h)
21	r.t.	91	24
23	50	73	4
19	65	70	2

Insight into the reactivity was gleaned from a few previous studies of aerobic copper catechol oxidations. When working with Bn<sub>3</sub>tacn, Tolman and coworkers noticed the formation of a copper-semiquinonate species from 3,5-di-*tert*-butylcatechol at low temperature; in this case, coordination was planar to form a square pyramidal complex (Figure 12A).<sup>96</sup> Stack and coworkers found that a side-on peroxo dicopper species supported by N,N'-di-*tert*-butylethylenediamine (DBED) at low temperatures generated an intermediate in the oxidation of 3,5-di-*tert*-butylcatechol, which was confirmed to be a copper(II) semiquinonate (Figure 12C).<sup>97</sup> The *tert*-butyl substituents caused a significant

distortion compared to a similar copper(II) semiquinonate supported by the less-bulky N,N,N',N'-tetramethylcyclohexane-1,2-diamine (TMCD) (Figure 12B), which generated a square pyramidal complex with tetrahydrofuran. Lumb and coworkers noticed the formation of a similar semiquinone intermediate with copper-DBED systems upon reaction with 4-*tert*-butylphenol; the distortion from planarity still occurred, albeit with a less pronounced deviation, even without a *tert*-butyl group ortho to a coordinating oxygen.<sup>95</sup>

In the aforementioned oxidations of phenol or catechol derivatives, a copper semiquinonate species was formed. To address the possibility of a semiquinonate intermediate, an air-free reaction was performed in a J. Young NMR tube in *d*<sub>4</sub>-methanol between **3**(OTf)<sub>2</sub> and 3,5-di-*tert*-butylcatechol. The solution slowly changed from dark brown to dark green. However, <sup>1</sup>H NMR analysis showed no product formation, even after a day. It should be noted that small, broad peaks in the 25-35 ppm range were detected, consistent with the presence of a paramagnetic species (Figure S19). Though copper paramagnetic species had often gone undetected due to the relatively slow paramagnetic relaxation delay of copper(II) complexes, broadened resonances beyond 4.5 Å from the copper center had been reported.<sup>98-99</sup> To help assess whether the species generated was an intermediate in the catalytic cycle to catechol oxidation or an off-cycle species generated in the absence of oxygen, the NMR tube was subsequently exposed to air. Four hours after the NMR tube was unsealed, the solution began to darken. Analysis of the reaction by <sup>1</sup>H NMR revealed complete consumption of starting material with the formation of product, suggesting that the species detected in the absence of oxygen was an intermediate in the reaction. Although a copper semiquinonate species supported by <sup>t</sup>Bu<sub>3</sub>tacn was never structurally characterized, the results point to the possibility of the generation of a

paramagnetic species, likely square pyramidal as seen with the paramagnetic  $\text{Bn}_3\text{tacn}$  (Figure 12D). A square pyramidal, paramagnetic copper semiquinonate was unexpected given the work by Stack and Lumb with DBED,<sup>95,97</sup> but the geometry observed by Tolman and coworkers<sup>96</sup> could be enforced by the macrocyclic nature of the tacn scaffold and the large *tert*-butyl group on the axial nitrogen. Indeed, a sterically unfavorable square planar adduct could have promoted product dissociation and helped catalyst turnover. However, though the observations were consistent with the formation of a copper-semiquinonate intermediate, more structural and kinetic evidence would be required to establish a clearer mechanistic picture.

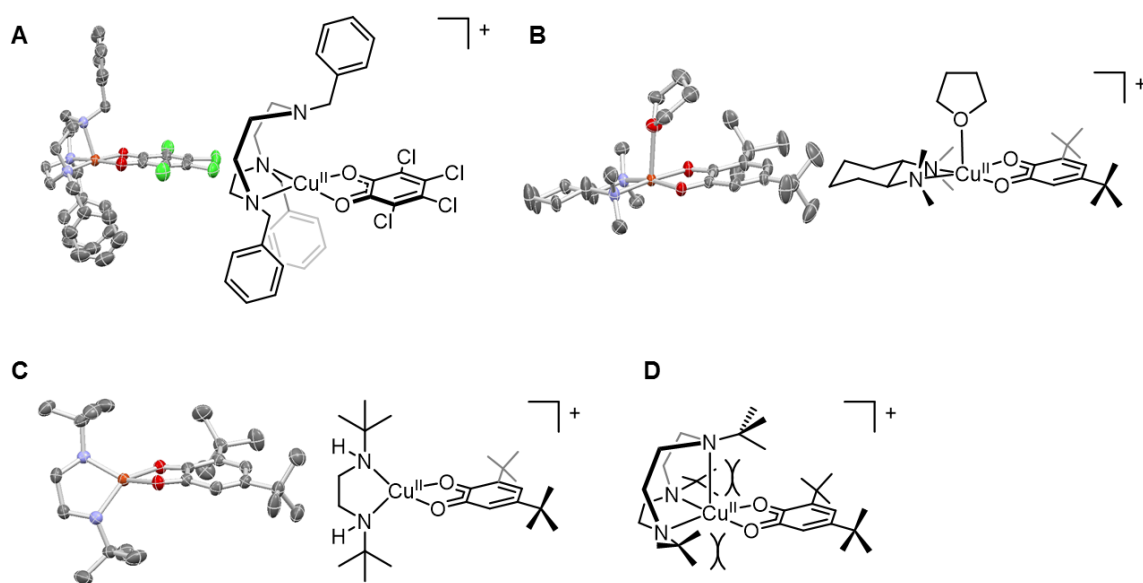


**Figure 12** Comparison of copper semiquinonate crystal structures with corresponding skeletal structures supported by (A)  $\text{Bn}_3\text{tacn}$ ,<sup>96</sup> (B)  $\text{TMCD}$ ,<sup>97</sup> and (C)  $\text{DBED}$ .<sup>97</sup> (D) Skeletal structure of potential copper semiquinonate intermediate supported by  $t\text{Bu}_3\text{tacn}$  highlighting steric clash.

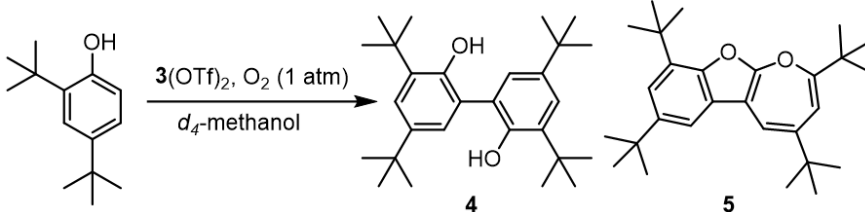
It should be noted here that the characteristics of  $\mathbf{3}(\text{OTf})_2$  with respect to reactivity with 3,5-di-*tert*-butylcatechol against phenol is strikingly similar to the characteristics of hemocyanin proteins toward phenol and catechol. Although hemocyanin proteins contain the same side-on peroxo isomer found in tyrosinase enzymes, hemocyanin proteins often

lack reactivity with phenolic substrates.<sup>4</sup> Structural variants with inefficient but present activity toward phenols have been shown, suggesting that the protein sterically prevents access of phenols to the  $[\text{Cu}_2\text{O}_2]^{2+}$  active site in hemocyanin proteins lacking tyrosinase reactivity. Similarly, the *tert*-butyl substituents of the ligand in  $\mathbf{3}(\text{OTf})_2$  may prevent access to the active site until an oxidation event occurs. Furthermore, a case of catechol reactivity with a hemocyanin protein has been reported, with spectroscopic data and reactivity suggestive of the generation of a semiquinone species.<sup>100</sup> Much like hemocyanin,  $\mathbf{3}(\text{OTf})_2$  does not oxidize phenols, possibly due to steric inaccessibility, but may be able to open for a sufficiently electron-rich catechol.

As  $\mathbf{3}$  did not exhibit tyrosinase reactivity with unsubstituted phenols or catechols but did display reactivity with 3,5-di-*tert*-butylcatechol, it was tested toward reactivity with 2,4-di-*tert*-butylphenol, a more commonly used phenol derivative. Again, no tyrosinase reactivity occurred, as there was no detectable 3,5-di-*tert*-butylcatechol or 3,5-di-*tert*-butyl-*o*-quinone. There was, however, formation of two other products detected by  $^1\text{H}$  NMR on reactions performed in *d*<sub>4</sub>-methanol. Based upon alternative side-on peroxo reactivity observed in a few previous studies, the products were assigned to 3,3',5,5'-tetra-*tert*-butyl-2,2'-dihydroxybiphenyl (**4**) and 2,4,7,9-tetra-*tert*-butyloxepino[2,3-*b*]benzofuran (**5**).<sup>59, 101</sup> The identity of **4** and **5** were confirmed through independent synthesis<sup>101</sup> and comparison of  $^1\text{H}$  NMR spectra from authentic samples in *d*<sub>4</sub>-methanol. Product **4** was hypothesized to derive from oxidative C—C coupling of an intermediate phenoxy radical, while **5** had been established to be the product of further oxidation of **4**.<sup>101-105</sup> Quantification of the products with an internal standard showed that, with 19 mol% loading of  $\mathbf{3}(\text{OTf})_2$ , **4** and **5** were formed in 36% yield and 2% yield, respectively, over the

course of 66 hours (Table 2); therefore, **3**(OTf)<sub>2</sub> was shown to be catalytic with respect to a 2-electron oxidation process. As only small amounts of **5** were formed under ambient conditions, the reaction was followed at elevated temperatures. At 50 °C with 20 mol% **3**(OTf)<sub>2</sub>, **4** and **5** were formed in 52% yield and 15% yield, respectively, over the course of 3 hours; at 65 °C with 21 mol% **3**(OTf)<sub>2</sub>, **4** and **5** were formed in 29% yield and 15% yield, respectively, over the course of 3 hours. It should be noted that, at elevated temperatures, unidentified side-products were formed, which was likely the cause for the decreased yield of **4** at 65 °C compared to 50 °C. Furthermore, no formation of **4** or **5** was noted without the presence of **3**(OTf)<sub>2</sub>. By comparison, [(<sup>i</sup>Pr<sub>3</sub>tacnCu)<sub>2</sub>(O<sub>2</sub>)](SbF<sub>6</sub>)<sub>2</sub>, in a solution primarily consisting of the side-on peroxo isomer, had been shown to react with excess 2,4-di-*tert*-butylphenol only at -80 °C stoichiometrically under a dioxygen atmosphere to form **4**.<sup>106</sup>

**Table 2. Catalytic Aerobic Oxidation of 2,4-Di-*tert*-butylphenol**



Catalyst Loading (mol%)	Temperature (°C)	Yield <b>4</b> (%)	Yield <b>5</b> (%)	Time (h)
19	r.t.	36	2	66
20	50	52	15	3
21	65	29	15	3

As **3**(OTf)<sub>2</sub> generated products consistent with H-atom abstraction, the complex was tested generally as an oxidant, focusing on alcohols geminal to homolytically weak C—H bonds. One alcohol particularly susceptible to oxidation was benzoin; the alcohol was both benzylic and adjacent to a ketone, and it had been shown to react with a previous

copper dioxygen complex at low temperature.<sup>107</sup> Upon reaction with 20 mol% **3**(OTf)<sub>2</sub> in *d*<sub>4</sub>-methanol at room temperature, benzoin was catalytically converted to benzil in 92% yield after four hours (Table 3). By raising the temperature to 50 °C, 20 mol% **3**(OTf)<sub>2</sub> converted benzoin to benzil in 100% yield in one hour. As the reaction occurred rather quickly with 20 mol% **3**(OTf)<sub>2</sub> at elevated temperatures, the reaction was run with 5 mol% **3**(OTf)<sub>2</sub> at 50 °C, leading to formation of 93% benzil in 29 hours. As with 2,4-di-*tert*-butylphenol, no benzoin reaction occurred when **3**(OTf)<sub>2</sub> was not present. Additionally, use of urea-hydrogen peroxide as the oxidant for benzoin did not efficiently generate benzil, instead forming another unidentified product; this suggested that the complex was not simply generating free hydrogen peroxide from air to act as the surrogate oxidant for benzoin oxidation.

**Table 3. Catalytic Aerobic Oxidation of Benzoin**

Catalyst Loading (mol%)	Temperature (°C)	Yield (%)	Time (h)
20	r.t.	92	4
20	50	100	1
5	50	93*	29

\*The reaction was run open to air.

Throughout the course of the reactions monitored by <sup>1</sup>H NMR in *d*<sub>4</sub>-methanol, **3**(OTf)<sub>2</sub> would naturally decompose over time; this came to no surprise, given its half-life value of 13.05 hours under an atmosphere of dioxygen. However, the main decomposition products were observed to be diamagnetic. The first product, a red-green species, was formed more rapidly at elevated temperatures, as determined by <sup>1</sup>H NMR and UV-Vis. Unfortunately, attempts to crystallize the diamagnetic products, particularly the initial diamagnetic product, led to further reaction and decomposition to **2**. This intermediate

species appeared to be similarly competent for benzoin catalysis, as oxidation still occurred at elevated temperatures, when the intermediate was the dominant observed species by  $^1\text{H}$  NMR. However, it should be noted that during the benzoin reaction at room temperature,  $\mathbf{3}(\text{OTf})_2$  was the only species observed throughout and at the end of the reaction.

Given that  $\mathbf{3}(\text{OTf})_2$  exhibited a half-life of 13.05 hours under a dioxygen atmosphere, it was peculiar that it was the only species observed after four hours of reaction with benzoin. This suggested the possibility that the presence of a good substrate for  $\mathbf{3}(\text{OTf})_2$  may promote the integrity of the complex, potentially by reacting with an unstable intermediate. Indeed, the half-life of  $\mathbf{3}(\text{OTf})_2$  in methanol increased from 13.05 hours to 13.48 hours when measured in the presence of benzoin (Table 4; Figures S4-S10). When measured in the presence of 2,4-di-*tert*-butylphenol, the half-life increased even more to 17.1 hours. Thus, under aerobic conditions in solution, complex  $\mathbf{3}$  was shown to maintain its concentration in solution for longer when in the presence of a suitable substrate.

**Table 4. Solution Half-Life of  $\mathbf{3}$**

<b>Solvent</b>	<b>Conditions</b>	<b>Half-Life (<math>\lambda</math>)</b>
<b>Water</b>	$\text{NaH}_2\text{PO}_4$ , $\text{N}_2$	$6.71 \pm 0.016$ days (398 nm)
<b>Water</b>	$\text{Na}_2\text{HPO}_4$ , $\text{N}_2$	$9.6$ days $\pm 0.12$ (398 nm)
<b>MeCN</b>	$\text{N}_2$	$2.524 \pm 0.0043$ hours (553 nm)
<b>MeOH</b>	$\text{N}_2$	$14.25 \pm 0.025$ hours (400 nm)
<b>MeOH</b>	$\text{O}_2$	$13.05 \pm 0.065$ hours (400 nm)
<b>MeOH</b>	Benzoin, $\text{O}_2$	$13.48$ hours $\pm 0.073$ (400 nm)
<b>MeOH</b>	2,4-di- <i>tert</i> -butylphenol, $\text{O}_2$	$17.1 \pm 0.18$ hours (554 nm)

As **3**(OTf)<sub>2</sub> showed that it could perform as an alcohol oxidation catalyst with benzoin, the less active alcohol, benzyl alcohol, was chosen as a substrate. Benzyl alcohol was reacted with **3**(OTf)<sub>2</sub> in methanol at room temperature, 50 °C, and 65 °C, and the reactions were monitored by gas chromatography (GC) with 1,3,5-tri-*tert*-butylbenzene as an internal standard (Table 5). At room temperature, **3**(OTf)<sub>2</sub> did not convert benzyl alcohol to benzaldehyde above the detection limits of the GC. However, the reaction did occur at elevated temperatures: after 76 hours, 9% yield and 34% yield of benzaldehyde were formed upon reaction with one equivalent of **3**(OTf)<sub>2</sub> at 50 °C and 65 °C, respectively. At all temperatures, no benzaldehyde product was detectable by GC without the addition of **3**(OTf)<sub>2</sub>, suggesting that **3**(OTf)<sub>2</sub> was involved in the observed substrate oxidation process. Given the necessity of stoichiometric loading of **3**(OTf)<sub>2</sub> and requirement of elevated temperatures for observable reactivity, it appeared that benzyl alcohol represented the limit of alcohol reactivity with **3**(OTf)<sub>2</sub>. Nevertheless, the reaction produced no detectable overoxidation to benzoic acid, consistent with the results of some recent aerobic copper oxidation reactions deriving from ill-defined active species.<sup>108-111</sup>

**Table 5. Aerobic Oxidation of Benzyl Alcohol**

c1ccc(cc1)CO  $\xrightarrow[\text{CH}_3\text{OH}]{\text{3(OTf)}_2 \text{ (1 equiv), O}_2}$  c1ccc(cc1)C=O

Temperature (°C)	Yield (%)	Time (h)
r.t.	0	N/A
50	9	76
65	34	76

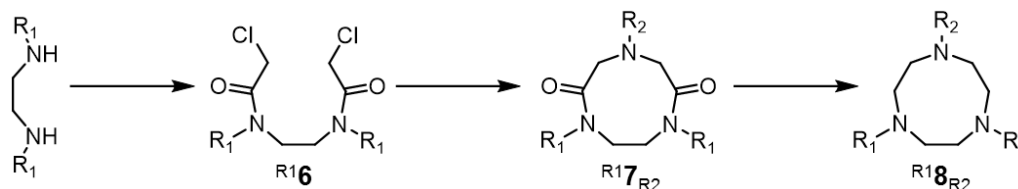
### *C. Modification of the Synthesis of 1,4,7-Tri-*tert*-butyl-1,4,7-triazacyclononane*

Studies analyzing the use of <sup>t</sup>Bu<sub>3</sub>tacn to support copper complexes required routine synthesis of the ligand using the methods of Bradshaw and Izatt<sup>71</sup> and expanded upon by Scarborough and coworkers<sup>74</sup> (Scheme 7). However, the synthesis of the ligand based upon



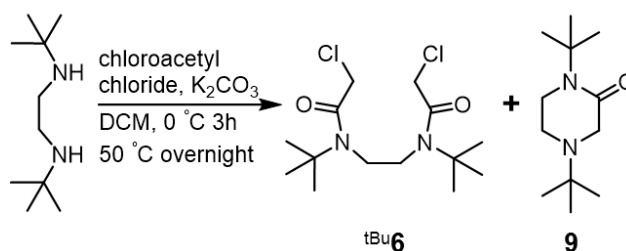
the previous literature report<sup>74</sup> required over a week. Furthermore, there were major reproducibility problems with the first step of the reaction, a chloroacetylation. Therefore, the synthesis of <sup>t</sup>Bu<sub>3</sub>tacn was targeted for procedural optimization.

### Scheme 7. A General Synthesis of Substituted Tacn Derivatives



The chloroacetylation step presented a few serious problems. The reaction generated a large amount of side product, identified as 1,4-di-*tert*-butylpiperazin-2-one (**9**); at times, more **9** was formed than major product, <sup>t</sup>Bu**6** (Scheme 8). Secondly, the yield of <sup>t</sup>Bu**6** varied greatly, and a yield as high as 69% was never obtained after the initial report.

### Scheme 8. Unoptimized Chloroacetylation Reaction



The generation of the side product **9** can be rationalized by examining the mechanism. DBED has two equivalent nucleophilic amines. However, the electrophile, chloroacetyl chloride, has two positions susceptible to nucleophilic attack: the carbonyl position and the  $\alpha$ -position of the carbonyl. The desired product requires each amine to perform acyl substitution at the more reactive carbonyl carbon of two different chloroacetyl chloride molecules. However, after acyl substitution of the first amine, the second amine can presumably perform  $\alpha$ -substitution to displace the other chlorine, which leads to **9**. Though S<sub>N</sub>2 displacement of alkyl chlorides is less favorable than acyl substitution of acid

chlorides, the barrier for the displacement of chloride in the  $\alpha$ -position of a carbonyl is lowered. Furthermore, as the less favorable substitution to **9** is intramolecular in nature, the reaction is likely to occur faster than an intermolecular substitution and is effectively irreversible under the reaction conditions, forming a six-membered ring in the process.

In order to promote the formation of the desired product <sup>tBu</sup>**6**, intermolecular reaction of the monoacylated intermediate must occur before intramolecular cyclization. In the original procedure for the diacylation, chloroacetyl chloride is added slowly to a solution of DBED. This process may favor the formation of **9**, the undesired product; the concentration of chloroacetyl chloride is then always low, lowering the likelihood of the intermediate encountering another chloroacetyl chloride with which to react. However, if the process is reversed, and DBED is exposed to a higher concentration of chloroacetyl chloride, this may bias the reaction toward the desired product <sup>tBu</sup>**6** over the observed undesired product **9**.

Another noteworthy observation regarding reaction optimization occurs in the quench. In theory, potassium carbonate is added to the reaction to act as a base. However, upon the addition of water to quench the reaction, the solution vigorously bubbles, requiring a careful addition of water to avoid eruption. This suggests a large buildup of acid that is not quenched until water is added to dissolve the potassium carbonate. Therefore, the potassium carbonate may not be necessary during the course of the reaction; it may be safely added as an aqueous solution during the quenching procedure.

These ideas were tested as modifications to the diacylation reaction.<sup>A, B</sup> By adding DBED dropwise to a solution of chloroacetyl chloride in dichloromethane, a similar turbid mixture was generated; however, with this procedure, the turbid mixture was white instead

of yellow. The reaction was quenched by pouring the contents into a mixture of aqueous potassium carbonate and ice and stirring for 30 minutes. Extraction from this mixture consistently led to isolation of a crude lacking impurity **9**. Further optimization, such as shortening the reaction time to two to four hours as well as cooling the solution in an ice bath during diamine addition consistently resulted in high yields (>90%) of product as a white solid without the need for crystallization. The crude product not only exhibited a clean  $^1\text{H}$  NMR, but was found to be pure by internal standard.

The next reaction in the synthesis involved the cyclization of  $^{\text{tBu}}\mathbf{6}$  around *tert*-butylamine. This reaction reportedly required three days of heating to complete. Furthermore, as a large amount of high-boiling (153 °C) DMF (the reaction required dilution to a 0.125M solution of  $^{\text{tBu}}\mathbf{6}$ ) was used, separation of DMF from the product  $^{\text{tBu}}\mathbf{7}_{\text{tBu}}$  was a laborious process, requiring distillation prior to extraction.

In an effort to minimize reaction time, the reaction was monitored by  $^1\text{H}$  NMR spectroscopy. From this, it was found that product formation did not proceed past four hours of heating, with most product formation complete after two hours of heating. Stopping the reaction at this time led to extraction of a crude solid, which could be similarly crystallized to afford the product  $^{\text{tBu}}\mathbf{7}_{\text{tBu}}$ .

Although the reaction time was decreased almost 20-fold, the use of a large volume of DMF was an obstacle, requiring a particularly lengthy distillation for large-scale reactions. The dilute reaction conditions were initially utilized to avoid a potential polymerization problem: if the intermediate, formed after initial  $\text{S}_{\text{N}}2$  displacement of the chloride, encountered another molecule of  $^{\text{tBu}}\mathbf{6}$ , it may add to that instead of performing a cyclization. To test the effect of dilution on product formation, the reaction was attempted

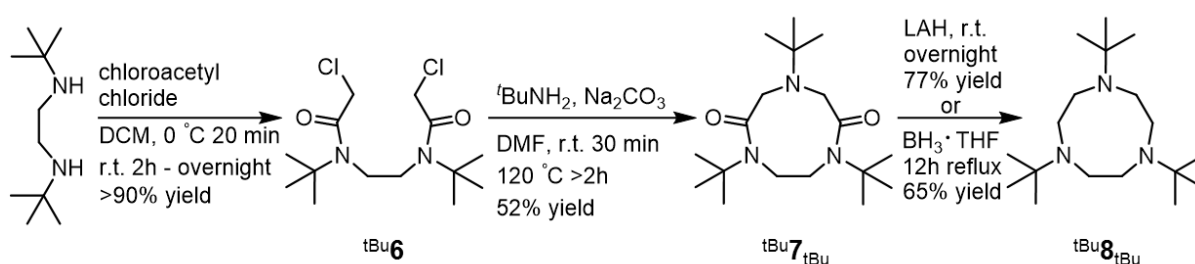
at increased concentrations. It was found that the reaction generated the product at concentrations as high as 1.0M in DMF, a concentration found to be essentially at the limit of solubility of the starting material. At this concentration, distillation was no longer required; the reaction could be extracted with ethyl acetate and washed several times with aqueous sodium chloride to separate DMF from the crude product. Though the crude isolated from extraction was often found to be impure by  $^1\text{H}$  NMR internal standard, the desired cyclization product was consistently the main material generated, and the isolated yield was generally about 10% lower than previously reported. Given the vast decrease in reaction time and solvent waste, the new procedure represented a significant improvement.

Though the final step of the reaction, the lithium aluminum hydride reduction, worked quite well, safer reagents were considered; indeed, the dangers of quenching pyrophoric lithium aluminum hydride were made evident by a quenching incident requiring medical treatment for a former coworker for burn injuries. Previous work on a related synthesis of macrocyclic ligands showed that borane-tetrahydrofuran ( $\text{BH}_3\cdot\text{THF}$ ), a significantly safer reagent, was a sufficient reductant for the amides in those processes.<sup>71</sup> Upon application of the same procedure to the formation of  $^t\text{Bu}_3\text{tacn}$ , the reaction was found to proceed in only slightly diminished yield to the desired product. Furthermore, due to the significantly attenuated reactivity of  $\text{BH}_3\cdot\text{THF}$ , the time required to safely quench the reaction was greatly reduced.

Taking all the steps together, the process to generate  $^t\text{Bu}_3\text{tacn}$  was significantly optimized and streamlined (Scheme 9). When performed efficiently, the entire ligand synthesis was executed in a 24 hour period with either reduction procedure. Compared to the previously reported synthesis, which required at least a week to perform, the optimized

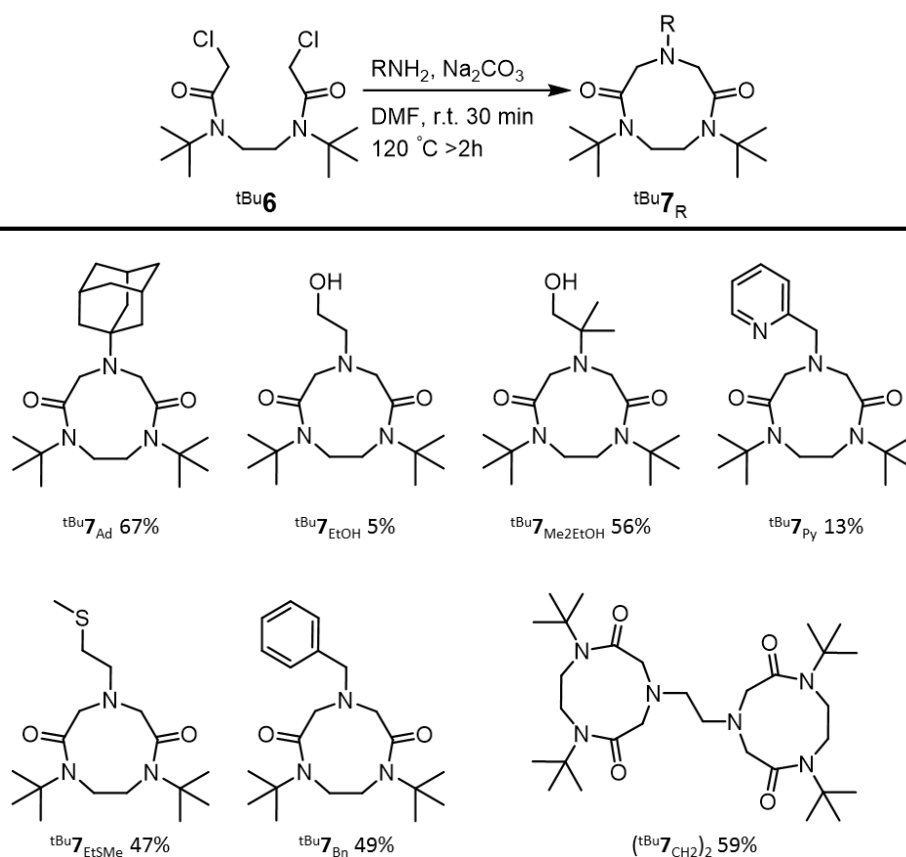
synthesis represented an 86% reduction in process time. Furthermore, due to the use of a less pyrophoric reagent during the reduction step, the process was made significantly safer. Due to the decreased reaction time and increased safety, the synthesis was even successfully performed in an undergraduate inorganic chemistry laboratory class. Thus, the modifications to the synthesis facilitated coordination chemistry with this ligand, as was already shown in an academic undergraduate laboratory.

### Scheme 9. Optimized Synthesis of <sup>t</sup>Bu<sub>3</sub>tacn (<sup>t</sup>Bu<sub>8</sub>tBu)



#### D. Exploring Modularity in the Synthesis of Derivatives of 1,4,7-Triazacyclononane

As previous work had shown that the second, cyclization step in the synthesis of <sup>t</sup>Bu<sub>3</sub>tacn could be applied to cyclization around each amine of benzylamine, ethylenediamine, and propylenediamine,<sup>A</sup> the scope of this reaction was investigated further,<sup>B</sup> initially with monoamines. From a series of reaction screens, the cyclization was found to occur with 1-adamantylamine, ethanolamine, 2-amino-2-methyl-1-propanol, 2-picolylamine, and 2-(methylthio)ethylamine (Table 6). From these initial screens, it was determined that the cyclization worked with alkylamines of various substitution patterns and tolerated alcohols, thioethers, and pyridyl groups.

**Table 6. Scope of Amine Cyclization Toward  $t\text{Bu}7_{\text{R}}$ .**

Unfortunately, a variety of nitrogen nucleophilic groups were unable to affect cyclization. Aryl substituents could not be incorporated into the tacn synthesis via this route, as anilines would not provide the cyclized product. Hydroxylamine would not cleanly form a desired N-hydroxy functionalization of the ring, instead forming a mixture of unidentified products. In an attempt to incorporate biologically relevant side chains as well as chirality, cyclization was attempted with amino acids L-methionine, L-tyrosine, and L-tryptophan; unfortunately, these reactions also led to mixtures of unknown products by  $^1\text{H}$  NMR. Fortunately, amino acid side chains could be incorporated without the carboxyl groups, as was shown by the successful cyclization around 2-(methylthio)ethylamine as a methionine surrogate.

Given the prior successes of cyclizations around ethylenediamine and propylenediamine,<sup>A</sup> other polyamines were attempted. Diethylenetriamine (dien) and tris(2-aminoethyl)amine (tren) were thus utilized as reagents. In either case, results were promising but not unambiguous. The <sup>1</sup>H NMR spectra of the reactions showed consumption of starting material and contraction of the proton resonances at the  $\alpha$ -amino positions, consistent with the patterns seen from previous successful nine-membered ring cyclizations. Unfortunately, the  $\alpha$ -amino peaks broadened considerably, and the reactions were not completely pure. Attempts to crystallize the products generated oil in each case, and species in the crude were immobile on silica. However, mass spectrometry on the crude products were highly promising, showing the desired mass (Figure 13). The results were consistent either with the formation of the desired product or the formation of large macrocycles with the same molecular formulae, inclusively. Reduction of these species led to similar results; the <sup>1</sup>H NMR results were highly suggestive of the products, (tBu<sub>2</sub>tacn)<sub>2</sub>dien and (tBu<sub>2</sub>tacn)<sub>3</sub>tren, but crystal structures were never obtained.

Given the ring-size ambiguity associated with polyamine cyclization, it became important to assess whether cyclization around multiple alkylamines was possible for tBu<sub>6</sub>. To address the question, the reactivity of tBu<sub>6</sub> was probed with excess benzylamine (Scheme 10, Figure S31). With ten equivalents of benzylamine, there was primarily the formation of the desired cyclized nine-membered ring **10**, with the formation of a noticeable amount of undesired acyclic product **11** (ratio 1.98:1 **10:11**). This result was particularly striking given the concentration of benzylamine: there were approximately equal volumes of benzylamine and DMF. Finally, heating tBu<sub>6</sub> in neat benzylamine (ten equivalents) led to the formation of **10** along with the formation of the **11** in a 0.82:1 ratio.

These results suggested that, although incorporation of two primary amines for each <sup>t</sup>Bu<sub>6</sub> was possible under extreme conditions, the pathway was less favorable than cyclization around a single primary amine.

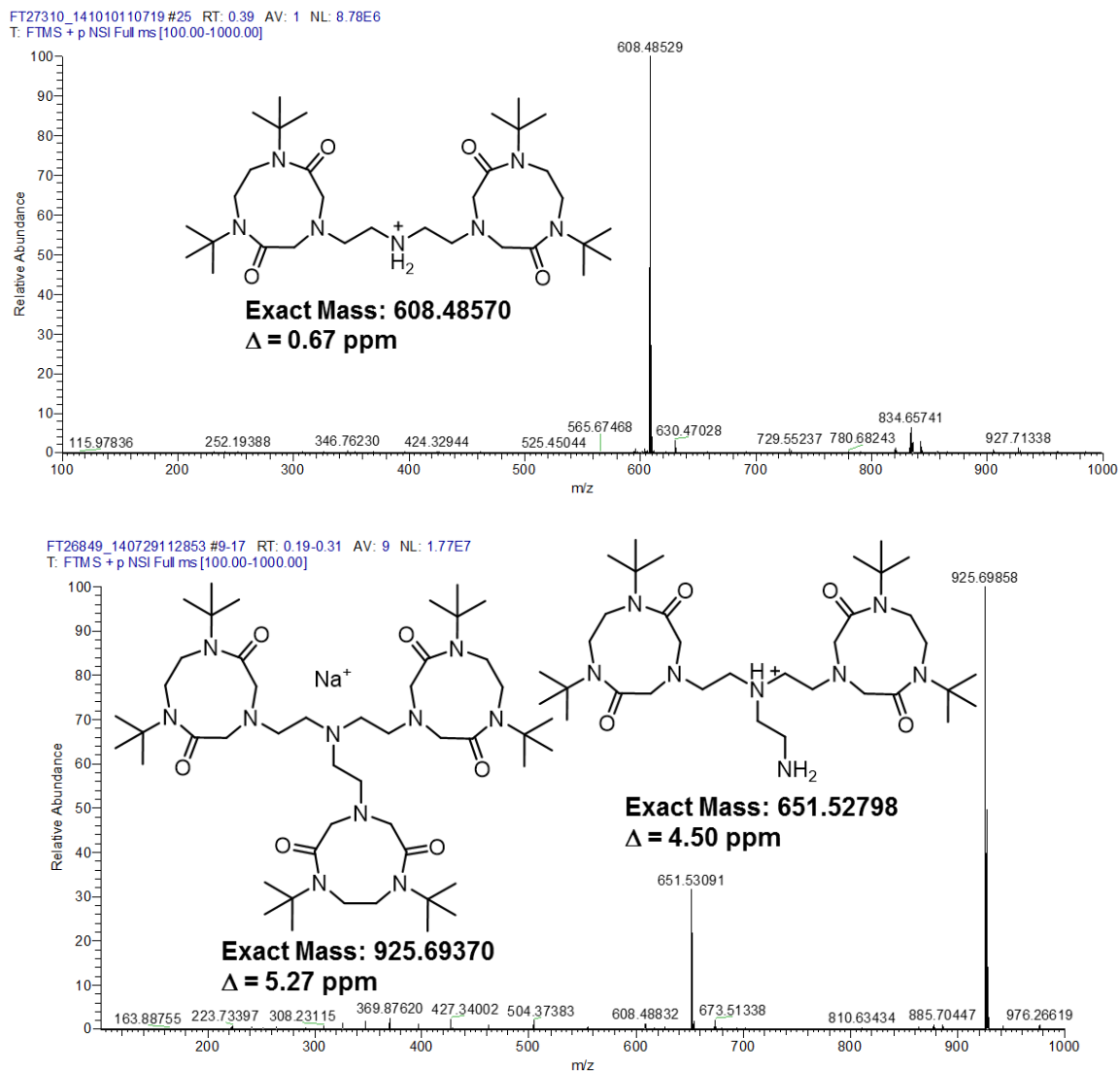
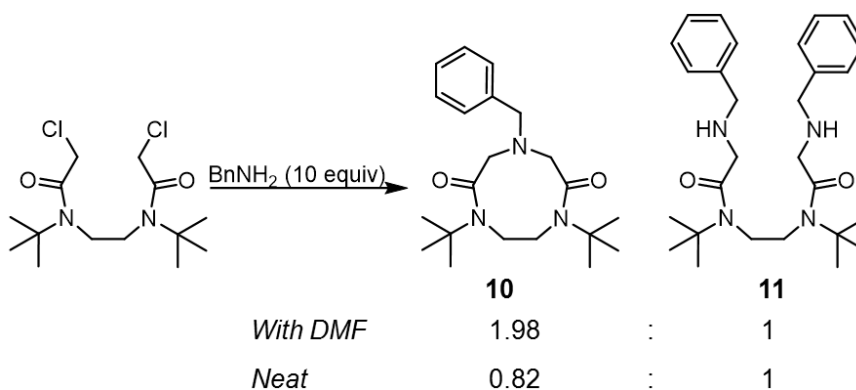


**Figure 13.** Mass spectrometry results of cyclization reactions with dien (top) and tren (bottom).



**Scheme 10. Single vs. Double Amination: Competition Experiment**

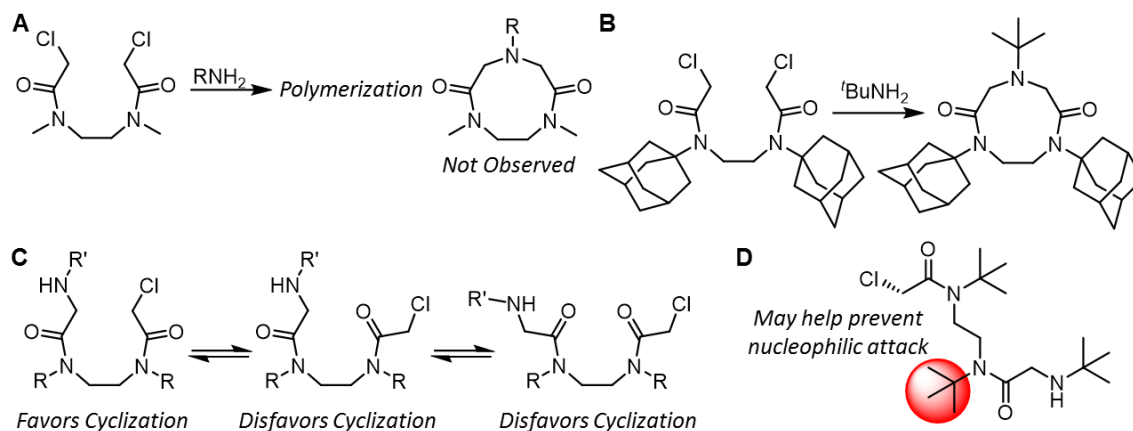


That cyclization to form a strained nine-membered ring would occur over formation of acyclic diamines and polymers even under conditions favoring the latter was naturally a curious occurrence. Considering the possibility that it may have something to do with the steric influence of tertiary alkyl N-substituents on the amides led to the investigation as to whether steric factors had a part to play in the reaction pathway. Indeed, previous experiments with <sup>Me</sup>**6** under the same cyclization conditions did not lead to noticeable formation of the desired product, with the production of highly insoluble solids consistent with polymerization (Figure 14A).<sup>A</sup> Furthermore, the tertiary alkyl N-substituted <sup>Ad</sup>**6** not only cyclized around 1-adamantylamine,<sup>74</sup> but it was also found to cyclize around *tert*-butylamine (Figure 14B).

The reactivity of <sup>tBu</sup>**6** and <sup>Ad</sup>**6** toward cyclization implicates substituent steric bulk as a potential reason for the success of the reactions. One quality that the sterics of N-substituted amides are known to affect is the equilibrium of amide rotamers. An amide C—N bond is capable of rotation, allowing the amide to equilibrate between *cis* and *trans* conformations. The resulting rotational isomers, or rotamers, can be affected by several factors;<sup>112-113</sup> however, in the case of fully substituted acyclic amides, steric effects are the major forces behind rotamer selection. Amides with a bulky alkyl group tend to favor the

rotamer with this group *syn* to the amide oxygen (Figure 14C, left), as this is the smallest group on the amide, often leading to the *cis* isomer as the major rotamer in solution.

This rotamer selection is likely important for the cyclization step in the synthesis of tacn derivatives bearing tertiary alkyl substituents. If the alkyl N-substituents on the bis(chloroacetamide)ethylenediamine (**6**) are large, such as with *tert*-butyl or adamantyl, then the *cis* rotamer allows for cyclization (Figure 14C, left). Furthermore, even when the ethyl bridge connecting the two amides twists into a disfavored conformation, the large alkyl substituents may help prevent intermolecular nucleophilic attack (Figure 14D). If this hypothesis is correct, then small N-substituents may favor polymerization under conditions in which large N-substituents favor cyclization.

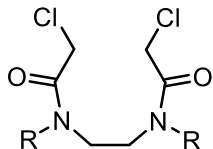
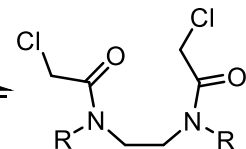
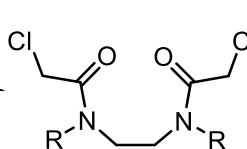


**Figure 14.** Cyclization does not occur with (A) <sup>Me</sup>**6**, likely favoring polymerization, but does occur with (B) <sup>Ad</sup>**6** and <sup>tBu</sup>**6** to form <sup>Ad</sup>**7**. (C) Only one amide rotamer combination (left) leaves the intermediate in the second step of a tacn synthesis likely to cyclize. (D) Large N-substituted amides may also help prevent intermolecular attack by a second amine.

To test this idea, derivatives of **6** were made with methyl (<sup>Me</sup>**6**), benzyl (<sup>Bn</sup>**6**), and isopropyl (<sup>iPr</sup>**6**) amide substituents. The derivatives were each crystallized, and the <sup>1</sup>H NMR spectra were analyzed (Figures S21, S23, and S25). The first derivative analyzed, <sup>iPr</sup>**6**, displayed significantly more resonances in its <sup>1</sup>H NMR than could be justified by one isomer. Furthermore, repeated synthesis of <sup>iPr</sup>**6** led to similar ratios of the NMR resonance

integrations. Similar isomeric features were found with <sup>Me</sup>6 and <sup>Bn</sup>6. These features were consistent with the presence of the predicted amide rotamers (Figure 13C). Indeed, heating <sup>iPr</sup>6 led to coalescence of the resonances into what appeared to be one isomer (Figure S26); heating of <sup>Me</sup>6 (Figure S22) and <sup>Bn</sup>6 (Figure S24) began to, but did not completely, converge to one isomer. Several 1D NOE experiments on <sup>Me</sup>6, <sup>Bn</sup>6, and <sup>iPr</sup>6 provided some evidence toward correlation between sets of <sup>1</sup>H NMR resonances to rotamer through the integration of enhanced peaks (Figures S27-S30). However, the assignments were ambiguous: not only did irradiated resonances equilibrate during enhancement, but irradiation of resonances from one amide could enhance resonances of another, as seen with <sup>tBu</sup>6 (Figure S30). However tenuous, the peak assignments to rotamers allowed for the establishment of rotamer ratios by NMR (Table 7).

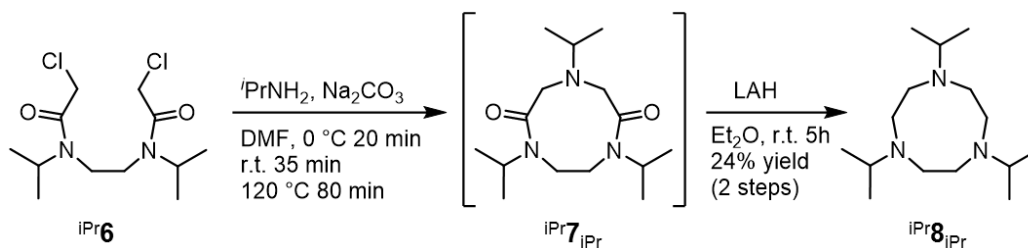
**Table 7. Estimated Percent Rotamer Population in Solution**

R Group			
Me		32%	68%
Bn	50%	46%	4%
<sup>i</sup> Pr	76%	24%	
<sup>t</sup> Bu	100%		

Given the evidence for the existence of multiple equilibrating structures in solution and rotamer assignments, the reactivity of each toward amine donors was tested. In attempted cyclizations of <sup>Me</sup>6 and <sup>Bn</sup>6 with amines, polymerization was the only evident process, generating spongy, insoluble solids; a similar event was noted with <sup>iPr</sup>6 and ethylenediamine. However, when <sup>iPr</sup>6 and isopropylamine were treated to the cyclization

conditions, an impure white solid formed. A  $^1\text{H}$  NMR of the solid contained resonances suggestive of cyclization to  ${}^{\text{iPr}}\mathbf{7}_{\text{iPr}}$ , and mass spectrometry results were consistent with this assignment. Reduction of  ${}^{\text{iPr}}\mathbf{7}_{\text{iPr}}$  led to the formation of  ${}^{\text{iPr}}\mathbf{3}\text{tacn}$  ( ${}^{\text{iPr}}\mathbf{8}_{\text{iPr}}$ ) as a clear, colorless, hygroscopic, air-sensitive oil in low yield (24% over two steps) (Scheme 11).

**Scheme 11. Synthesis of  ${}^{\text{iPr}}\mathbf{3}\text{tacn}$  ( ${}^{\text{iPr}}\mathbf{8}_{\text{iPr}}$ ).**



Based upon the results of the reactivity studies, it appears that cyclization around a single amine is dependent upon the steric bulk of the amide N-substituent. The correlation between amide rotamers and reactivity to form the desired 9-membered ring provides evidence for the hypothesis that the correct amide rotamer is necessary, and potentially sufficient, for affecting cyclization. The results show that secondary alkyl substituents represent a boundary toward formation of tacn derivatives utilizing the present conditions, with tertiary alkyl substituents ( ${}^{\text{tBu}}\mathbf{6}$  and  ${}^{\text{Ad}}\mathbf{6}$ ) representing the way toward clean cyclizations. Additionally, given the ease of removal of *tert*-butyl groups from amines,<sup>B</sup> the present synthesis provides a rapid route to a variety of tacn derivatives.

### III. Conclusions

The aforementioned work shows that <sup>t</sup>Bu<sub>3</sub>tacn is an oxidatively robust ligand capable of the generation of the most persistent copper-dioxygen complex known. Extensive characterization of the copper dioxygen complex unambiguously demonstrates the formation of **3**(OTf)<sub>2</sub> upon exposure of **2** to air. The ability of the supporting ligand to effectively bury the active copper dioxygen core may be responsible for the stability of the complex. Furthermore, unlike other copper dioxygen complexes supported by tacn derivatives, the ligand prevents formation of more active bis(μ-oxo) complexes, as the contraction of the copper-copper distance to form this highly active form is precluded by the steric bulk of the ligands. Consequently, **3**(OTf)<sub>2</sub> is relatively unreactive compared to other known side-on peroxo complexes.

The ligand synthesis work shows new utility of 1,4,7-triazacyclononane ligands as targets for the rapid synthesis of bulky scaffolds. Due to the modularity introduced in the second step of the tacn synthesis, groups representing a variety of steric and electronic features can be incorporated through the use of simple amines. The tendency of <sup>R</sup>**6**, where R is a tertiary alkyl substituent, to cyclize around a single amine finds use in the potential synthesis of tethered polyamines. Unfortunately, <sup>R</sup>**6** derivatives with smaller R groups perform less satisfactorily: when R is the secondary alkyl group isopropyl, cyclization around a single amine occurs in low yield at best, while smaller R groups form material consistent with polymerization. Evidence from NMR experiments point to the necessity of tertiary alkyl substituents on <sup>R</sup>**6** to ensure that amine rotamer equilibrium favors intramolecular cyclization.

## IV. Future Directions

### A. Synthesis and Utility of Tethered Tacn Derivatives

The generation of polytacn ligands, such as (<sup>t</sup>Bu<sub>2</sub>tacn)<sub>2</sub>dien and (<sup>t</sup>Bu<sub>2</sub>tacn)<sub>3</sub>tren, may be useful for bringing metals together, particularly for cluster generation. Significant advancements in template chemistry have been performed by the research laboratories of Agapie<sup>114</sup> and Holm,<sup>115-116</sup> toward the assembly of cluster models of the oxygen evolving complex and an iron-sulfur cluster (Figure 15A). However, FeMo-co, the cluster responsible for nitrogen fixation in proteins, has yet to be fully formed; work by Holm has led to similar clusters (Figure 15B),<sup>117</sup> yet assembly with the proper atom identities, particularly with the central carbon,<sup>118</sup> has yet to be attained. Only recently has an iron complex been synthesized that is bound to both sulfur and carbon and shows some potential for dinitrogen activation (Figure 15C).<sup>119</sup> Hence, the potential synthesis of (<sup>t</sup>Bu<sub>2</sub>tacn)<sub>2</sub>dien and (<sup>t</sup>Bu<sub>2</sub>tacn)<sub>3</sub>tren may lead to advancement in the study of active metal clusters.

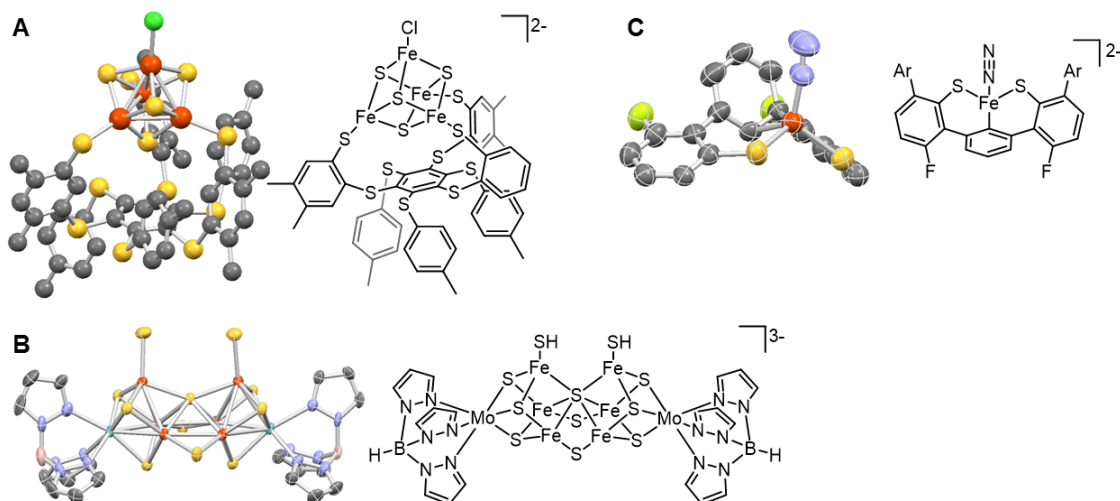


**Figure 15.** (A) Crystal and skeletal structures of a templated iron-sulfur cluster (thermal ellipsoid data not available; ball-and-stick model used instead; counterions and solvent omitted for clarity).<sup>115</sup> (B) Crystal and skeletal structures of a cluster similar to the cluster found in nitrogenase enzymes (counterions and solvent omitted for clarity).<sup>117</sup> (C) Crystal and skeletal structures of an iron-dinitrogen complex supported by sulfur and carbon donor atoms, similar to a portion of the metal cluster in nitrogenase (counterions, solvent, and aryl groups omitted for clarity; Ar = 2,4-diisopropylphenyl).<sup>119</sup>

The bulk and modularity of tethered polytacn ligands may allow for greater control of cluster size. As the tether length between bound tacn derivatives is easily modified, variation in metal distance can be manipulated. Furthermore, the steric bulk required in the aforementioned syntheses of tethered tacn derivatives may constrain cluster size. The ease of such chain incorporation through tether modification may be useful for studying how enzymes cooperatively facilitate cluster formation. The potential for rapid formation of a variety of tethered tacn derivatives bearing tertiary alkyl substituents may not only facilitate the formation of metal clusters similar to those in biology, but it may additionally pave the way toward the synthesis and study of novel metal complexes.

*B. Ambient Electrochemical and Chemical Reduction of Peroxo Complexes Toward the Active Site of Particulate Methane Monooxygenase*

One of the original motivations behind the formation of a stable  $[\text{Cu}_2(\mu\text{-}\eta^2\text{:}\eta^2\text{-O}_2)]^{2+}$  complex was to study the core generated upon single-electron reduction,  $[\text{Cu}_2\text{O}_2]^+$ , for its suggested role in methane oxidation in pMMO.<sup>58</sup> Preliminary work with  $\mathbf{3}(\text{OTf})_2$  electrochemistry in organic solvents led to complicated cyclic voltammograms. As the only cyclic voltammetry experiment on a dicopper dioxygen complex was performed at  $-80^\circ\text{C}$ ,<sup>33</sup> the temperature dependence of the cyclic voltammograms of  $\mathbf{3}(\text{OTf})_2$  were tested. In DMF at room temperature,  $\mathbf{3}(\text{OTf})_2$  showed a species partially decaying upon reduction with what appeared to be electrochemically irreversible but somewhat chemically reversible reoxidation at fast (500 mV/s) scan rates located around -1.3 V vs.  $\text{Ag}/\text{Ag}^+$  (Figure 16A). At  $-42^\circ\text{C}$ , however, a solution of  $\mathbf{3}(\text{OTf})_2$  displayed different behavior (Figure 16B). The reduction event split into two discrete reduction events, and the reoxidation events occurred at higher potentials. Though low temperature work could have

suggested that the reduction event at room temperature could be multielectron, it also highlighted the necessity for ambient electrochemical studies for comparison with biological examples of copper dioxygen complexes such as pMMO.

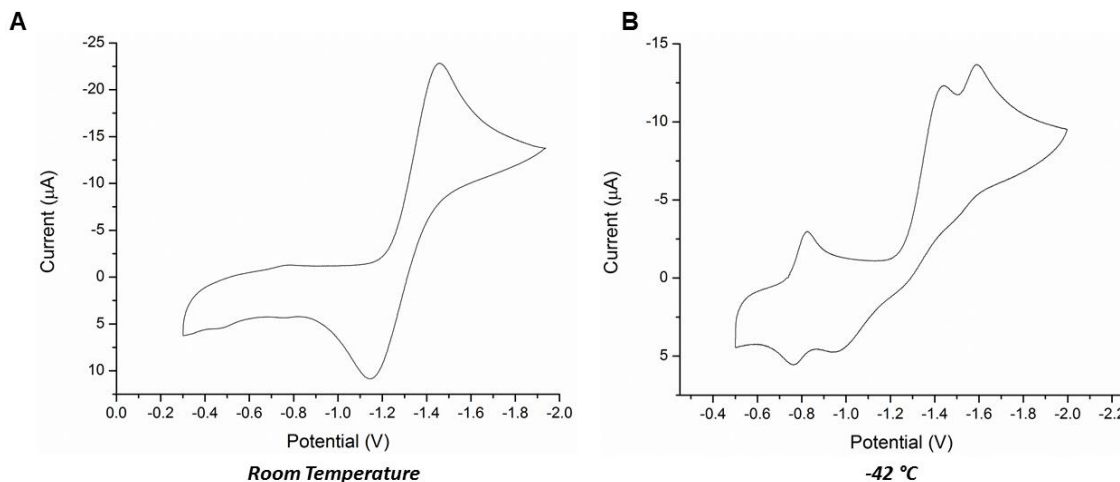


**Figure 16.** Cyclic voltammetry experiments of **3** in DMF at (A) room temperature and (B)  $-42\text{ }^{\circ}\text{C}$ .

Electrochemistry was then performed in water, in which **3** was determined to be most stable. As **3** was found to be somewhat water soluble with phosphate anions, solutions were generated by mixing  $\mathbf{3}(\text{OTf})_2$  with phosphates of various acidity using  $\text{Na}_2\text{HPO}_4$ ,  $\text{NaH}_2\text{PO}_4$ , and  $\text{H}_3\text{PO}_4$ . It was expected that with greater solution acidity, the reduction potential would become more positive. However, cyclic voltammetry experiments in water, referenced to  $\text{Ag}/\text{AgCl}$ , suggested the opposite trend (Figure 17). The reduction potential of **3** in water became more negative with increasing acidity:  $-0.48$  at pH 9;  $-0.56$  at pH 7;  $-0.61$  at pH 4;  $-0.66$  at pH 2. Unfortunately, no hypothesis for this behavior was developed.

In the hopes of studying the species generated by reduction of  $\mathbf{3}(\text{OTf})_2$ , bulk electrolysis was performed, in collaboration with Dongmei Xiang of the Dyer laboratory at Emory University. Bulk electrolysis of  $\mathbf{3}(\text{OTf})_2$  in DMSO at room temperature led to the



formation of a light green species. To determine whether the ligand was still intact after reduction, ammonium hydroxide was added to this species to demetallate the complex soon after formation; this led to vigorous bubbling and eruption of the flask contents, suggesting gas release from the solution. Investigation into the identity of the gas was not performed.

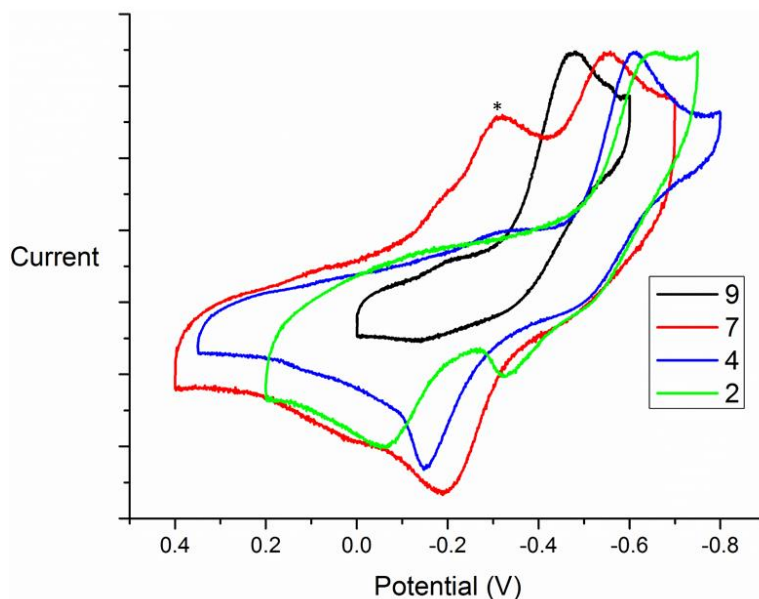


**Figure 17.** Cyclic voltammetry of **3** in water in solutions of various pH values (shown in key; pH values approximated from pH test strips). The voltammograms were scaled by the peak current of the reduction wave for ease of comparison. Peak reduction potentials are as follows:  $-0.48$  at pH 9;  $-0.56$  at pH 7;  $-0.61$  at pH 4;  $-0.66$  at pH 2. \*Reduction wave present in background solution and thus not attributed to reduction of **3**.

Attempts to assemble the product of single electron reduction were led by some preliminary results using superoxide. In the hopes of generating a mononuclear copper(II)-superoxide complex to compare with intermediates in the reaction of  $\mathbf{3}(\text{OTf})_2$  with substrates,  ${}^t\text{Bu}_3\text{tacnCuOTf}_2$  was exposed to potassium superoxide ( $\text{KO}_2$ ) and 18-crown-6 (used to dissolve  $\text{KO}_2$ ) in 1,2-dimethoxyethane (DME). Unexpectedly, crystallization and x-ray diffraction of the resulting green species revealed formation of complex **12**, a trinuclear copper cluster with C-H insertion into the unactivated primary C-H bonds of a *tert*-butyl group in each of two bound ligands (Figure 18A). As this may have derived initially from a dinuclear copper(II)-superoxo, which is the one-electron oxidized form of

**3**, this method was utilized toward the one-electron reduced form of **3**. Addition of  $\text{KO}_2$  and 18-crown-6 to **2** in DME generated a black solid, which, upon filtration and dissolution in methanol, generated a red-green species (Figure 18B). However, allowing a reaction to persist led to isolation of **3**. Attempts to get a pure form of a complex resulting from the reduction of **3** instead often led to **3**, a further demonstration of the stability of the complex.

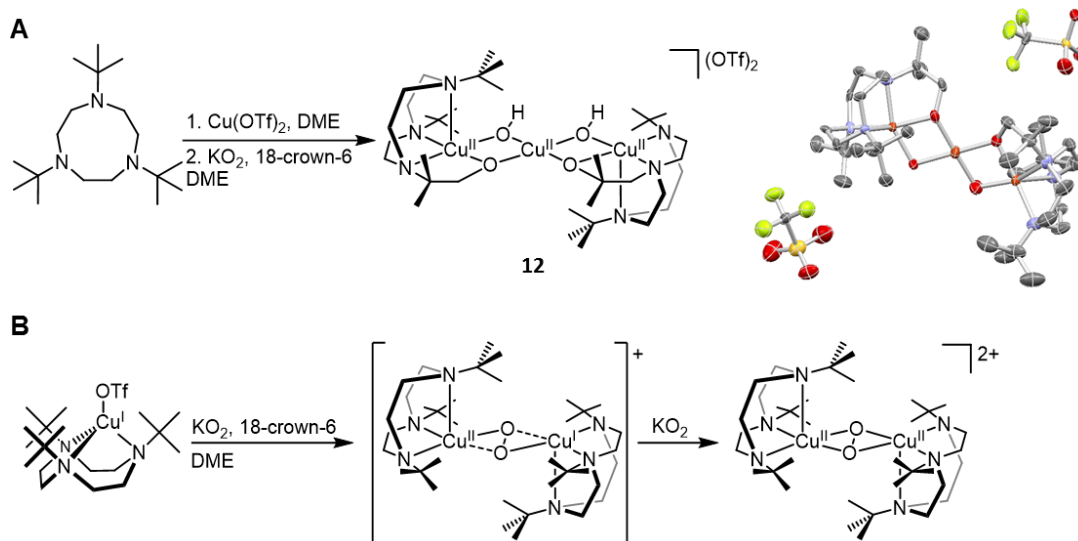


**Figure 18.** (A) Synthesis of complex **12** (left) along with crystal structure (right; hydrogen atoms omitted for clarity). (B) Attempted assembly of complex resulting from one electron reduction of **3**.

To avoid buildup of potassium superoxide, a solution of potassium superoxide in DMSO was added dropwise to a stirring solution of **2** in DMSO under inert atmosphere. With each drop, the solution transiently darkened and quickly flashed to yellow. By the end of the addition, the solution was green. In an attempt to extract the ligand, ammonium hydroxide was added to the solution; the solution immediately bubbled so vigorously that the contents erupted from the vial. The similar behavior of this solution to the solution generated via bulk electrolysis could suggest a similar nature of the species.

Future work on the electrochemistry of **3** may explain the behavior in water, as it is most biologically relevant to methane oxidation chemistry. Determination of the gas

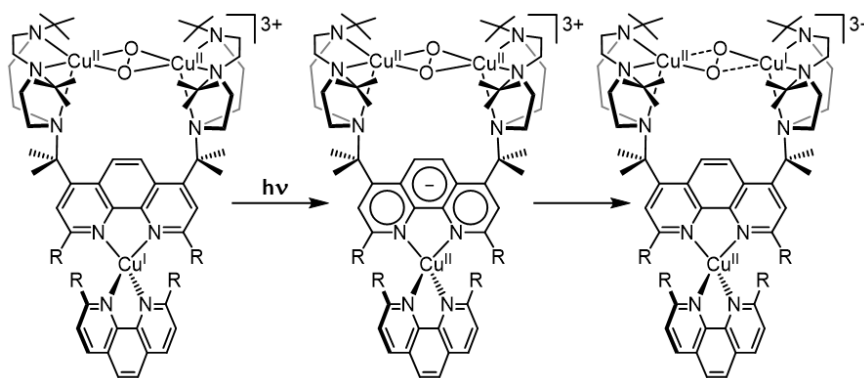
released upon water addition to a DMSO solution of the complex formed from reduction of **3** may be slowly monitored by gas uptake of a bulk electrolysis of the reduction of **3** performed in water. This process may be studied further by measurement of resonance Raman spectra during bulk electrolysis to track the stretching frequency of the O—O bond during the reduction process.

Additionally, isolation of a complex generated from single-electron reduction of **3** or another side-on peroxo dicopper complex may be a goal of future work. Unfortunately, due to reduction wave coalescence, it may be difficult to affect a single-electron reduction. At low temperature, however, the reduction events appears to be more resolvable. Furthermore, the single-electron reduced species appears to decay at room temperature. Thus, low temperature formation and isolation of a  $[\text{Cu}_2\text{O}_2]^+$  complex may be possible.

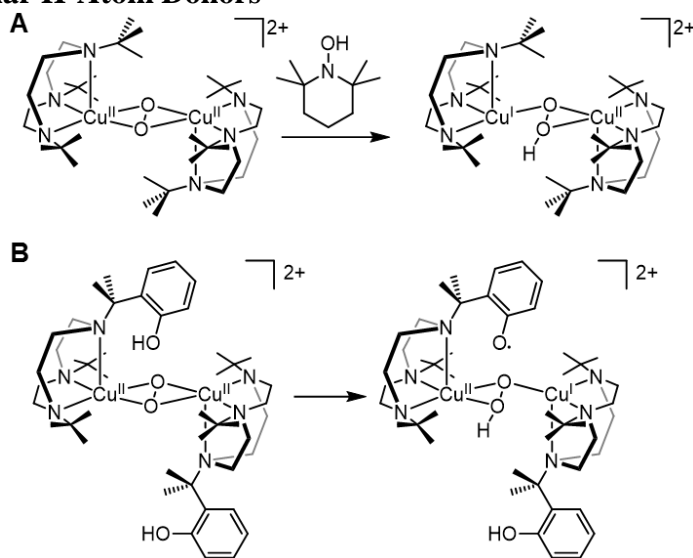
If stability of a  $[\text{Cu}_2\text{O}_2]^+$  complex derived from **3** is a problem, then transient absorption spectroscopy may help identify a species. If a tacn complex is tethered to a photoreductant with a relatively long-lived excited state, such as a bis(phenanthroline)copper(I) system,<sup>120</sup> then excitation of the photoreductant may induce intramolecular single-electron transfer to the side-on peroxo (Scheme 12). Although the species may be short-lived, transient absorption spectroscopy may be able to resolve the formation of an intermediate species. Transient absorption spectroscopy involving dicopper side-on peroxo systems is not unprecedented,<sup>121</sup> but using the technique to observe a photoreduced species has never been reported. Although not specifically an isolation of the desired  $[\text{Cu}_2\text{O}_2]^+$  species, spectroscopic observation may set the foundation for future identification of the complex, particularly in proteins such as pMMO.

Furthermore, as recent calculations suggest that the active site of pMMO may be formed not just through reduction but through H-atom transfer from a nearby tyrosine residue,<sup>57</sup> H-atom transfer to **3** to form a  $[\text{Cu}_2\text{O}_2\text{H}]^{2+}$  complex may be a useful process to investigate. The H-atom transfer agent ideally forms a stable radical species during the process. Therefore, 1-hydroxy-2,2,6,6-tetramethylpiperidine (TEMPOH) may be a good reagent for the transfer of a single H-atom to **3**, as the product, 2,2,6,6-tetramethylpiperidine N-oxide (TEMPO) is a stable radical species (Scheme 13A). Additionally, a phenolic group could be incorporated into the tacn ligand scaffold to generate a source of a single H-atom in a complex (Scheme 13B). Although the latter case may more directly probe the species generated in proteins, the phenolic oxygen may also coordinate. Regardless, spectroscopic observation and characterization of a  $[\text{Cu}_2\text{O}_2\text{H}]^{2+}$  complex may also be useful for identification of the species responsible for methane oxidation in pMMO.

### Scheme 12. Hypothetical Photophysical Generation of $[\text{Cu}_2\text{O}_2]^{+}$ Core



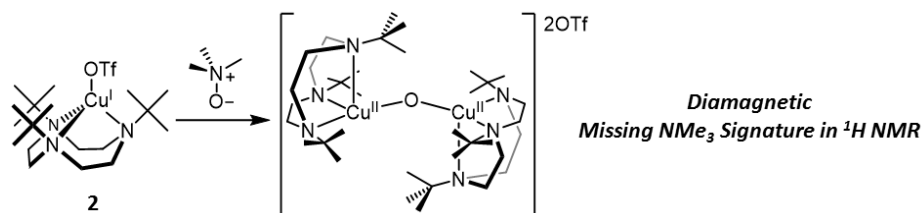
**Scheme 13. Hypothetical Formation of  $[\text{Cu}_2\text{O}_2\text{H}]^{2+}$  Through the Use of (A) Inter- and (B) Intramolecular H-Atom Donors**



On this note, it is worth addressing the possibility that the species responsible for methane oxidation in pMMO is a mono( $\mu$ -oxo), the same as in copper zeolites capable of similar methane oxidation. Therefore, isolation of this species through the use of oxidatively robust tacn derivatives, such as  $t\text{Bu}_3\text{tacn}$ , as the supporting ligands may be a target for future work. This may be accomplished through the exposure of **2** to O-atom transfer agents, such as iodosoarenes and N-oxides. Preliminary work shows that upon exposure of **2** to trimethylamine N-oxide, an orange species is formed (Scheme 14). Analysis of the orange species by  $^1\text{H}$  NMR spectroscopy in  $d_6$ -DMSO shows the formation of a diamagnetic complex, consistent either with a copper(I) species or an oxidized dinuclear copper species exhibiting antiferromagnetic coupling (Figure S20). Though adducts of copper(I) with trimethylamine N-oxide are known, the  $^1\text{H}$  NMR of the orange species does not display resonances corresponding with protons on trimethylamine N-oxide, suggesting the possible expulsion of trimethylamine. This result is consistent with O-atom transfer to a copper center, which, given the diamagnetic nature of the complex,

may suggest formation of the desired mono( $\mu$ -oxo). However, further spectroscopic work is necessary to determine the structure of the complex formed, particularly X-ray diffraction data and resonance Raman spectroscopy.

**Scheme 14. Reaction of Complex 2 with Trimethylamine N-oxide**



*C. Investigation of Steric Modularity of Tacn on Copper Dioxygen Cluster*

*Formation, Stability, and Reactivity*

The synthesis of oxidatively robust tacn ligands allows for the study of copper dioxygen complexes normally unstable under ambient conditions, as is shown by the work with **3**. The modularity of the synthesis also expedites the generation of a variety of tertiary-alkyl substituted tacn derivatives, facilitating the study of steric effects on the formation of copper dioxygen complexes supported by a three-coordinate ligand. Though the scientific literature contains reports linking steric effects to the formation of copper dioxygen complexes of this type,<sup>17</sup> the ability to carefully modify substitution patterns generating non-C<sub>3</sub>-symmetric tacn derivatives allows for a more in-depth study of controlling the coordination in copper dioxygen complexes.

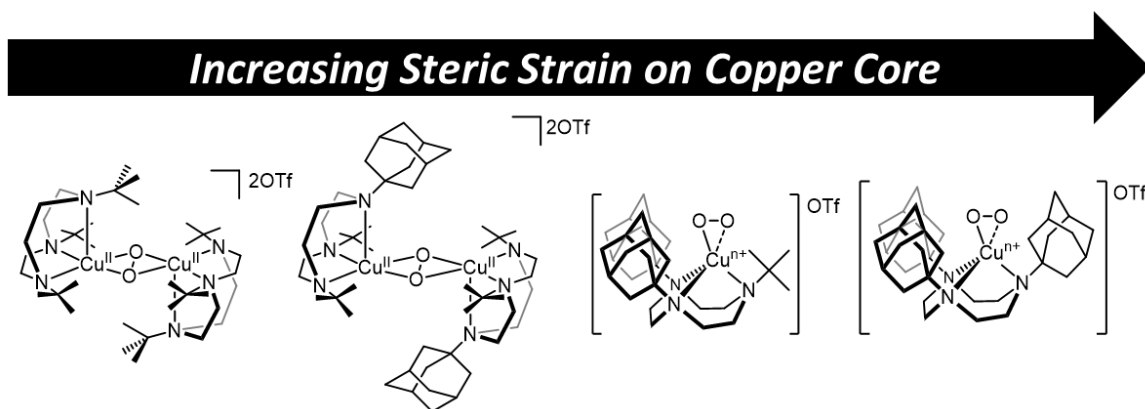


**Figure 19.** Through sequential replacement of *tert*-butyl substituents with adamantyl substituents, the strain induced by formation of a dinuclear copper dioxo complex may begin to favor the formation of mononuclear complexes.

Preliminary work focused on <sup>t</sup>Bu $\mathbf{8}_{Ad}$ , <sup>Ad</sup> $\mathbf{8}_{tBu}$ , and <sup>Ad</sup> $\mathbf{8}_{Ad}$  (Figure 19). Upon synthesis of the ligands, complexation with copper(I) trifluoromethanesulfonate benzene complex and exposure to air led to the formation of a series of complexes. The dioxo complex **13**, generated from exposure of air to a copper complex of <sup>t</sup>Bu $\mathbf{8}_{Ad}$ , displayed UV-Vis features consistent with a side-on peroxo complex (Figure 20A). The visible transitions in the UV-Vis spectrum (407 nm, 580 nm) were red-shifted compared to **3** (400 nm, 550 nm), consistent with poorer orbital overlap between copper  $d_{xy}$  orbitals and peroxo  $\pi^*$  and  $\sigma^*$  orbitals (Figure 7B). Resonance Raman spectroscopy showed a resonance at  $775.4\text{ cm}^{-1}$ , a very small shift from the O-O stretching frequency of **3** ( $773.1\text{ cm}^{-1}$ ), but still consistent with decreased backbonding of copper into the peroxo  $\sigma^*$  orbital (Figure 20A, inset). Furthermore, two additional resonances at 595 and  $918\text{ cm}^{-1}$  appeared, consistent with the presence of a possible mononuclear copper-dioxo complex.<sup>17</sup> An equilibrium of the dinuclear and mononuclear copper dioxo complexes supported by <sup>t</sup>Bu $\mathbf{8}_{Ad}$  would be consistent with the steric effects between supporting ligands imparted by incorporation of an adamantyl group (Figure 20B).

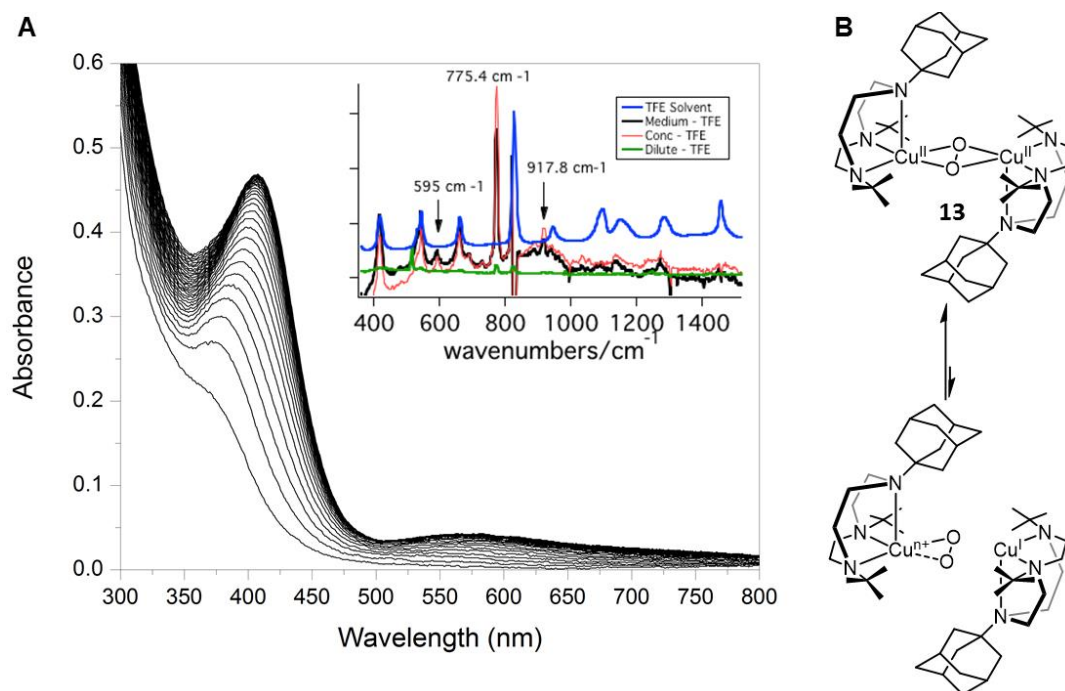


**Figure 20.** (A) UV-Vis of dioxygen uptake to a solution primarily consisting of **13**; inset resonance Raman spectrum (514.5 nm excitation) in trifluoroethanol showing formation of species indicative of a mononuclear dioxygen complex. (B) Process depicting possible dinuclear-mononuclear peroxo complex equilibrium.

The dioxygen complex generated from exposure of air to a copper complex of <sup>Ad</sup>**8**<sub>tBu</sub> displayed slightly different UV-Vis features to **3** and **13** (Figure 21A). The visible transitions in the UV-Vis were similar to a side-on peroxo complex, but the location of the peaks (400 nm and 528 nm) was shifted in the opposite direction expected for a side-on peroxo complex; addition of another adamantyl group should push the copper centers of a dinuclear side-on peroxo farther apart, leading to a general decrease in the energy of transitions with increasing copper distances. The shift back to higher energy was indicative of a mononuclear side-on peroxo complex **14**, which had been shown to possess similar, yet weaker, visible transitions to a dinuclear complex.

If the hypothesis is correct that a copper dioxygen complex supported by <sup>Ad</sup>**8**<sub>tBu</sub> generates **14**, <sup>Ad</sup>**8**<sub>tBu</sub> represents the ligand beyond the steric limit of dinuclear copper complexes, with <sup>tBu</sup>**8**<sub>Ad</sub> supporting copper complexes at the border of dinuclear and



mononuclear. The effect of the second adamantyl group toward formation of the mononuclear complex may be rationalized by the coordination geometry seen in complex **3**. Each copper in **3** possesses a square planar geometry, displaying axial elongation of one Cu—N bond. The steric strain between ligands in a dinuclear complex **13** can be partially relieved through the placement of the largest substituent, adamantyl, in the axial position. However, upon the incorporation of a second adamantyl group in the supporting ligand  $^{\text{Ad}}\mathbf{8}_{\text{tBu}}$ , a dinuclear complex is forced to position at least one adamantyl group in an equatorial position. A dinuclear complex supported by  $^{\text{Ad}}\mathbf{8}_{\text{tBu}}$  would nearly eclipse a *tert*-butyl substituent of one ligand with an adamantyl substituent of another ligand (Figure 21B). The requirement of at least one equatorial adamantyl group may represent the limit for dinuclear copper complexes.

The spectroscopic results for **3**, **13**, and **14** begin to paint a picture of the limit of dinuclear complex formation. Preliminary work with **14** suggests that it may be a mononuclear copper(II)-superoxo or copper(III)-peroxo complex. Further resonance Raman and X-ray crystallographic data may provide stronger evidence for this assignment. Resonance Raman and UV-Vis data show that **13** is the primary species in solution, but may equilibrate to a small but detectable amount mononuclear complex in solution. Resonance Raman on a solution of the copper complex of  $^{\text{tBu}}\mathbf{8}_{\text{Ad}}$  exposed to  $^{18}\text{O}_2$  may provide stronger evidence for the assignment of 595 and 918  $\text{cm}^{-1}$  frequencies to a mononuclear complex. The only detectable copper dioxygen complex supported by  $^{\text{tBu}}\mathbf{3}_{\text{tacn}}$  in solution is **3**. However, the reactivity of complex **3** may be associated with equilibrium to a small amount of another complex, such as a mononuclear complex; similar

equilibria between dinuclear complexes have been implicated in previous reactivity studies involving dinuclear side-on peroxo complexes.

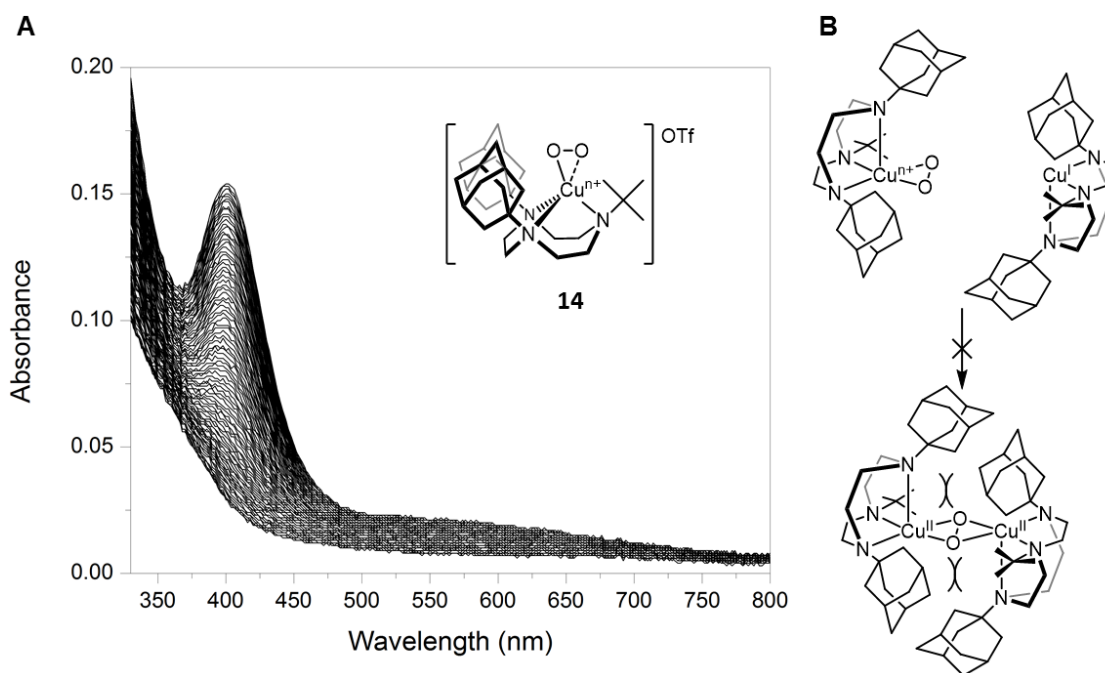


**Figure 21.** (A) UV-Vis of dioxygen uptake to a solution of what may be complex **14**. (B) Depiction of equatorial steric strain, hypothesized to be the primary reason for prevention of the formation of a dinuclear complex.

Indeed, identification of a system incapable of forming a dinuclear complex (**14**) and a complex generating a small but noticeable amount of mononuclear complex in solution (**13**) may provide an ideal system for addressing the reactivity observed with **3**. Complex **14** can be screened for reactivity against the same substrates used for **3**. If **14** is capable of the same reactivity, then the reactivity of **3** may be associated with an equilibrium to this species. The reactivity of **13** can be compared to that of **14** and **3**. If slower kinetics compared to **14** is shown at equivalent starting copper concentrations, this may add evidence to a hypothesis that some amount of **3** is equilibrating to a mononuclear dioxygen adduct in solution. Furthermore, it may be possible to favor the mononuclear complex derived from **13** by heating a solution of the complex. If the reactivity is more in

line with that of **14** at the same elevated temperature, then reactivity can likely be attributed to a mononuclear complex. This may help unravel the reaction mechanism of **3** toward a variety of substrates.

Intriguingly, the trend established with copper dioxygen complexes supported by <sup>t</sup>Bu<sub>3</sub>tacn (<sup>t</sup>Bu**8**<sub>tBu</sub>), <sup>t</sup>Bu**8**<sub>Ad</sub>, and <sup>Ad</sup>**8**<sub>tBu</sub>, became complicated when moving to <sup>Ad</sup>**8**<sub>Ad</sub>. Exposure of a copper complex of <sup>Ad</sup>**8**<sub>Ad</sub> rapidly generated a green species, completely lacking the buildup of a complex with a mid-visible charge-transfer feature (Figure 22). Attempts to crystallize the green species led to the formation of two different complexes. One species, a light brown, crystalline solid, was revealed by x-ray diffraction to be a copper(I)-copper(II) mixed valence carbonate complex **15** (Figure 23A); a carbonate complex had previously been shown to form from Cu(II) hydroxide complexes.<sup>91</sup> Another species, a blue-green crystal, was also generated, with data from x-ray diffraction revealing a trinuclear copper cluster **16** as a product of O-atom insertion into adamantyl C—H bonds (Figure 23B). Additionally, attempts to dissolve the green species in chloroform immediately led to formation of a yellow decomposition complex, and dissolution in THF led to a purple solution. The complex initially generated clearly lacked the stability afforded to previous tacn derivatives bearing tertiary alkyl substituents, and likely required low temperature work to identify the initial copper peroxo adduct formed upon reaction with dioxygen.

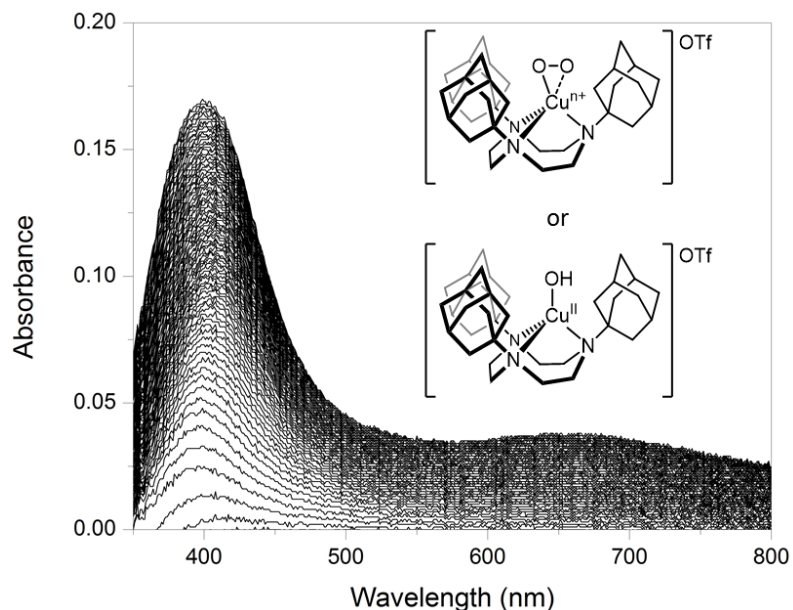


**Figure 22.** UV-Vis spectrum of dioxxygen uptake of a copper(I) complex supported by  $^{\text{Ad}}\mathbf{8}_{\text{Ad}}$ . Potential structures associated with the UV-Vis features are featured.

It is worth noting that a colleague's work on cyclization of  $^{\text{tBu}}\mathbf{6}$  around ammonia<sup>B</sup> allows the similar procedure for the synthesis of  $^{\text{Ad}}\mathbf{8}_{\text{H}}$ . Complexation using copper(I) trifluoromethanesulfonate benzene complex leads to the formation of a green species. X-ray crystallography data of green crystals from this solution indicate the formation of a mononuclear copper complex **17**, with O-atom insertion into an adamantyl C—H bond (Figure 24). Though **17** presumably derives from a copper dioxxygen adduct, the fate of the remaining oxygen has yet to be identified. This mononuclear complex suggests that the two adamantyl groups are sufficient for formation of a mononuclear complex, as a colleague's work with a copper complex supported by  $^{\text{tBu}}\mathbf{8}_{\text{H}}$  shows a similar complex as a dicopper dimer.<sup>C</sup> This result is also consistent with the hypothesis that an equatorial adamantyl group on copper cannot be tolerated in a dinuclear copper complex.

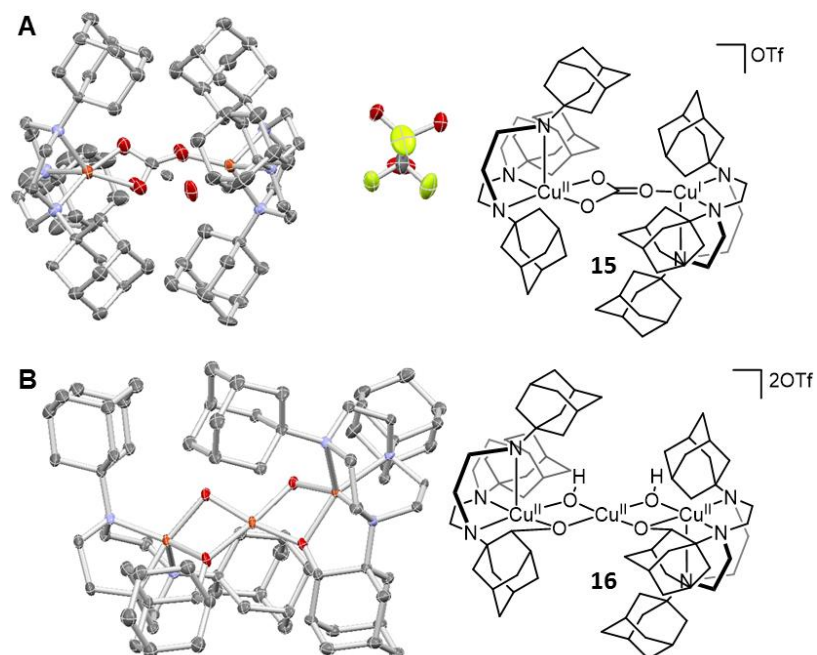


**Figure 23.** Crystal and skeletal structures of (A) **15** and (B) **16**, products of dioxygen uptake of a copper complex supported by  $\text{Ad}_8\text{Ad}$ .

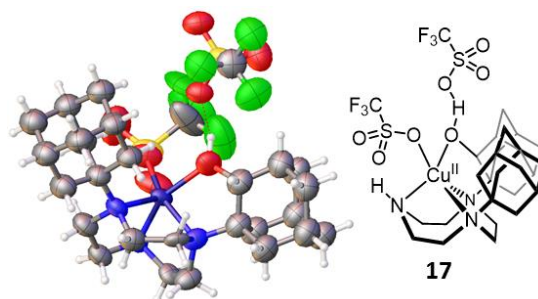


**Figure 24.** Crystal and skeletal structure of complex **17**.

#### *D. Stabilization of Mononuclear Copper Nitrene*

As  $\text{tBu}_3\text{tacn}$  is an oxidatively robust, bulky ancillary ligand, it may be a good ligand to support another, highly active copper complex: a copper nitrene. A copper nitrene is a predicted mononuclear copper species generated from the reaction of copper(I) with a nitrene source, such as an alkyl azide, chloramine, or iminoiodinane.<sup>122</sup> The predicted structure can be described with resonance structures between a copper(II) bound to a nitrogen radical and a copper(III) bound to a nitrogen anion (Figure 25A). The mixture of

copper(I) complexes with nitrene sources is often not only capable of alkene aziridination, but the system is commonly used to perform C—H functionalization of alkanes as robust as cyclohexane.<sup>122</sup> Although dinuclear copper complexes supporting electron-deficient alkyl amines are known, the unambiguous identification of the active mononuclear complex by x-ray crystallography remains elusive. Only one report describes the potential spectroscopic observation of a mononuclear “copper nitrene” complex (Figure 25B) at  $-90$  °C in DCM by UV-Vis, x-ray absorption spectroscopy (XAS), and resonance Raman spectroscopy.<sup>122</sup> Furthermore, an unassigned  $^1\text{H}$  NMR of the complex at low temperature shows a variety of resonances consistent with a diamagnetic species. Though the evidence supporting the formation of this copper nitrene species is far from providing an absolute structural assignment, the data are suggestive of the formation of a diamagnetic copper nitrene species. The supporting ligand in this study is a triamine, similar to  $^t\text{Bu}_3\text{tacn}$ , but with nitrogen atoms bearing methyl groups instead of more robust *tert*-butyl groups. Use of  $^t\text{Bu}_3\text{tacn}$  to form a nitrene complex **R18** (Figure 25C) may help avoid decomposition of a copper nitrene by preventing easy access of the reactive electrophilic nitrogen to vulnerable solvent molecules (Figure 25D).

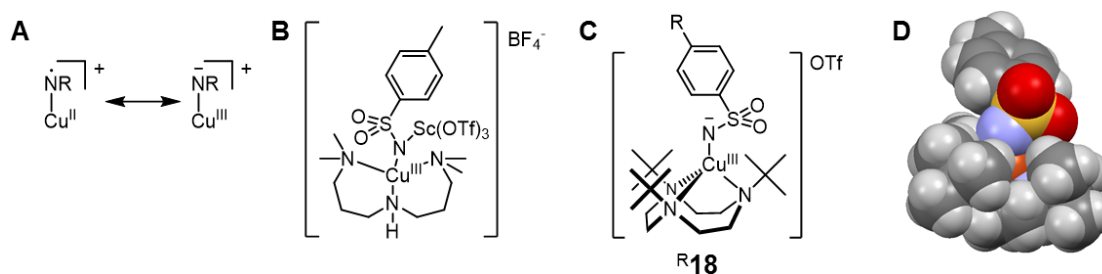


**Figure 25.** (A) A copper nitrene adduct described through resonance structures. (B) Proposed structure of previously reported copper nitrene adduct. (C) Synthetic copper nitrene target (R =  $\text{CH}_3$  (Me) or H). (D) Spacefilling model depicting steric protection of potential copper nitrene adduct from intermolecular reactivity (formed from the crystal structure of  $^{\text{Me}}\mathbf{19}$ ).

Therefore, in an attempt to generate the desired complex **18**, **2** was exposed to nitrene sources. Although no reaction was observed with *tert*-butyl azide, reactions with chloramine T-hydrate (Scheme 15A), [N-(*p*-toluenesulfonyl)imino]phenyliodinane (PhINTs) (Scheme 15A), and [N-(benzenesulfonyl)imino](2-*tert*-butylsulfonyl)phenyliodinane (**20**) (Scheme 15B) led to the formation of a red solution in DCM. At room temperature, the red color was formed and persisted for hours. UV-Vis of the species generated (487 nm and 811 nm from the use of chloramine-T hydrate; 488 nm and 800 nm from the use of PhINTs; 467 nm and 790 nm from the use of **20**) appeared to be similar to the species previously hypothesized as a copper nitrene adduct at low temperatures, with absorption maxima at 530 nm ( $3500 \text{ M}^{-1} \text{ cm}^{-1}$ ) and 750 nm ( $580 \text{ M}^{-1} \text{ cm}^{-1}$ ). Indeed, the immediate decomposition product of a copper nitrene via H-atom abstraction, a copper(II) amido, was found in a previous report to be a green species lacking a charge-transfer transition in the visible region of its UV-Vis spectrum.<sup>122</sup> As a fit for the decomposition could not be established, a quantitative half-life for the complex in solution was not found; however, the nitrene species formed from **20** qualitatively seemed to persist longest (Figure 26).

Crystallization of a solution from the reaction of **2** with PhINTs in DCM at room temperature (Figure 27A) provided x-ray crystal data showing a copper complex of *t*-Bu<sub>3</sub>tacn bound to a tosylated nitrogen, **Me19**, as a hydrogen bond dimer (Figure 27B). Preliminary EPR spectroscopy on the red species in DCM displayed a paramagnetic copper(II) spectrum (Figure 27A, inset), consistent with **Me19**. However, the amount of paramagnetic species was not quantified and decomposition was not followed against an

EPR internal standard, making it unclear whether the signal derived from decomposition to or from <sup>Me</sup>19.

### Scheme 15. Synthesis and Decomposition of Copper Nitrene Adducts

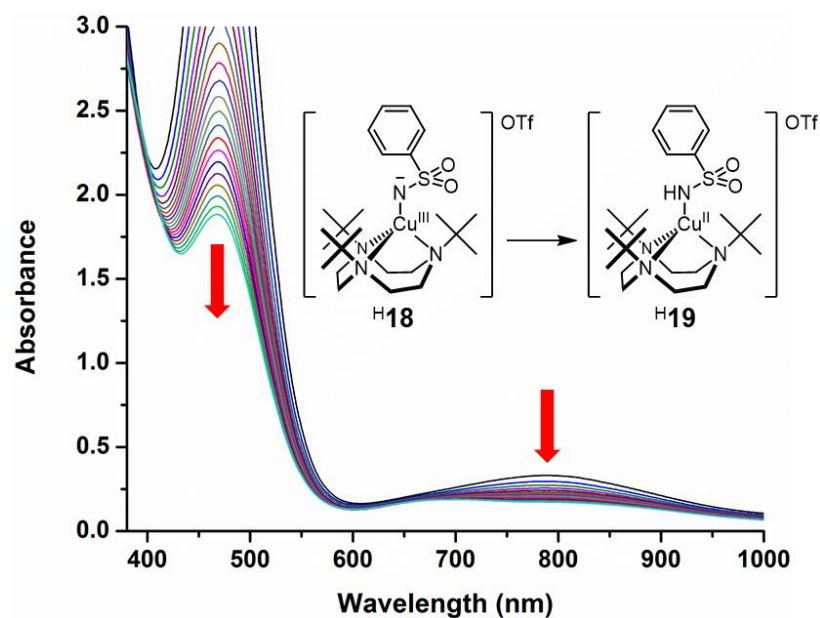
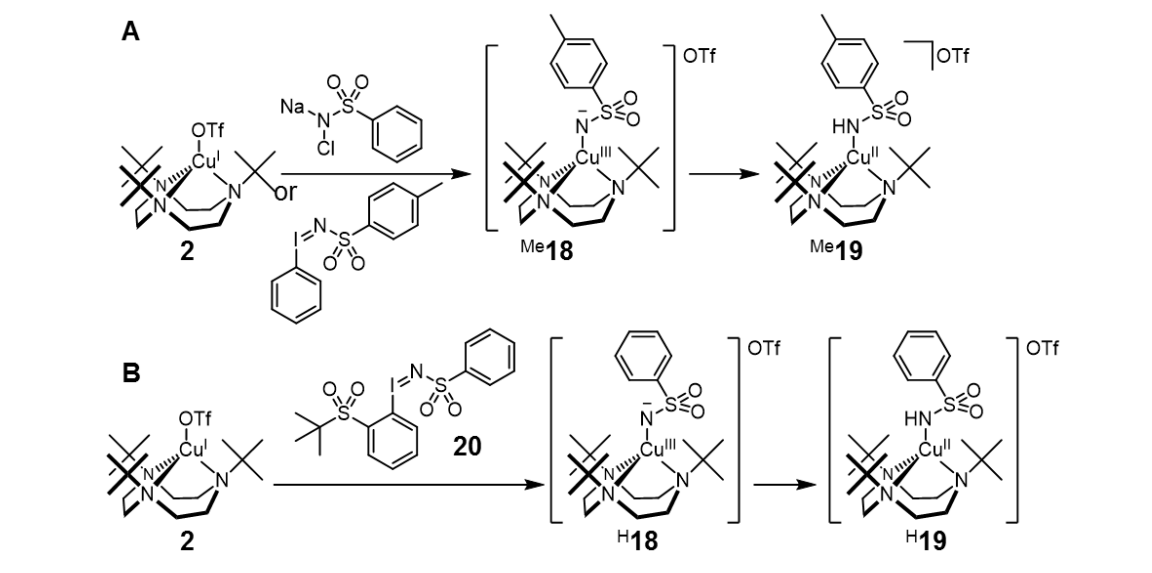


**Figure 26.** UV-Vis spectra of a species formed from **2** and **20**, potentially showing a decomposition from <sup>H</sup>18 to <sup>H</sup>19. UV-Vis spectra were taken hourly; the red arrows indicate the decay of peak intensity over time.

As <sup>tBu</sup>8<sub>H</sub> was synthesized by a colleague,<sup>B</sup> a copper species supported by this ligand,

**21**, was reacted with **20**. As expected, the solution decayed much more rapidly, flashing a



pale orange before rapidly changing to a bright yellow. It is thus hypothesized that the charge transfer responsible for a red-orange color corresponds to a “copper nitrene” species when supported by tacn. As the previous spectroscopic observation of a copper nitrene species was performed in the presence of scandium(III) trifluoromethanesulfonate ( $\text{Sc}(\text{OTf})_3$ ), complexes **2** and **21** were each reacted with **20** in the presence of  $\text{Sc}(\text{OTf})_3$ . Unfortunately, the red species formed from **2** decomposed more rapidly to orange and then yellow, while **21** decomposed directly to a yellow solution.

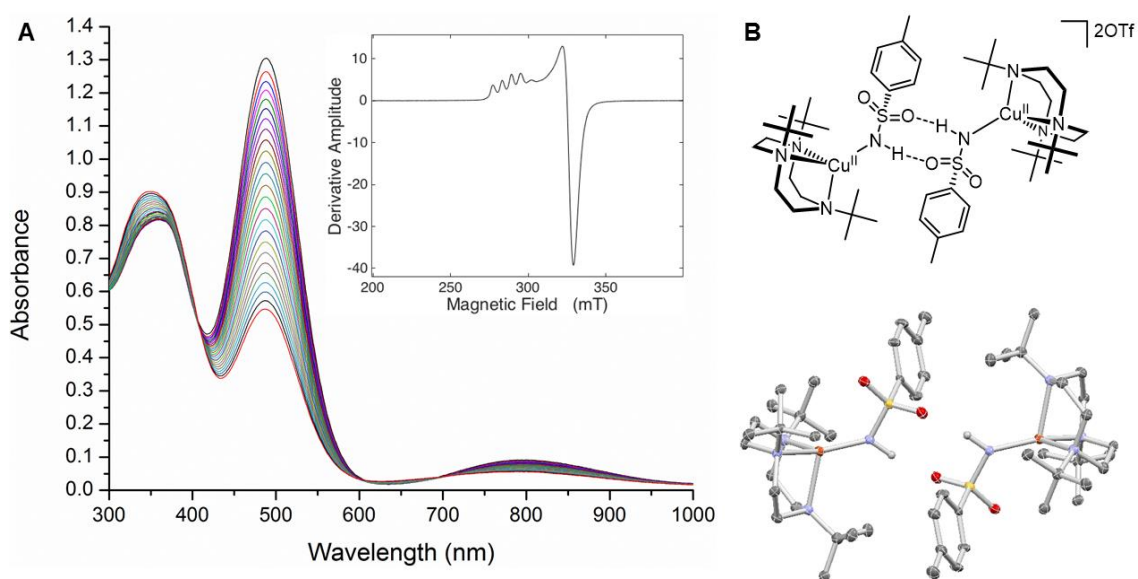
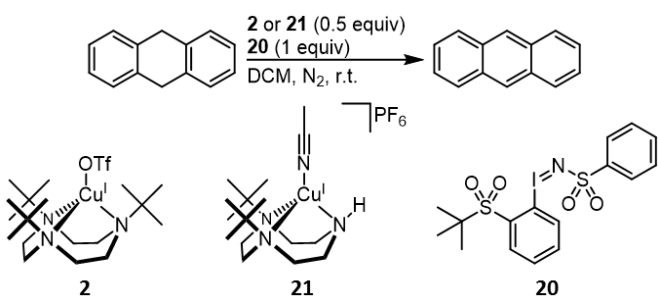


**Figure 27.** (A) UV-Vis spectrum of decomposition of red species in DCM formed from reaction of **2** with PhINTs (spectra taken every 30 minutes for 12 hours), with an EPR inset of a similarly prepared solution indicating the presence of a paramagnetic species in solution. (B) Crystal and skeletal structures of  $\text{Me}^{19}$  as a hydrogen-bond dimer.

Given the stability of the species in solution, the reactivity of dihydroanthracene was tested with potential copper nitrene species (Figures S32-S37). In each case, the substrate reactivity was tested in solution with **20** with or without  $\text{Sc}(\text{OTf})_3$ , in the presence of **2**, **21**, or no copper complex. The results of the reactivity are shown in Table 8. In all cases, conversion to anthracene was substoichiometric. The presence of  $\text{Sc}(\text{OTf})_3$  with **2** and **21** led to a decreased yield of anthracene. There was also a small amount (3%) of

background conversion to anthracene when  $\text{Sc}(\text{OTf})_3$  was present. The less reactive nature of **2** was consistent with poor accessibility of substrate to the active copper complex, as the *tert*-butyl substituents could hinder substrate. In contrast, the opening provided by one unsubstituted amine in **21** likely provided access to the active copper complex. However, the results of mixing **21** and **20** in the absence of substrate suggested the possibility that the product of nitrene decomposition, a copper(II) amido, could instead be the active oxidant toward the formation of anthracene.

**Table 8. Dihydroanthracene Reactivity with Copper and Nitrene Source**



Copper Source	Additive	Yield (%)*
<b>2</b>	-	30%
<b>2</b>	$\text{Sc}(\text{OTf})_3$	3%
<b>21</b>	-	40%
<b>21</b>	$\text{Sc}(\text{OTf})_3$	29%
-	-	0%
-	$\text{Sc}(\text{OTf})_3$	3%

\*Yield by  $^1\text{H}$  NMR based on 1,3,5-tri-*tert*-butylbenzene internal standard.

Clearly there is much work left to establish whether **2** forms **R18** at room temperature. Independent synthesis of **R19** from a copper(II) complex of  $t\text{Bu}_3\text{tacn}$  and comparison of the UV-Vis data would be helpful to compare UV-Vis signatures.

Furthermore, comparison of the reactivity of authentic <sup>H</sup>**19** to mixtures of **2** with **20** may help identify which species is truly performing the oxidation of dihydroanthracene; the oxidation of substrates by a copper(II) amido is not unprecedented.<sup>123</sup> If the results of future work rule out <sup>R</sup>**19** as the identity of the species responsible for the visible charge transfer, then collaboration to perform XAS on a solution of **2** and **20** may identify <sup>H</sup>**18** if it is truly present in solution through the location of the rising edge of a copper(III) species.

## V. Supporting Information

### A. General Considerations

All reactions were performed under a nitrogen atmosphere using Schlenk technique unless otherwise specified. All glove box manipulations were performed using a UNI-LAB MBRAUN glove box. The solvents  $\text{CH}_2\text{Cl}_2$  and  $\text{Et}_2\text{O}$  used in reactions were obtained from a solvent purification system (MB-SPS MBRAUN). All other solvents were obtained from commercial sources and used as received. Tetrakis(acetonitrile)copper(I) was purchased from Strem Chemicals and used as received. Copper(I) trifluoromethanesulfonate benzene complex (technical grade, 90%, Sigma Aldrich) required purification as follows: In a glove box, the crude solid was heated in benzene for 30 minutes at 75-80°C. The resulting solution was then filtered hot over celite, and the solvent removed *in vacuo* to obtain a white air/solvent sensitive powder. Purification was performed immediately prior to usage for best results. N,N'-di-tert-butylethylenediamine (TCI America) was stored in a Strauss flask under  $\text{N}_2$  to avoid decomposition. N,N'-diisopropylethylenediamine (Alfa Aesar) was kept in a glove box to avoid decomposition. All other chemicals and solvents were obtained from commercial sources and used as received.

### B. Experimental Procedures

**Complex Syntheses.** [ $t\text{Bu}_3\text{tacn}\text{Cu}^{\text{I}}(\text{MeCN})$ ][ $\text{PF}_6$ ] (**1**). The following procedure is modified from the original report. In a round-bottom flask equipped with a stir bar, tetrakis(acetonitrile)copper(I) hexafluorophosphate (1.24 g, 3.33 mmol, 1 equiv) and  $t\text{Bu}_3\text{tacn}$  (1.02 g, 3.43 mmol, 1.03 equiv) were dissolved/suspended in acetonitrile. The reaction mixture was stirred for 30 min, at which time the solution appeared to be clear and colorless. The reaction mixture was filtered over Celite through a glass-sintered frit. The solvent was removed to yield 1.74 g (3.17 mmol, 95% yield) of pure copper complex as a white solid. The characteristics of the  $^1\text{H}$  NMR and IR spectra matched spectroscopic values reported previously for this compound.<sup>74</sup>

$t\text{Bu}_3\text{tacn}\text{Cu}^{\text{I}}(\text{OTf})$  (**2**). In a glovebox, copper(I) trifluoromethanesulfonate benzene complex (0.1218 g, 0.242 mmol, 1 equiv) and  $t\text{Bu}_3\text{tacn}$  (0.144 g, 0.484, 2 equiv) were added to a 20 mL glass vial with a stir bar. Benzene (10 mL) was added to the vial, which was then capped, and the solution was stirred for 1 h. The solvent was removed in vacuo to yield the product as an off-white powder (0.2288 g, 0.449 mmol, 92%). Note that **1** is very reactive to trace acetonitrile in the glovebox atmosphere, forming [ $t\text{Bu}_3\text{tacn}\text{Cu}^{\text{I}}(\text{MeCN})$ ][ $\text{OTf}$ ] (**1**), and was accordingly handled in only an acetonitrile-free glovebox:  $^1\text{H}$  NMR (400 MHz,  $\text{C}_6\text{D}_6$ )  $\delta$  2.43–2.26 (6H, m), 1.59–1.41 (6H, m), 1.10 (27H, s); IR (KBr) 3019, 2976, 2911, 2844, 1638, 1497, 1480, 1449, 1402, 1368, 1265 (br, sh), 1226, 1195, 1165, 1150, 1097, 1033, 935, 892, 845, 804, 759, 726, 690, 638, 571, 518, 474  $\text{cm}^{-1}$ .

$[(t\text{Bu}_3\text{tacn}\text{Cu}^{\text{I}})_2(\mu\text{-}\eta^2\text{:}\eta^2\text{-O}_2)]\text{[OTf]}_2$  (**3**). A vial containing **2** (0.2288 g, 0.449 mmol) was removed from the glovebox. DCM (10 mL) was added to the vial exposed to air, causing

the resulting solution to immediately flush dark brown. The vial was left open to the air overnight for slow evaporation. The resulting crystals were washed with chloroform to yield the product as dark brown crystals (0.1996 g, 0.423 mmol, 84%):  $^1\text{H NMR}$  (400 MHz,  $\text{CD}_3\text{OD}$ )  $\delta$  3.31–3.20 (12H, m), 2.68–2.54 (12H, m), 1.85–1.10 (54H, br s); positive-mode NSI-MS  $m/z$  (relative intensity, formula, ppm) 360.24400 {39.40%, [ $^t\text{Bu}_3\text{tacn}$ ] $\text{Cu}$ } $^+$  ( $\text{C}_{18}\text{H}_{39}^{63}\text{CuN}_3^+$ ),  $\Delta = 1.5$  ppm}, 362.24231 {18.09%, [ $^t\text{Bu}_3\text{tacn}$ ] $\text{Cu}$ } $^+$  ( $\text{C}_{18}\text{H}_{39}^{65}\text{CuN}_3^+$ ),  $\Delta = 1.8$  ppm}, 752.47890 {97.51%, [ $^t\text{Bu}_3\text{tacn}$ ] $_2\text{Cu}_2\text{O}_2$ } $^+$  ( $\text{C}_{36}\text{H}_{78}^{63}\text{Cu}_2\text{N}_6\text{O}_2^+$ ),  $\Delta = 1.5$  ppm}, 754.47673 {100.00%, [ $^t\text{Bu}_3\text{tacn}$ ] $_2\text{Cu}_2\text{O}_2$ } $^+$  ( $\text{C}_{36}\text{H}_{78}^{65}\text{Cu}_2\text{N}_6\text{O}_2^+$ ),  $\Delta = 1.7$  ppm}, 756.47494 {21.35%, [ $^t\text{Bu}_3\text{tacn}$ ] $_2\text{Cu}_2\text{O}_2$ } $^+$  ( $\text{C}_{36}\text{H}_{78}^{65}\text{Cu}_2\text{N}_6\text{O}_2^+$ ),  $\Delta = 1.0$  ppm}, 869.44213 {37.84%, [ $^t\text{Bu}_3\text{tacn}$ ] $_2\text{Cu}_2(\text{OTf})$ } $^+$  ( $\text{C}_{37}\text{H}_{78}^{63}\text{Cu}_2\text{F}_3\text{N}_6\text{O}_3\text{S}^+$ ),  $\Delta = 3.1$  ppm}, 871.43957 {37.02%, [ $^t\text{Bu}_3\text{tacn}$ ] $_2\text{Cu}_2(\text{OTf})$ } $^+$  ( $\text{C}_{37}\text{H}_{78}^{65}\text{Cu}_2\text{F}_3\text{N}_6\text{O}_3\text{S}^+$ ),  $\Delta = 2.2$  ppm}, 873.43693 {7.95%, [ $^t\text{Bu}_3\text{tacn}$ ] $_2\text{Cu}_2(\text{OTf})$ } $^+$  ( $\text{C}_{37}\text{H}_{78}^{65}\text{Cu}_2\text{F}_3\text{N}_6\text{O}_3\text{S}^+$ ),  $\Delta = 1.2$ }; negative-mode NSI-MS  $m/z$  (relative intensity, formula, ppm) 658.15131 {100.00%, [ $^t\text{Bu}_3\text{tacn}$ ] $\text{Cu}(\text{OTf})_2$ } $^-$  ( $\text{C}_{20}\text{H}_{39}^{63}\text{CuF}_6\text{N}_3\text{O}_6\text{S}_2^-$ ),  $\Delta = 4.1$  ppm}, 660.14991 {47.21%, [ $^t\text{Bu}_3\text{tacn}$ ] $\text{Cu}(\text{OTf})_2$ } $^-$  ( $\text{C}_{20}\text{H}_{78}^{65}\text{CuF}_6\text{N}_3\text{O}_6\text{S}_2^-$ ),  $\Delta = 4.7$  ppm}. Elemental Anal. Calcd for  $\text{C}_{38}\text{H}_{78}\text{Cu}_2\text{F}_6\text{N}_6\text{O}_8\text{S}_2$ : C, 43.37; H, 7.47; N, 7.99; F, 10.83. Found: C, 43.39; H, 7.33; N, 7.89; F, 11.02.

Note: Copper metallations involving  $^t\text{Bu}\mathbf{8}_{\text{Ad}}$ ,  $^{\text{Ad}}\mathbf{8}_{\text{tBu}}$ , and  $^{\text{Ad}}\mathbf{8}_{\text{Ad}}$  were performed following methods utilized for  $^t\text{Bu}_3\text{tacn}$  complexes. As the results were preliminary, characterization of pure copper(I) complexes have not yet been gathered.

**Aerobic Oxidations with Complex 3.** *Oxidation of Benzoin.* With 20 mol % catalyst loading, the procedure is as follows. In a 20 mL glass vial with a stir bar, benzoin (0.02116 g, 99.7  $\mu\text{mol}$ , 1 equiv) and complex **3** (0.02089 g, 19.9  $\mu\text{mol}$ , 19.9 mol %) were dissolved in  $d_4$ -methanol (3 mL). Mesitylene (0.01406 g, 117  $\mu\text{mol}$ , 1.2 equiv) was then added as an

internal standard. The vial was sealed with an inverted septum and fitted with an O<sub>2</sub> balloon. The reaction mixture was stirred at room temperature and monitored by <sup>1</sup>H NMR spectroscopy until the reaction was complete.

With 20 mol % catalyst loading at 50 °C, the procedure is as follows. In a 20 mL glass vial with a stir bar, benzoin (0.02012 g, 94.7 μmol, 1 equiv) and complex **3** (0.02036 g, 19.3 μmol, 20.4 mol %) were dissolved in *d*<sub>4</sub>-methanol (3 mL). Then, 1,3,5-trimethoxybenzene (0.00831 g, 49.4 μmol, 0.52 equiv) was added as an internal standard. The vial was sealed with an inverted septum and fitted with an O<sub>2</sub> balloon. The reaction mixture was stirred at room temperature and monitored by <sup>1</sup>H NMR spectroscopy until the reaction was complete.

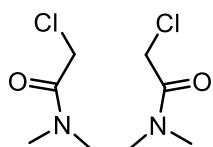
With 5 mol % catalyst loading, the procedure is as follows. In a 20 mL glass vial with a stir bar, benzoin (0.02145 g, 101 μmol, 1 equiv) and complex **3** (0.00512 g, 4.87 μmol, 4.8 mol %) were dissolved in *d*<sub>4</sub>-methanol. Then, 1,3,5-trimethoxybenzene (0.00587 g, 34.9 μmol, 0.35 equiv) was added as an internal standard. The vial was sealed with an inverted septum. The reaction mixture was stirred at 50 °C open to air and monitored by <sup>1</sup>H NMR until the reaction was complete.

*Oxidation of 2,4-Di-tert-butylphenol.* In a 20 mL glass vial, 2,4-di-*tert*-butylphenol (0.04134 g, 200 μmol, 1 equiv) and 1,3,5-trimethoxybenzene (0.00557 g, 33.1 μmol, 0.17 equiv) were dissolved in *d*<sub>4</sub>-methanol (8 mL) to make a stock solution. Then complex **3** [0.00497 g (room temperature), 4.72 μmol, 18.9 mol %; 0.00531 g (50 °C), 5.07 μmol, 20.1 mol %; 0.00567 g (65 °C), 5.39 μmol, 21.5 mol %] was added to an NMR tube. To each tube with complex **3** was added 1.0 mL of the stock solution. The tubes were capped, fitted with an O<sub>2</sub> balloon, and heated to their respective temperatures. The reactions were monitored by <sup>1</sup>H NMR spectroscopy until they were complete.

*Oxidation of 3,5-Di-tert-butylcatechol.* In a 20 mL glass vial, 3,5-di-*tert*-butylcatechol (0.04100 g, 184  $\mu\text{mol}$ , 1 equiv) and 1,3,5-tri-*tert*-butylbenzene (0.01262 g, 51.2  $\mu\text{mol}$ , 0.28 equiv) were dissolved in *d*<sub>4</sub>-methanol (8 mL) to make a stock solution. Then complex **3** [0.00512 g (room temperature), 4.87  $\mu\text{mol}$ , 21.1 mol %; 0.00560 g (50 °C), 5.32  $\mu\text{mol}$ , 23 mol %; 0.00450 g (65 °C), 4.28  $\mu\text{mol}$ , 18.6 mol %] was added to an NMR tube. To each tube with complex **3** was added 1.0 mL of the stock solution. The tubes were capped, fitted with an O<sub>2</sub> balloon, and heated to their respective temperatures. The reactions were monitored by <sup>1</sup>H NMR spectroscopy until they were complete.

*Oxidation of Benzyl Alcohol.* In a 100 mL volumetric flask, benzyl alcohol (0.01146 g, 106  $\mu\text{mol}$ , 1 equiv) and 1,3,5-tri-*tert*-butylbenzene (0.00726 g, 29.5  $\mu\text{mol}$ , 0.28 equiv) were dissolved in methanol to a volume of 100 mL as a stock solution. To 25 mL three-necked flasks equipped with stir bars and reflux condensers was added complex **3** [0.01028 g (room temperature), 9.77  $\mu\text{mol}$ , 0.92 equiv; 0.01098 g (50 °C), 10.4  $\mu\text{mol}$ , 0.98 equiv; 0.01036 g (65 °C), 9.84  $\mu\text{mol}$ , 0.93 equiv]. To each flask with complex **3** was added 10 mL of the stock solution. Each reaction mixture was fitted with an O<sub>2</sub> balloon atop the condenser, and the reaction mixtures were stirred and heated to their respective temperatures. The reactions were monitored by gas chromatography.

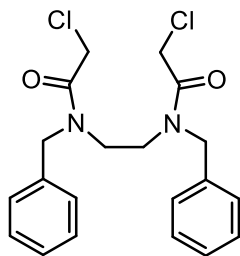
### Synthesis of Triazacyclononanes



*N,N'*-(ethane-1,2-diyl)bis(2-chloro-*N*-methylacetamide) (*Me***6**). To an oven-dried, N<sub>2</sub>-purged round bottom flask equipped with a stir bar, DCM (75 mL) was added. Then, chloroacetyl chloride (9.3 mL, 116 mmol, 3.0 equiv) was added, and the



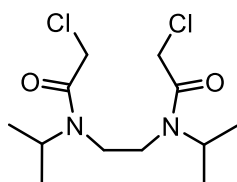
flask was cooled in an ice bath with stirring for 15 minutes. By syringe pump over 20 minutes, N,N'-dimethylethylenediamine (5.0 mL, 47 mmol, 1.0 equiv) was added. The flask was then allowed to warm to room temperature and stirred overnight. To a beaker filled with ice and saturated aqueous potassium carbonate, the reaction was added, washing the flask with DCM into the beaker. The biphasic mixture was stirred about 30 minutes. The contents of the beaker were poured into a separatory funnel. The DCM phase was collected, and the aqueous phase was washed once more with DCM. The combined DCM extracts were washed once with saturated aqueous potassium carbonate and once with brine. The organic phase was collected, dried with anhydrous MgSO<sub>4</sub>, and filtered. The filtrate was concentrated *in vacuo* to obtain the crude as a white powder. The crude material is crystallized in DCM/pentane to obtain the product as a colorless crystalline solid (6.88g, 72% yield). Main Form: <sup>1</sup>H NMR (CDCl<sub>3</sub>) δ 3.99 (s, 4 H), 3.54 (s, 4 H), 3.05 (s, 6 H); <sup>13</sup>C NMR (CDCl<sub>3</sub>) δ 167.17, 45.26, 41.54, 36.07; Asymmetric Form: <sup>1</sup>H NMR (CDCl<sub>3</sub>) δ 4.08 (s, 2 H), 4.04 (s, 2 H), 3.49 (s, 4 H), 3.08 (s, 3 H), 2.95 (s, 3 H); Asymmetric Form: <sup>13</sup>C NMR (CDCl<sub>3</sub>) δ 47.70, 47.25, 41.24, 40.82, 37.37, 34.29 (Note: carbonyl peak not detected, likely due to concentration of minor asymmetric form). Positive Mode NSI-MS m/z (relative intensity, formula, ppm) 241.05064 (0.59%, C<sub>8</sub>H<sub>15</sub>Cl<sub>2</sub>N<sub>2</sub>O<sub>2</sub><sup>+</sup> ([M+H]<sup>+</sup>), Δ = 0.54).



*N,N'*-(ethane-1,2-diyl)bis(*N*-benzyl-2-chloroacetamide) (*Bn*6). To an

oven-dried, N<sub>2</sub>-purged round bottom flask equipped with a stir bar, DCM (135 mL) was added. Then, chloroacetyl chloride (20.3 mL, 255 mmol, 3.0 equiv) was added, and the flask was cooled in an ice bath with stirring for 15 minutes. By syringe pump over 20 minutes, *N,N'*-dibenzylethylenediamine (20 mL, 85 mmol, 1.0 equiv) was added. The flask was then allowed to warm to room temperature and stirred overnight. To a beaker filled with ice and saturated aqueous potassium carbonate, the reaction was added, washing the flask with DCM into the beaker. The biphasic mixture was stirred about 30 minutes. The contents of the beaker were poured into a separatory funnel. The DCM phase was collected, and the aqueous phase was washed once more with DCM. The combined DCM extracts were washed once with saturated aqueous potassium carbonate and once with brine. The organic phase was collected, dried with anhydrous MgSO<sub>4</sub>, and filtered. The filtrate was concentrated *in vacuo* to obtain the crude as a white powder. The crude material is crystallized in DCM/pentane to obtain the product as a colorless crystalline solid (21.96g, 66% yield). Main Form: <sup>1</sup>H NMR (CDCl<sub>3</sub>) δ 4.66 (s, 4 H), 4.06 (s, 4 H), 3.61 (s, 4 H). Asymmetric Form: <sup>1</sup>H NMR (CDCl<sub>3</sub>) δ 4.49 (s, 4 H), 4.13 (s, 2 H), 4.11 (s, 2 H), 3.39-3.33 (m, 2 H), 3.33-3.26 (m, 2 H). Minor Symmetric Form: <sup>1</sup>H NMR (CDCl<sub>3</sub>) δ 4.56 (s, 4 H), 3.96 (s, 4 H), 3.41 (s, 4 H). Note: Aryl C-H bonds not mentioned in the assigned peaks. Although we could not deconvolute them, they appear as a complex multiplet between 7.42-7.10 ppm and presumably account for 10 H for each species. Combined <sup>13</sup>C

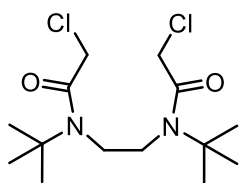
NMR (CDCl<sub>3</sub>)  $\delta$  167.56, 167.41, 167.14, 136.67, 135.90, 135.22, 129.30, 129.14, 128.73, 128.56, 128.23, 128.00, 127.74, 127.07, 126.46, 53.11, 51.50, 49.20, 45.88, 44.27, 43.09, 41.56, 41.17, 41.03; Positive Mode NSI-MS  $m/z$  (formula, ppm) 393.11293 (C<sub>20</sub>H<sub>23</sub>Cl<sub>2</sub>N<sub>2</sub>O<sub>2</sub><sup>+</sup> ([M+H]<sup>+</sup>),  $\Delta = 0.46$ ).



*N,N'*-(ethane-1,2-diyl)bis(2-chloro-*N*-isopropylacetamide) (*iPr***6**). To a

flame-dried, N<sub>2</sub>-purged round bottom flask equipped with a stir bar, DCM (180 mL) was added. Then, chloroacetyl chloride (26.4 mL, 332 mmol, 3.0 equiv) was added, and the flask was cooled in an ice bath with stirring for 15 minutes. By syringe pump over 20 minutes, N,N'-diisopropylethylenediamine (20 mL, 111 mmol, 1.0 equiv) was added. The flask was then allowed to warm to room temperature and stirred overnight. To a beaker filled with ice and saturated aqueous potassium carbonate, the reaction was added, washing the flask with DCM into the beaker. The biphasic mixture was stirred about 30 minutes. The contents of the beaker were poured into a separatory funnel. The DCM phase was collected, and the aqueous phase was washed once more with DCM. The combined DCM extracts were washed once with saturated aqueous potassium carbonate and once with brine. The organic phase was collected, dried with anhydrous MgSO<sub>4</sub>, and filtered. The filtrate was concentrated *in vacuo* to obtain the crude as an off-white powder. The crude was purified through dissolution in minimal DCM and crashing out the product with excess pentane to yield a white powder (25.7212g, 78% yield). Main Form <sup>1</sup>H NMR (CDCl<sub>3</sub>)  $\delta$  4.11 (s, 4 H), 3.98 (sept,  $J = 6.6$  Hz, 2 H), 3.34 (2, 4 H), 1.29 (d,  $J = 6.6$  Hz, 12 H); <sup>13</sup>C NMR (CDCl<sub>3</sub>)  $\delta$  166.55, 49.76, 42.01, 39.53, 21.05. Asymmetric Form <sup>1</sup>H NMR (CDCl<sub>3</sub>)

$\delta$  4.64 (sept,  $J = 6.8$  Hz, 2 H), 4.36 (s, 2 H), 4.10 (s, 2 H), 3.33-3.30 (m, 2 H), 3.30-3.28 (m, 2 H), 1.26 (d,  $J = 6.6$  Hz, 6 H), 1.18 (d,  $J = 6.8$  Hz, 6 H). Total  $^{13}\text{C}$  NMR ( $\text{CDCl}_3$ )  $\delta$  166.49, 49.69, 49.29, 46.52, 42.17, 41.98, 41.75, 41.54, 41.23, 39.49, 21.51, 21.01, 20.52. Positive Mode NSI-MS  $m/z$  (relative intensity, formula, ppm) 295.09740 ( $\text{C}_{12}\text{H}_{21}\text{O}_2\text{N}_2\text{Cl}_2^+$  ( $[\text{M}-\text{H}]^+$ ,  $\Delta = 0.34\text{ppm}$ ).



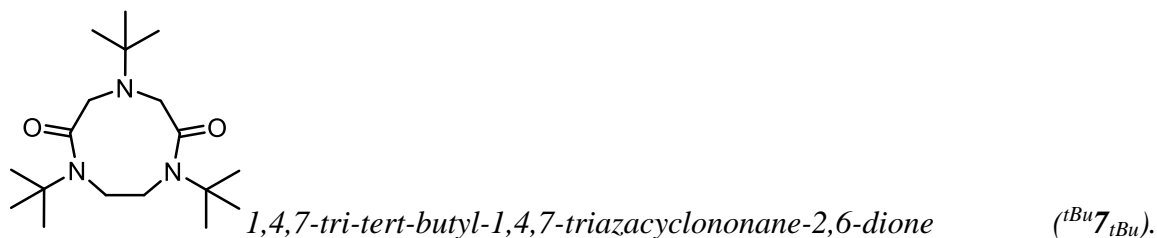
*N,N'*-(ethane-1,2-diyl)bis(*N*-(*tert*-butyl)-2-chloroacetamide) (*tBu6*). To

a flame-dried,  $\text{N}_2$ -purged round bottom flask equipped with a stir bar, DCM (150 mL) was added. Then, chloroacetyl chloride (22.0 mL, 276 mmol, 3.0 equiv) was added, and the flask was cooled in an ice bath with stirring for 15 minutes. By syringe pump over 20 minutes, *N,N'*-dimethylethylenediamine (20 mL, 93 mmol, 1.0 equiv) was added. The flask was then allowed to warm to room temperature and stirred overnight. To a beaker filled with ice and saturated aqueous potassium carbonate, the reaction was added, washing the flask with DCM into the beaker. The biphasic mixture was stirred about 30 minutes. The contents of the beaker were poured into a separatory funnel. The DCM phase was collected, and the aqueous phase was washed once more with DCM. The combined DCM extracts were washed once with saturated aqueous potassium carbonate and once with brine. The organic phase was collected, dried with anhydrous  $\text{MgSO}_4$ , and filtered. The filtrate was concentrated *in vacuo* to obtain the crude as a white powder (28.90g, 94% yield). The crude material can also be crystallized in DCM/pentane to obtain the product as a colorless crystalline solid if desired. Spectroscopic data matches literature.<sup>74</sup>  $^1\text{H}$  NMR

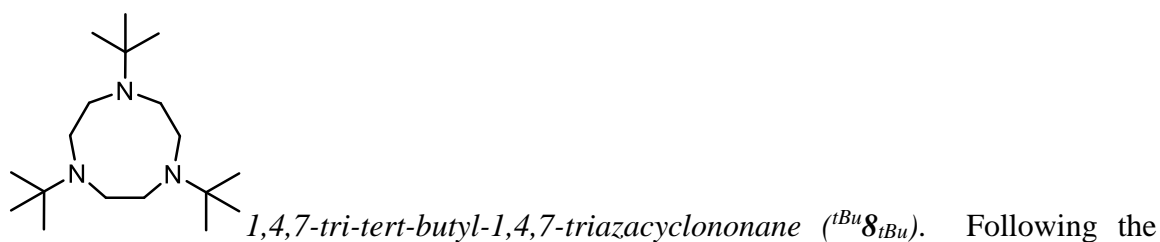
(CDCl<sub>3</sub>)  $\delta$  4.30 (s, 4 H), 3.47 (s, 4 H), 1.47 (s, 18 H).

General Procedure for Cyclization: In a flask equipped with a stir bar, N,N'-(ethane-1,2-diyl)bis(N-(tert-butyl)-2-chloroacetamide) (1 equiv) was dissolved in N,N-dimethylformamide (1 M). The contents of the flask were stirred, and sodium carbonate (2.5 equiv) was added. Then, amine (1.1 equiv) was added, and the contents were stirred 30-60 minutes at room temperature. Then, the reaction was heated to 120 °C and stirred 3-12 hours. The flask was then allowed to cool to room temperature. The contents were poured into a separatory funnel, washing with ethyl acetate and water. The ethyl acetate phase was separated, and the aqueous phase was washed once more with ethyl acetate. The combined ethyl acetate phases were washed with 5 portions of brine. The organic phase was then dried with anhydrous MgSO<sub>4</sub> and filtered. The filtrate was concentrated *in vacuo* to yield a crude cyclic diamide, often of sufficient purity for subsequent reduction.

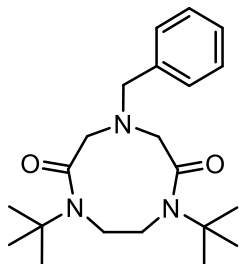
General Procedure for Reduction: In a glove box, lithium aluminum hydride pellets (5 equiv) were stirred in Et<sub>2</sub>O (25 mL/g LAH) overnight. The grey suspension was then filtered over celite into a round bottom flask with a stir bar. With stirring, cyclic diamide (1 equiv) was added in small portions. The reaction was stirred 3-12 hours at room temperature. The reaction was then removed from the glove box and cooled in an ice bath in a fume hood. With stirring, the reaction was quenched via the Feiser method. The quenched reaction was filtered, washing with Et<sub>2</sub>O, and the filtrate was concentrated *in vacuo* to afford the product.



Following the general procedure, N,N'-(ethane-1,2-diyl)bis(N-(tert-butyl)-2-chloroacetamide) (1.0014g, 3.1 mmol), N,N-dimethylformamide (3.0 mL), sodium carbonate (0.8285g, 7.8 mmol), and *tert*-butylamine (0.34 mL, 3.2 mmol) (heated for 3 hours) produced a crude, orange white solid (0.80g, 65% pure by NMR internal standard, 52% yield). The crude can be purified by crystallization from ethyl acetate/hexanes. Spectroscopic data matches literature.<sup>74</sup>

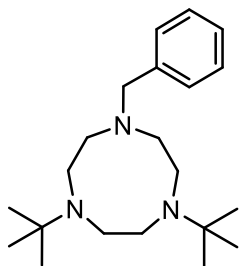


general procedure, lithium aluminum hydride pellets (17.5g, 461 mmol, 6.6 equiv), diethyl ether (440mL), and 1,4,7-tri-tert-butyl-1,4,7-triazacyclononane-2,6-dione (22.6g, 69 mmol) (stirred overnight) produced a yellow-white solid, which was crystallized from ethanol to yield the product as colorless needles (15.85g, 77% yield). Spectroscopic data matches literature.<sup>74</sup>



*4-benzyl-1,7-di-tert-butyl-1,4,7-triazacyclononane-2,6-dione* (<sup>tBu</sup>7<sub>Bn</sub>).

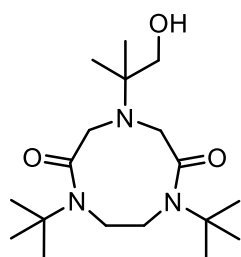
Following the general cyclization procedure, N,N'-(ethane-1,2-diyl)bis(N-(tert-butyl)-2-chloroacetamide) (10.12g, 31 mmol), N,N-dimethylformamide (31 mL), sodium carbonate (8.10g, 76.4 mmol), and benzylamine (3.5 mL, 32 mmol) (heated 8 hours) produced a crude pale yellow solid. The crude solid was dissolved in minimal ethyl acetate and precipitated with hexanes to afford the product as a white powder (5.53g, 49% yield). <sup>1</sup>H NMR (CDCl<sub>3</sub>) δ 7.37-7.22 (m, 5 H), 3.80 (s, 2 H), 3.77 (s, 4 H), 3.46 (s, 4 H), 1.44 (s, 18 H); <sup>13</sup>C NMR (CDCl<sub>3</sub>) δ 171.56, 137.90, 129.31, 128.58, 127.40, 59.47, 59.35, 57.76, 48.23, 29.10. Positive Mode NSI-MS m/z (formula, ppm) 360.26510 (C<sub>21</sub>H<sub>34</sub>N<sub>3</sub>O<sub>2</sub><sup>+</sup> ([M+H]<sup>+</sup>), Δ = 1.53).



*1-benzyl-4,7-di-tert-butyl-1,4,7-triazacyclononane* (<sup>tBu</sup>8<sub>Bn</sub>). Following

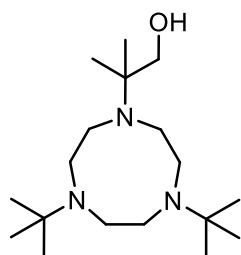
the general reduction procedure, lithium aluminum hydride pellets (1.9g, 50 mmol), diethyl ether (50mL), and 1-benzyl-4,7-di-tert-butyl-1,4,7-triazonane-2,6-dione (3.2654, 9.1 mmol) (stirred overnight) produced a pale yellow oil (59% of 3.4513g by internal standard, 68% yield; low internal standard yield appears to be due to difficulty removing CDCl<sub>3</sub> contaminant from previous NMR under high vacuum, see characterization data below). <sup>1</sup>H

NMR (CDCl<sub>3</sub>) δ 7.41 (d, *J* = 6.9 Hz, 2 H), 7.31 (t, *J* = 7.5 Hz, 2 H), 7.22 (t, *J* = 7.2 Hz, 1 H), 3.68 (s, 2 H), 2.97-2.90 (m, 4 H), 2.70-2.63 (m, 8 H), 1.06 (s, 18 H); <sup>13</sup>C NMR (CDCl<sub>3</sub>) δ 141.32, 128.96, 128.14, 126.60, 62.15, 55.62, 55.01, 53.05, 50.63, 27.21. Positive Mode NSI-MS *m/z* (formula, ppm) 332.30584 (C<sub>21</sub>H<sub>38</sub>N<sub>3</sub><sup>+</sup> ([M+H]<sup>+</sup>), Δ = 0.54).



1,7-di-tert-butyl-4-(1-hydroxy-2-methylpropan-2-yl)-1,4,7-

triazacyclononane-2,6-dione (<sup>*t*Bu</sup>7<sub>Me2EtOH</sub>). Following the general cyclization procedure, N,N'-(ethane-1,2-diyl)bis(N-(tert-butyl)-2-chloroacetamide) (5.0202g, 15 mmol), N,N-dimethylformamide (16 mL), sodium carbonate (4.2033g, 39.7 mmol), and 2-amino-2-methyl-1-propanol (1.6 mL, 16.8 mmol) (heated overnight) produced an off-white crude solid, which was purified by silica gel column chromatography (100 ethyl acetate, R<sub>f</sub> = 0.38) to yield the product as a white solid (2.96g, 56% yield). <sup>1</sup>H NMR (CDCl<sub>3</sub>) δ 3.78 (s, 4 H), 3.63 (s, 4 H), 3.46 (s, 2 H), 1.43 (s, 18 H), 1.12 (s, 6 H); <sup>13</sup>C NMR (CDCl<sub>3</sub>) δ 173.29, 69.69, 59.75, 58.68, 57.85, 47.14, 23.94, 21.24. Positive Mode NSI-MS *m/z* (formula, ppm) 342.27539 (C<sub>18</sub>N<sub>36</sub>N<sub>3</sub>O<sub>3</sub> ([M+H]<sup>+</sup>), Δ = 0.85).

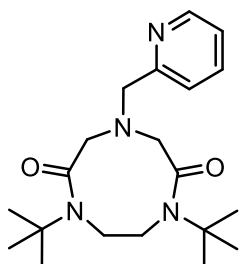


2-(4,7-di-tert-butyl-1,4,7-triazonan-1-yl)-2-methylpropan-1-ol

(<sup>*t*Bu</sup>8<sub>Me2EtOH</sub>). Following the general reduction procedure with a slight modification, lithium



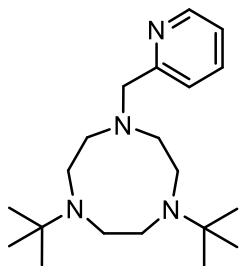
aluminum hydride solution (4.0M in Et<sub>2</sub>O, 10.5 mL), diethyl ether (25 mL), and 1,7-di-tert-butyl-4-(1-hydroxy-2-methylpropan-2-yl)-1,4,7-triazacyclononane-2,6-dione (2.88g, 8.4 mmol) (stirred overnight) was quenched and washed with chloroform, and the filtrate, concentrated *in vacuo*, produced a solid, which was purified by trituration with methanol and water to produce a white solid (1.4485g, 55% yield). <sup>1</sup>H NMR (CDCl<sub>3</sub>) δ 6.50 (br t, *J* = 6.6 Hz, 1 H), 3.50 – 2.00 (v br m, 14 H) 0.95 (s, 24 H); <sup>13</sup>C NMR (CDCl<sub>3</sub>) δ 70.12, 57.95, 55.73, 54.21, 53.76, 51.65, 26.69, 18.53. Positive Mode NSI-MS *m/z* (formula, ppm) 314.31676 (C<sub>18</sub>H<sub>40</sub>N<sub>3</sub>O ([M+H]<sup>+</sup>), Δ = 0.54).



*1,7-di-tert-butyl-4-(pyridin-2-ylmethyl)-1,4,7-triazonane-2,6-dione*

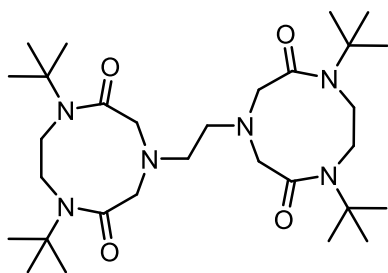
(<sup>*t*Bu</sup>7<sub>Py</sub>). Following the general cyclization procedure, N,N'-(ethane-1,2-diyl)bis(N-(tert-butyl)-2-chloroacetamide) (3.0084, 9.2 mmol), N,N-dimethylformamide (9 mL), sodium carbonate (2.4550, 23.2 mmol), and 2-picolylamine (1.00 mL, 9.7 mmol) produced a crude red solid. The crude can be purified by silica gel column chromatography (ethyl acetate, R<sub>f</sub> = 0.21) to yield a white solid (0.4234g, 13% yield) which may darken upon prolonged exposure to air. <sup>1</sup>H NMR (CDCl<sub>3</sub>) δ 8.53 (dtd, *J* = 5.1, 2.1, 1.0 Hz, 1 H), 7.68 (tt, *J* = 7.6, 2.0 Hz, 1 H), 7.52 (d, *J* = 7.6 Hz, 1 H), 7.16 (dddd, *J* = 7.2, 4.9, 2.3, 1.2 Hz, 1 H), 3.99 (s, 2 H), 3.75 (s, 4 H), 3.57 (s, 4 H), 1.44 (s, 18 H); <sup>13</sup>C NMR (CDCl<sub>3</sub>) δ 171.09, 158.39, 149.20, 136.61, 123.02, 122.11, 60.71, 59.07, 57.74, 48.25, 28.97. Positive Mode NSI-MS

m/z (formula, ppm) 361.25946 ( $C_{20}H_{33}N_4O_2^+$  ( $[M+H]^+$ ),  $\Delta = 0.94$ ).



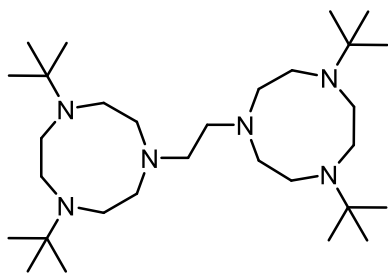
*1,4-di-tert-butyl-7-(pyridin-2-ylmethyl)-1,4,7-triazacyclononane*

( $tBu_8Py$ ). Following a modification of the general reduction procedure, in a glove box, in a round bottom flask with a stir bar, 1,7-di-tert-butyl-4-(pyridin-2-ylmethyl)-1,4,7-triazonane-2,6-dione (0.4234g, 1.17 mmol, 1 equiv) was dissolved in diethyl ether (15 mL). To this stirring solution, lithium aluminum hydride (0.4496g, 11.85 mmol, 10 equiv) was added portionwise. The reaction was stirred for 4.5 hours. Then, the reaction was quenched in the glove box through slow addition of ethyl acetate to the reaction. The quenched reaction was filtered over celite, and the solvent was removed *in vacuo*. The resulting viscous yellow oil with white solid was dissolved in chloroform and filtered over celite to yield the product as a viscous yellow oil (0.3221g, 37% pure by NMR internal standard, 31% yield). The product darkens rapidly (yellow to red-brown within 30 minutes) upon exposure to air.  $^1H$  NMR ( $CDCl_3$ )  $\delta$  8.43 (ddd,  $J = 4.9, 1.9, 1.0$  Hz, 1 H), 7.63 (d,  $J = 8.0$  Hz, 1 H), 7.56 (td,  $J = 7.6, 1.8$  Hz, 1 H), 7.04 (ddd,  $J = 7.4, 4.9, 1.4$  Hz, 1 H), 3.78 (s, 2 H), 2.96-2.91 (m, 4 H), 2.63-2.59 (m, 4 H), 2.59 (s, 4 H), 0.97 (s, 18 H);  $^{13}C$  NMR ( $CDCl_3$ )  $\delta$  161.95, 148.91, 136.35, 123.14, 121.66, 63.90, 55.82, 55.11, 53.39, 50.60, 27.23; Positive Mode NSI-MS m/z (formula, ppm) 333.30152 ( $C_{20}H_{37}N_4^+$  ( $[M+H]^+$ ),  $\Delta = 0.75$ ).



4,4'-(ethane-1,2-diyl)bis(1,7-di-tert-butyl-1,4,7-triazonane-

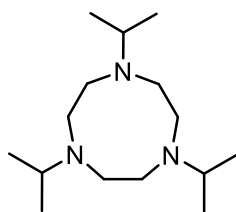
2,6-dione) ( $t^{Bu}7_{CH_2}$ )<sub>2</sub>. Following the general cyclization procedure, N,N'-(ethane-1,2-diyl)bis(N-(tert-butyl)-2-chloroacetamide) (10.09g, 31 mmol, 1 equiv), N,N-dimethylformamide (31 mL), sodium carbonate (7.98g, 75 mmol, 2.4 equiv), and ethylenediamine (1.03 mL, 15 mmol, 0.50 equiv) (heated overnight) produced a crude orange solid (7.28g, 71% pure by internal standard) of sufficient purity for reduction (see reduction below). If necessary, the product can be purified by silica gel column chromatography. <sup>1</sup>H NMR (CDCl<sub>3</sub>) δ 3.70 (s, 8 H), 3.50 (s, 8 H), 2.87 (s, 4 H), 1.41 (s, 36 H); <sup>13</sup>C NMR (CDCl<sub>3</sub>) δ 171.60, 60.39, 57.82, 52.31, 48.30, 29.10; Positive mode NSI-MS m/z (formula, ppm) (C<sub>30</sub>H<sub>57</sub>N<sub>6</sub>O<sub>4</sub><sup>+</sup> 565.44390 ([M+H]<sup>+</sup>), Δ = 0.57). 8.7603



1,2-bis(4,7-di-tert-butyl-1,4,7-triazacyclononan-1-

yl)ethane ( $t^{Bu}8_{CH_2}$ )<sub>2</sub>. Following a modification of the general reduction procedure, crude 4,4'-(ethane-1,2-diyl)bis(1,7-di-tert-butyl-1,4,7-triazonane-2,6-dione) (7.28g), lithium aluminum hydride solution (4.0M in Et<sub>2</sub>O, 34.6 mL), and diethyl ether (50mL) (overnight), produced a crude off-white solid. This solid was purified by trituration with methanol/water to purify the product as a white solid (1.3659g, 17% yield over 2 steps).

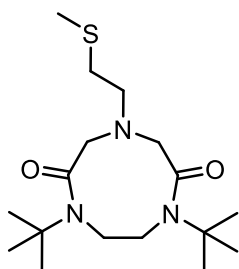
$^1\text{H}$  NMR ( $\text{CDCl}_3$ )  $\delta$  3.00-2.94 (m, 8 H), 2.68-2.64 (m 8 H), 2.62 (s, 4 H), 2.58 (s, 8 H), 1.03 (s, 36 H);  $^{13}\text{C}$  NMR ( $\text{CDCl}_3$ )  $\delta$  56.45, 55.97, 55.03, 53.01, 50.69, 27.21; Positive Mode NSI-MS  $m/z$  (formula, ppm) 509.52721 ( $\text{C}_{30}\text{H}_{65}\text{N}_6\text{O}^+$  ( $[\text{M}+\text{H}]^+$ ),  $\Delta = 1.35$ ), 525.52202 ( $\text{C}_{30}\text{H}_{69}\text{N}_6\text{O}_2^+$  ( $[\text{M}+\text{OH}]^+$ ),  $\Delta = 1.10$ ).



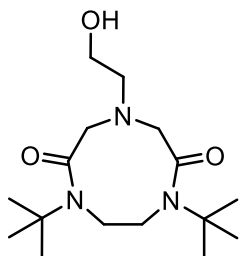
*1,4,7-triisopropyl-1,4,7-triazacyclononane* ( $i^{\text{Pr}}\mathbf{8}_{i^{\text{Pr}}}$ ). In a 100 mL round

bottom flask with stir bar, *N,N'*-(ethane-1,2-diyl)bis(*N*-(isopropyl)-2-chloroacetamide) (9.07g, 30.5 mmol, 1 equiv) was dissolved in *N,N*-dimethylformamide (30 mL). The contents were stirred, and sodium carbonate (8.1g, 76.3 mmol, 2.5 equiv) was added. The flask was cooled in an ice/water bath. Then, isopropylamine (2.9 mL, 33.6 mmol, 1.1 equiv) was added, and the flask was capped and stirred 20 minutes. The flask was then allowed to warm to room temperature over 35 minutes. The flask is then uncapped and heated to 120 °C for 80 minutes. The reaction was allowed to cool to room temperature. The contents were poured into a separatory funnel, washing with ethyl acetate and water. The ethyl acetate phase was separated, and the aqueous phase was washed once more with ethyl acetate. The combined ethyl acetate phases were washed with 5 portions of brine. The organic phase was then dried with anhydrous  $\text{MgSO}_4$  and filtered. The filtrate was concentrated *in vacuo* to yield a white solid (4.5371g). The white solid was added to a solution of lithium aluminum hydride in diethyl ether (from the filtrate of 3.2g lithium aluminum hydride in 75 mL diethyl ether; see general reduction procedure above) in a glove box, and the reaction was stirred 5 hours. The reaction was then removed from the

glove box and cooled in an ice bath in a fume hood. With stirring, the reaction was quenched via the Feiser method. The quenched reaction was filtered, washing with Et<sub>2</sub>O, and the filtrate was concentrated in vacuo to afford the product as a crude yellow hygroscopic and air-sensitive oil (2.29g, 82% pure by internal standard, 24% yield). <sup>1</sup>H NMR (CDCl<sub>3</sub>) δ 2.83 (sept, *J* = 6.5 Hz, 3 H), 2.39 (s, 12 H), 0.93 (d, *J* = 6.6 Hz, 18 H). Positive Mode NSI-MS *m/z* (formula, ppm) 256.27451 (C<sub>15</sub>H<sub>34</sub>N<sub>3</sub><sup>+</sup> ([M+H]<sup>+</sup>), Δ = 0.74).

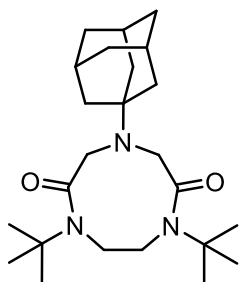


*1,7-di-tert-butyl-4-(2-(methylthio)ethyl)-1,4,7-triazacyclononane-2,6-dione* (<sup>*t*</sup>Bu7<sub>EtSMe</sub>). Following the general cyclization procedure, <sup>*t*</sup>Bu6 (0.5025 g, 1.5 mmol, 1 equiv), DMF (1.5 mL), sodium carbonate (0.4119 g, 3.9 mmol, 2.5 equiv), and 2-(methylthio)ethylamine (0.15 mL, 1.6 mmol, 1.05 equiv) generated a crude orange solid (0.4798g impure, 47% yield based on product mass by <sup>1</sup>H NMR using 1,3,5-trimethoxybenzene as internal standard). <sup>1</sup>H NMR (CDCl<sub>3</sub>) δ 3.76 (s, 4 H), 3.50 (s, 4 H), 2.89 (dd, *J* = 8.5 Hz, 6.1 Hz, 2 H), 2.68 (dd, *J* = 8 Hz, 5.6 Hz, 2 H) 2.11 (s, 3 H), 1.43 (s, 18 H). <sup>13</sup>C NMR (CDCl<sub>3</sub>) δ 171.51, 60.37, 57.85, 54.56, 48.16, 31.57, 29.03, 15.91.



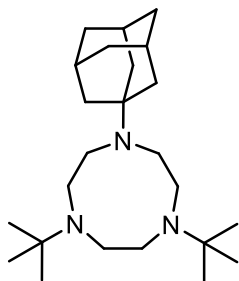
*1,7-di-tert-butyl-4-(2-hydroxyethyl)-1,4,7-triazacyclononane-2,6-*

dione (<sup>tBu</sup>7<sub>EtOH</sub>). Following the general cyclization procedure, <sup>tBu</sup>6 (0.5011 g, 1.5 mmol, 1 equiv), DMF (1.5 mL), sodium carbonate (0.4167 g, 3.9 mmol, 2.5 equiv), and ethanolamine (0.10 mL, 1.6 mmol, 1.05 equiv) generated a crude solid (0.0747g impure, 4% yield based on product mass by <sup>1</sup>H NMR using 1,3,5-trimethoxybenzene as internal standard). <sup>1</sup>H NMR (CDCl<sub>3</sub>) δ 3.76-3.72 (m, 2 H), 3.70 (s, 4 H), 3.53 (s, 4 H), 2.95-2.91 (m, 4 H), 1.45 (s, 18 H). Positive Mode NSI-MS m/z (formula, ppm) 314.24382 (C<sub>16</sub>H<sub>32</sub>N<sub>3</sub>O<sub>3</sub><sup>+</sup> ([M+H]<sup>+</sup>), Δ = 4.36).



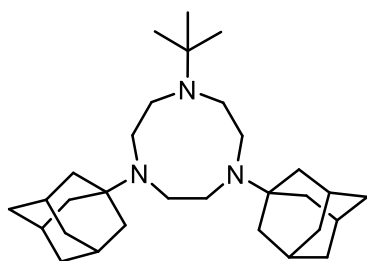
*1-(1-adamantyl)-4,7-di-tert-butyl-1,4,7-triazacyclononane* (<sup>tBu</sup>8<sub>Ad</sub>).

Following the general cyclization procedure, <sup>tBu</sup>6 (0.9665 g, 3.0 mmol, 1 equiv) DMF (3 mL), sodium carbonate (0.79, 7.5 mmol, 2.5 equiv), and 1-adamantylamine (0.4726 g, 3.1 mmol, 1.05 equiv) (heated 3 hours) produced a crude solid, which was purified by silica gel column chromatography (1:1 ethyl acetate:hexanes, R<sub>f</sub> = 0.2) to yield a white solid (0.7718g, 64% yield). <sup>1</sup>H NMR (CDCl<sub>3</sub>) δ 3.82 (s, 4 H), 3.63 (s, 4 H), 2.10-2.05 (br s, 3 H), 1.73-1.68 (br s, 6 H), 1.65-1.60 (br s, 6 H), 1.41 (s, 18 H).



*1-(1-adamantyl)-4,7-di-tert-butyl-1,4,7-triazacyclononane* (<sup>tBu</sup>**8**<sub>Ad</sub>).

Following a modification of the general reduction procedure, <sup>tBu</sup>**7**<sub>Ad</sub> (0.7203g, 1.8 mmol, 1 equiv) lithium aluminum hydride (0.60g, 16.0 mmol, 9 equiv) in diethyl ether (40 mL) were used to yield a waxy white solid (0.4945g, 74% yield,). <sup>1</sup>H NMR (CDCl<sub>3</sub>) δ 2.73-2.69 (m, 4 H), 2.64 (s, 4 H), 2.63-2.59 (m, 4 H), 2.06-2.00 (br m, 3 H), 1.65-1.62 (m, 6 H), 1.62-1.57 (m, 6 H), 1.00 (s, 1 H). <sup>13</sup>C NMR (CDCl<sub>3</sub>) δ 55.03, 54.85, 53.35, 52.97, 51.14, 39.85, 37.30, 29.94, 27.25.



*1,4-bis(1-adamantyl)-7-tert-butyl-1,4,7-triazacyclononane*

(<sup>Ad</sup>**8**<sub>tBu</sub>). Following a slight modification to the general cyclization procedure, <sup>Ad</sup>**6** (4.4581g, 9.3 mmol 1 equiv) DMF (10 mL), sodium carbonate (2.4535g, 23.1 mmol, 2.5 equiv), and *tert*-butylamine (2.92 mL, 27.8 mmol, 3 equiv) (heated 3 hours) produced an off-white crude solid, which was purified by silica gel column chromatography (1:1 ethyl acetate:hexanes, R<sub>f</sub> = 0.4) to yield a slightly impure white solid (1.12g). From this material, 0.95g was used following a modification to the general reduction procedure with lithium aluminum hydride (0.38g, 9.9 mmol, 5 equiv) in diethyl ether (20 mL) to yield a crude off-white solid, which was triturated with hot methanol to yield 0.72g (17% yield, two steps)

in an unoptimized process.  $^1\text{H}$  NMR ( $\text{CDCl}_3$ )  $\delta$  2.67-2.58 (m, 8 H), 2.57-2.51 (m, 4 H), 2.05-1.91 (m, 6 H), 1.66-1.45 (m, 24 H), 0.93 (s, 9 H).  $^{13}\text{C}$  NMR ( $\text{CDCl}_3$ )  $\delta$  54.76, 54.61, 53.02, 44.79, 39.61, 38.36, 37.07, 36.93, 29.70, 27.05.

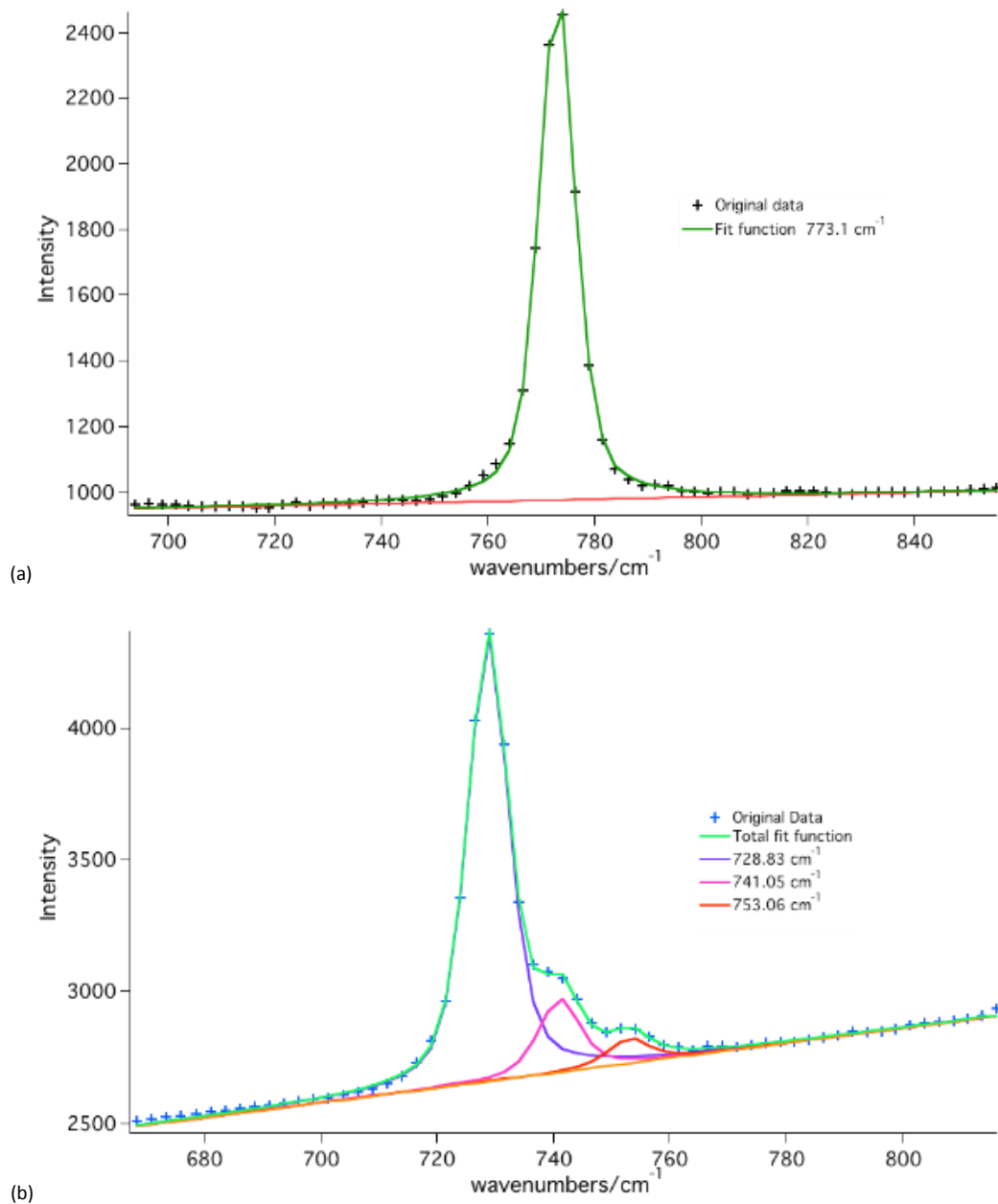


### *C. Resonance Raman Spectroscopy*<sup>90</sup>

Raman spectra were collected using excitation from the 514.5 nm line of an Ar<sup>+</sup> ion laser (Spectra Physics). Samples were dissolved in anhydrous methanol (EMD DriSolv) held in NMR tubes. Scattered light was collected by a 20X microscope objective (Olympus Plan Achromat, N.A.=.4) orthogonal to excitation beam. Rayleigh scattered excitation light was rejected by a super-notch holographic filter (Kaiser Optical) and the transmitted light was focused on the entrance slit (50  $\mu$ m) of a Holo-spec f/1.8 imaging spectrograph (Kaiser Optical) and dispersed on a Pixis 400 CCD camera (Princeton Instruments). Data acquisition was controlled by LabView software. The spectrometer was calibrated using a 1:1 toluene:acetonitrile standard and Raman shift data available from McCreery<sup>2</sup>. Integration times were set to 15-20 seconds and reported spectra are the result of 100 averages. Samples were stable at room temperature and under illumination conditions, as evidenced by lack of change in the Raman spectra on the timescale of the experiment.

Spectra were fit using a homebuilt nonlinear least squares fitting algorithm in the R language. Spectra were fit to pseudo-Voigt functions constructed as linear combinations of normalized lorentzian and gaussian functions and a linear baseline as in equation (1). The peaks were constrained to have the same full width at half maximum ( $\lambda$ ) and the same proportion of lorentzian and gaussian character ( $\eta$ ). The frequencies ( $x^0$ ), amplitudes, peak width and degree of gaussian or lorentzian character were allowed to vary for the individual peaks.

$$(1) \quad a + (1 - \eta)e^{-\left(\frac{1}{2}\right)\frac{(x-x^0)^2}{0.180336887(\lambda^2)}} + \eta \left[ 1 + \frac{(x-x^0)^2}{\left(\frac{\lambda}{2}\right)^2} \right]^{-1}$$

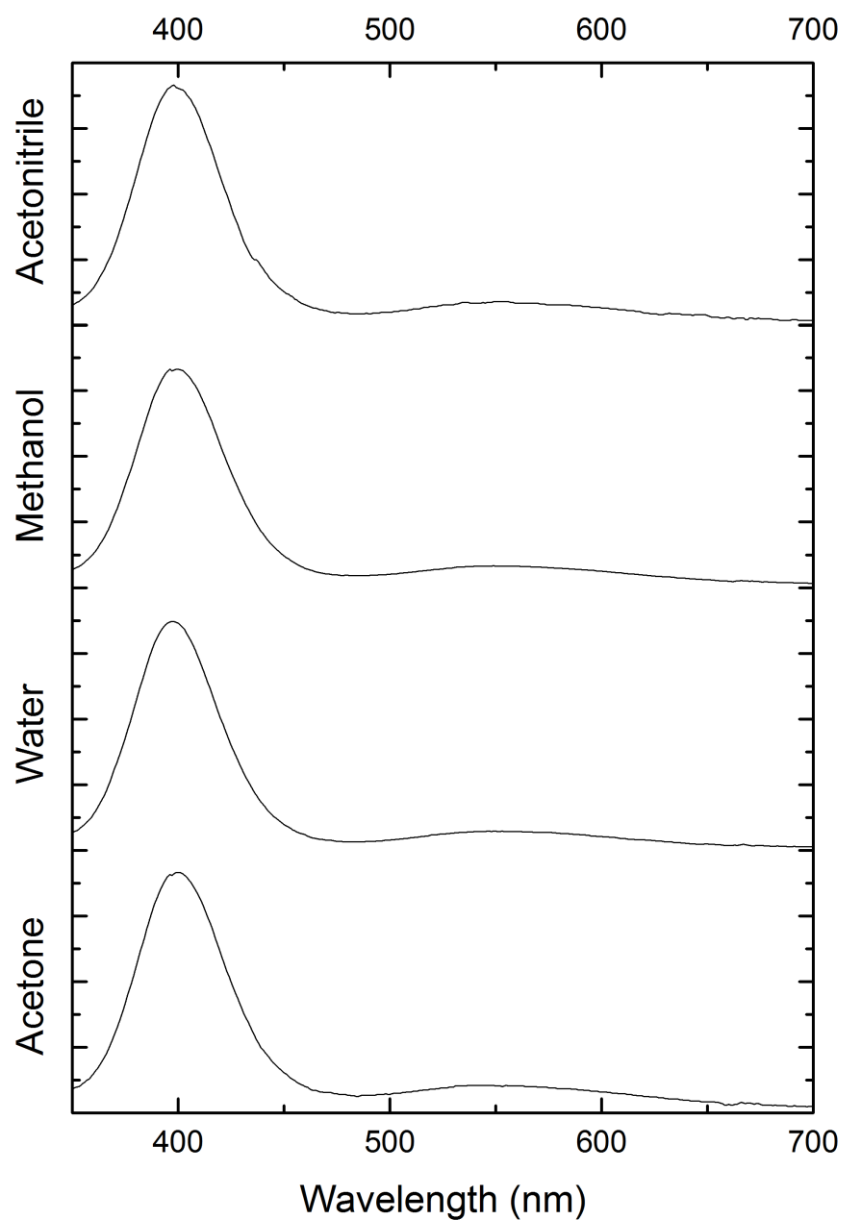


**Figure S1.** rR spectra and fits of and  $^{16}\text{O}_2$  (a) and  $^{18}\text{O}_2$  (b) labeled **3** complexes showing the O–O stretching vibration. Excitation at 514.5 nm.

FWHM of peaks :  $8.2 \text{ cm}^{-1}$

O <sub>2</sub> isotope	Observed energy (cm <sup>-1</sup> )	Predicted energy <sup>a</sup> (cm <sup>-1</sup> )
<sup>16</sup> O- <sup>16</sup> O	773.1	NA
<sup>18</sup> O- <sup>18</sup> O	728.83	728.8
<sup>18</sup> O- <sup>17</sup> O	741.05	739.53
<sup>18</sup> O- <sup>16</sup> O	753.06	751.3

<sup>a</sup>Isotope shifts based on harmonic oscillator approximation shift from the <sup>16</sup>O-<sup>16</sup>O peak.

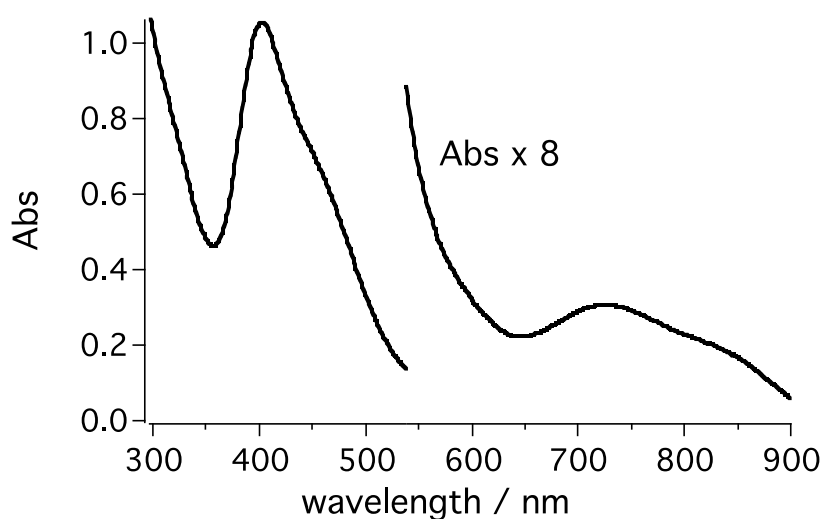
*D. UV-Vis Spectra*

**Figure S2.** UV-Vis spectra of complex **3** in acetonitrile, methanol, water, and acetone. The data was plotted using the same x-axis. For the spectra in acetonitrile, methanol, and acetone, complex **3** was dissolved in the corresponding solvent. For the water spectrum, complex **3** and an excess of KBr were stirred in water to allow for dissolution to occur.

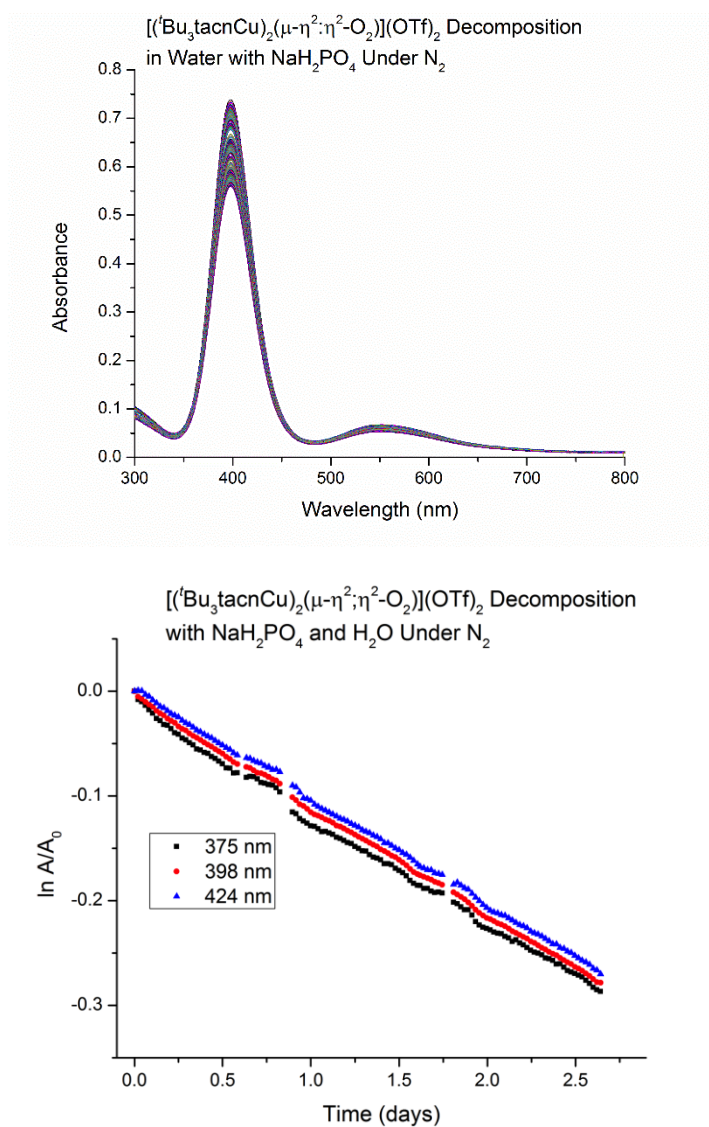
## Decomposition Studies<sup>90</sup>

### *Extended Decomposition by UV-Vis and Resonance Raman Spectroscopies*

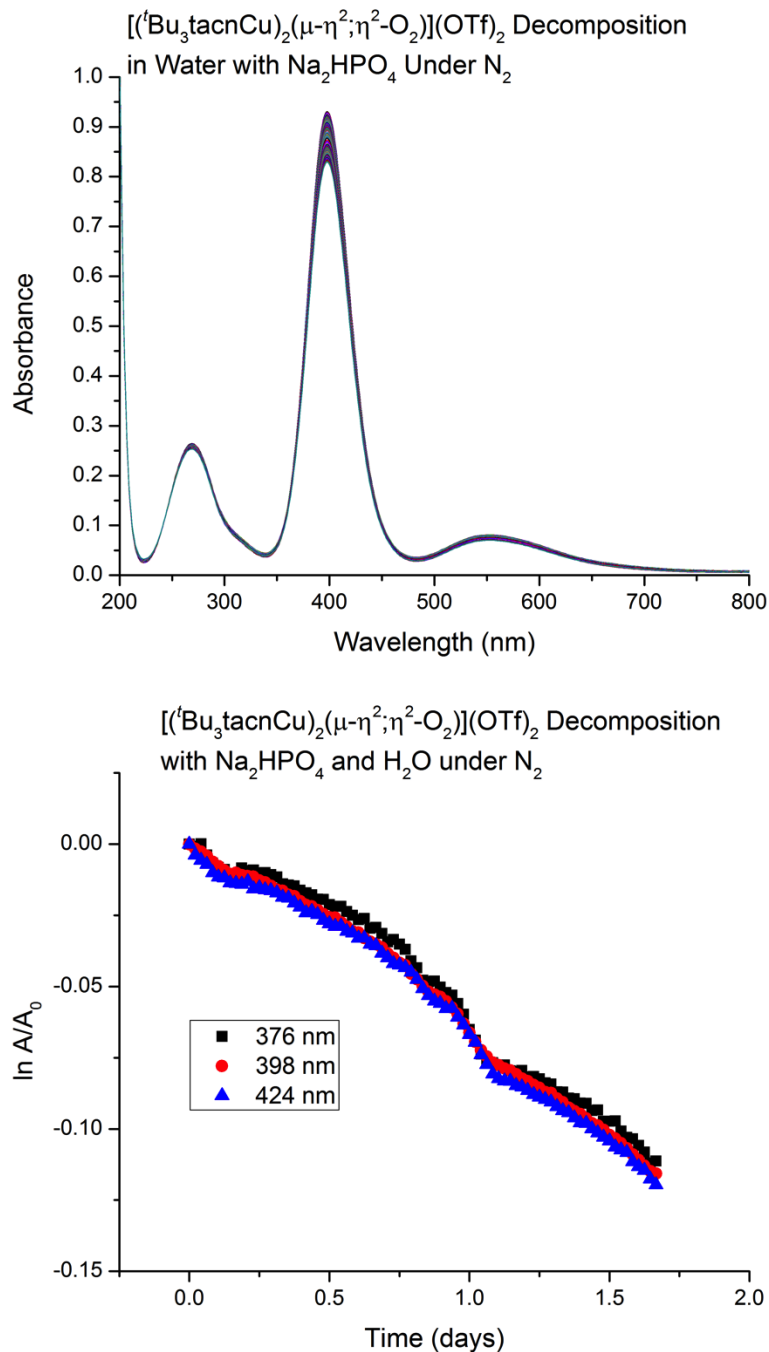
Solutions of **2** in methanol were allowed to sit under ambient atmosphere in the dark for several days. Decomposition of **3** was evident by decay of the absorption bands at 400nm and 550nm. Further decomposition of **3** in methanol revealed formation of at least one other species with absorption bands centered at ~460 and ~730 nm once the strongly absorbing **3** had sufficiently decayed (Figure S3). Raman spectra of this new gold colored species (mixture of species) were acquired and shown in Figures 9-10. Formation of this species was evident for spectra acquired using both 514.5 and 632.8 nm.



**Figure S3.** Representative absorption spectrum of **3** after 4 days in the dark in MeOH solution under ambient atmosphere. The region from 550nm to 900 nm has been scaled to show more detail.

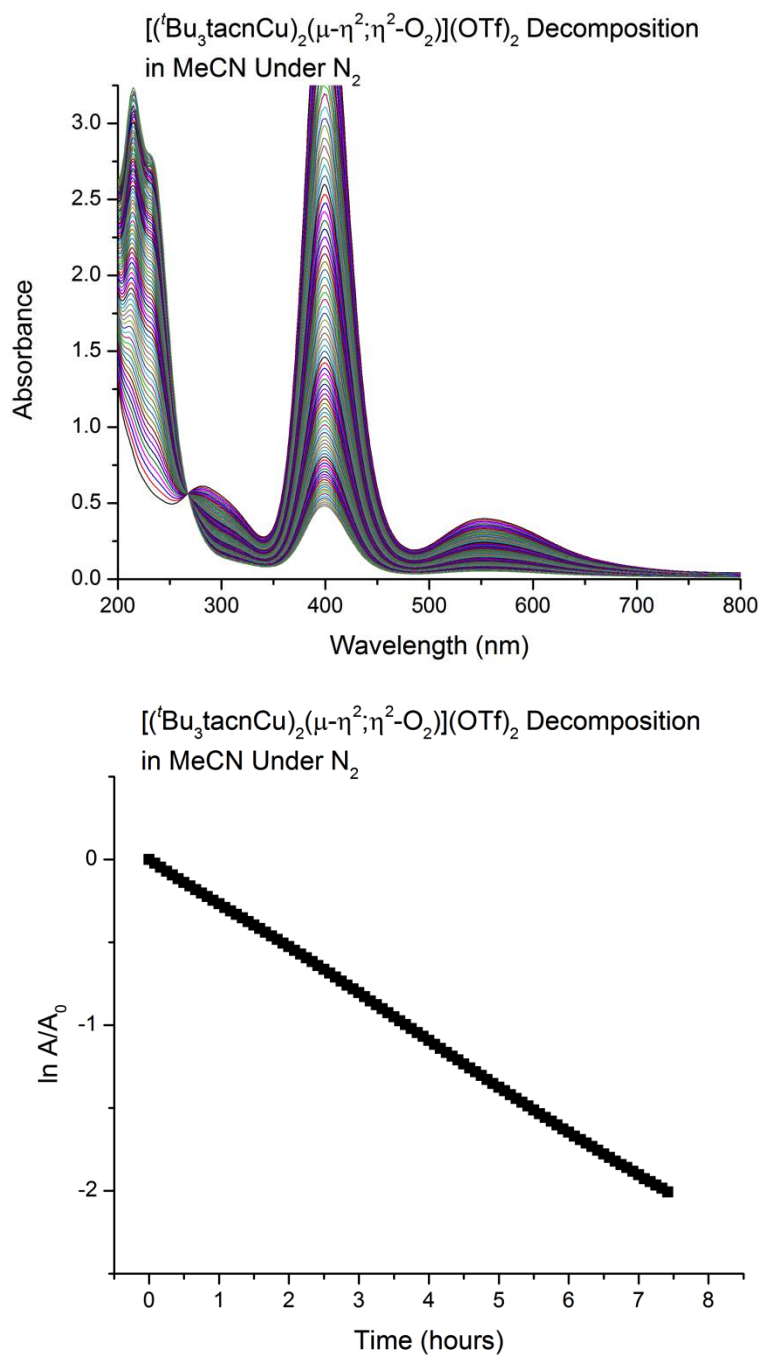
*Half-life measurements*

**Figure S4.** Decomposition of complex **3** in water with NaH<sub>2</sub>PO<sub>4</sub> as monitored by UV-Vis (Top – full spectra; bottom – pseudo first-order decay plot). Shown are representative wavelengths from full spectra taken every 10 minutes. The sample was made in the following manner: Complex **3** (0.00344g, 3.27 μmol) and NaH<sub>2</sub>PO<sub>4</sub>·H<sub>2</sub>O (0.57420g, 4.16 mmol) were dissolved in deionized water (100mL). Then 4 mL of this solution was filtered over celite/cotton into a cuvette. The cuvette was sealed with a septum-topped cap and purged by bubbling N<sub>2</sub> gas through the solution with an outlet. The septum was covered with parafilm to ensure the seal for analysis of the sample by UV-Vis.



**Figure S5.** Decomposition of complex **3** in H<sub>2</sub>O with Na<sub>2</sub>HPO<sub>4</sub> as monitored by UV-Vis (Top – full spectra; bottom – pseudo first-order decay plot). Shown are representative wavelengths from full spectra taken every 30 minutes. The sample was made in the following manner: Complex **3** (0.00383g, 3.64 μmol) and Na<sub>2</sub>HPO<sub>4</sub>·7H<sub>2</sub>O (0.87937g, 3.28 mmol) were dissolved in H<sub>2</sub>O (100mL). The resulting solution was filtered over celite. Then 4 mL of this solution was filtered over celite/cotton into a cuvette. The cuvette was sealed with a septum-topped cap and purged by bubbling N<sub>2</sub> gas through the solution with an outlet. The septum was covered with parafilm to ensure the seal for analysis of the sample by UV-Vis.

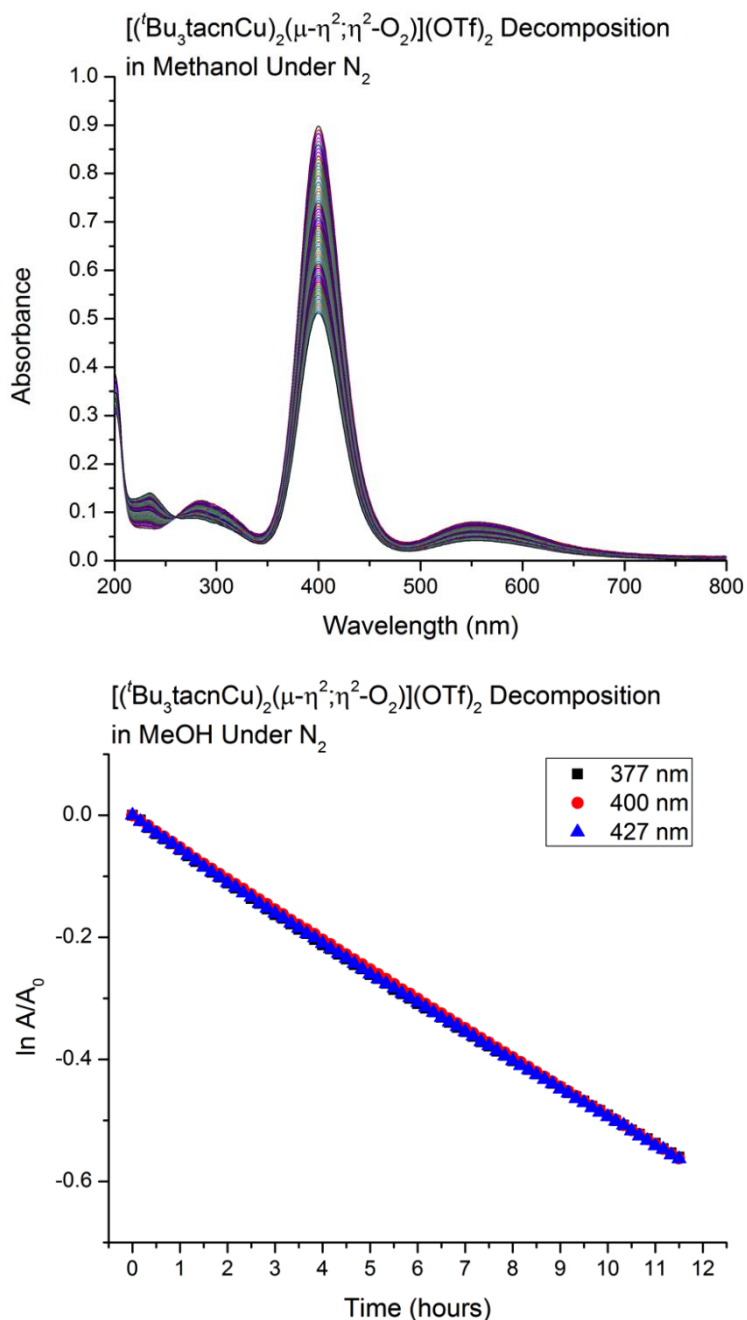
Solvent: Acetonitrile



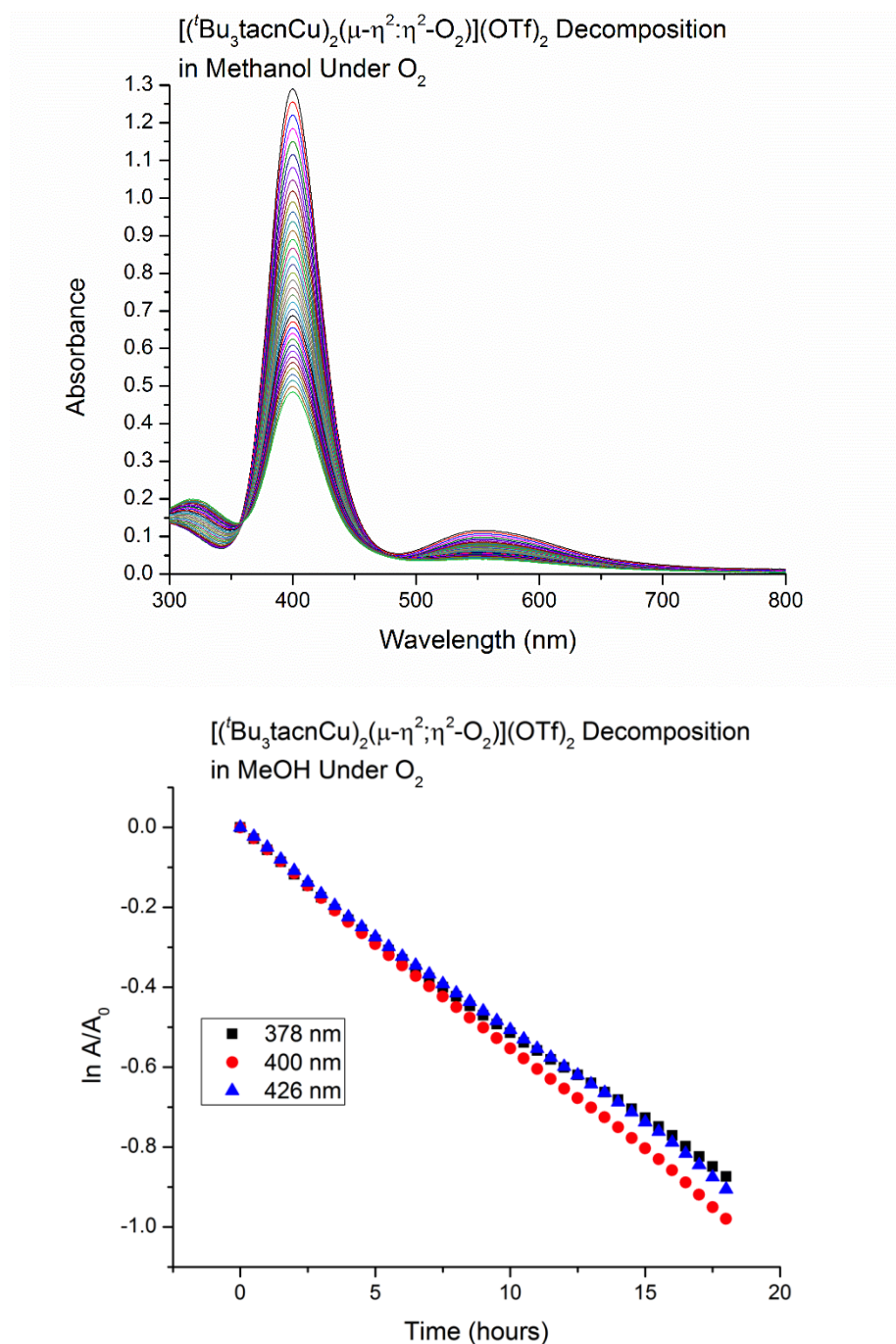
**Figure S6.** Decomposition of complex **3** in acetonitrile as monitored by UV-Vis (Top – full spectra; bottom – pseudo first-order decay plot). Shown are data from 553 nm from full spectra taken every 5 minutes. The sample was made in the following manner: Complex **3** (0.00180g, 1.71  $\mu\text{mol}$ ) was dissolved in acetonitrile (10mL). Then 4 mL of this solution was filtered over celite/cotton into a cuvette. The cuvette was sealed with a septum-topped cap and purged by bubbling  $\text{N}_2$  gas through the solution with an outlet. The septum was covered with parafilm to ensure the seal for analysis of the sample by UV-Vis.



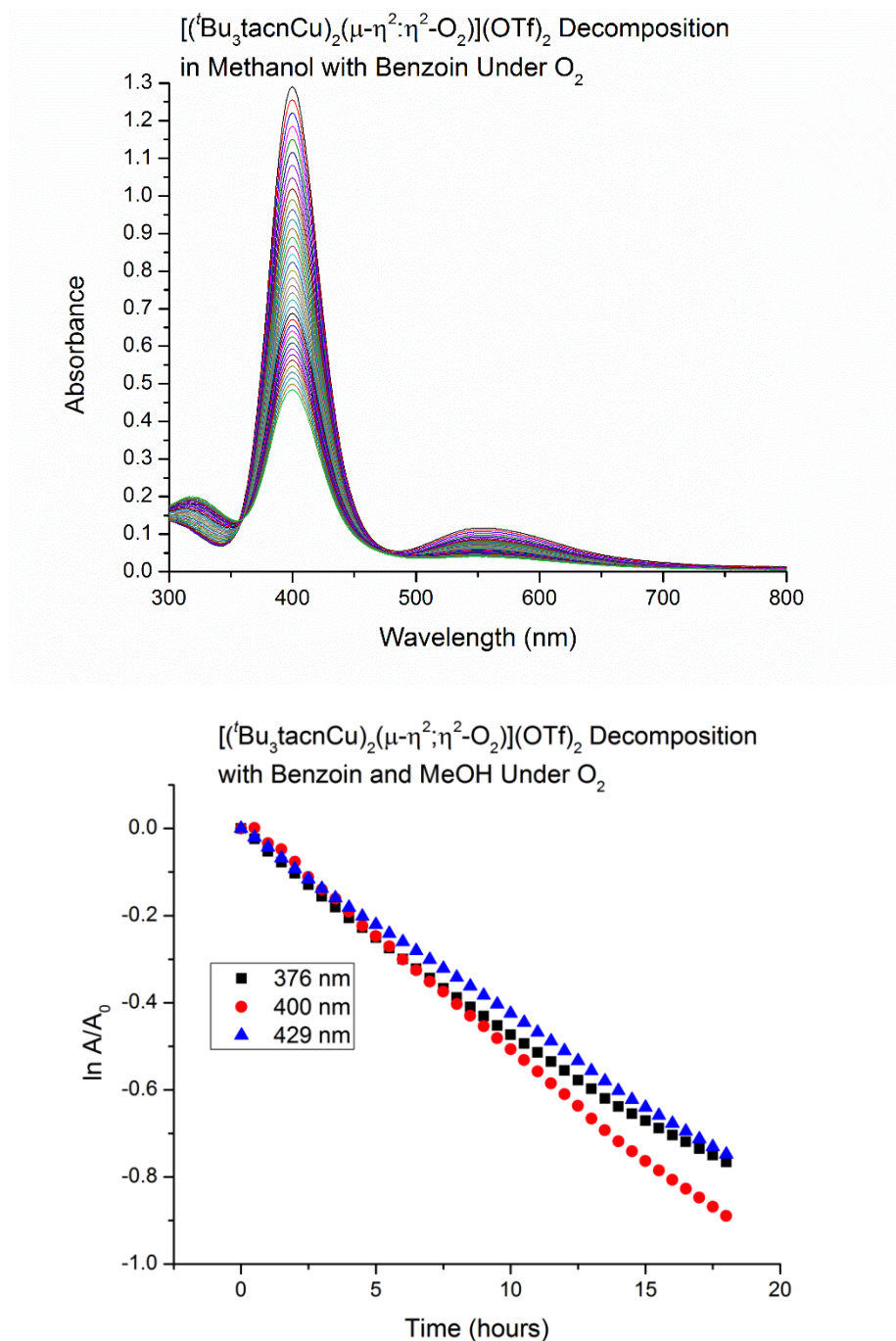
Solvent: Methanol



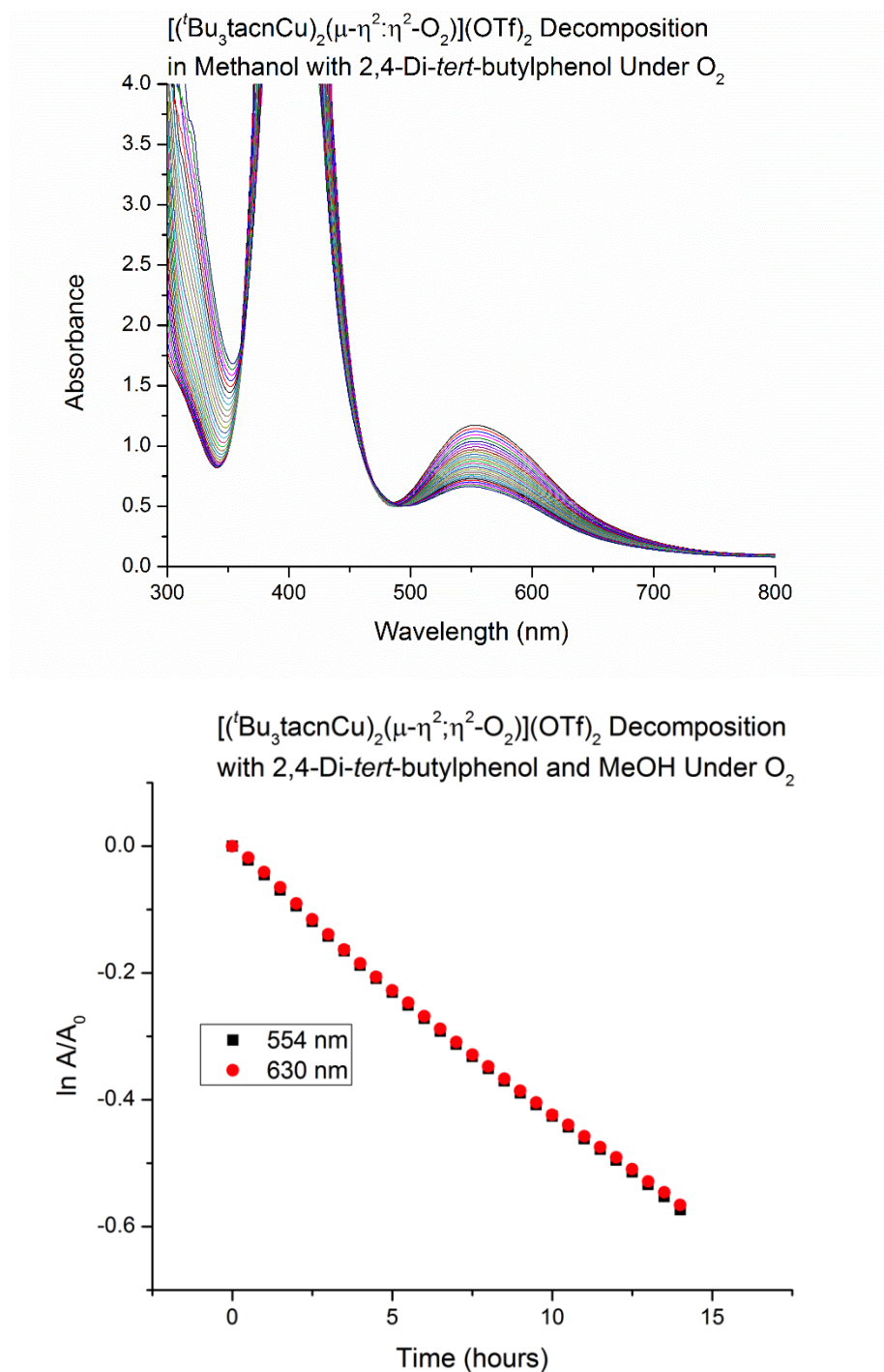
**Figure S7.** Decomposition of **3** in methanol as monitored by UV-Vis (Top – full spectra; bottom – pseudo first-order decay plot). Shown are representative wavelengths from full spectra taken every 10 minutes. The sample was made in the following manner: In a glove box, complex **3** (0.00756g, 7.18 μmol) was dissolved in anhydrous methanol (10mL). Upon complete dissolution, 0.5 mL of this solution was removed and diluted further with methanol to 10mL. Then 4 mL of this solution was transferred to a cuvette and sealed for analysis by UV-Vis.



**Figure S8.** Decomposition of complex **3** in methanol as monitored by UV-Vis (Top – full spectra; bottom – pseudo first-order decay plot). Shown are representative wavelengths from full spectra taken every 30 minutes. The sample was made in the following manner: Complex **3** (0.00538g, 5.11 μmol) was dissolved in methanol (100mL). The resulting solution was filtered over celite. Then 4 mL of this solution was filtered over celite/cotton into a cuvette. The cuvette was sealed with a septum-topped cap and purged by bubbling a balloon of O<sub>2</sub> gas through the solution with an outlet. Another O<sub>2</sub> balloon was fitted onto the septum for analysis of the sample by UV-Vis.

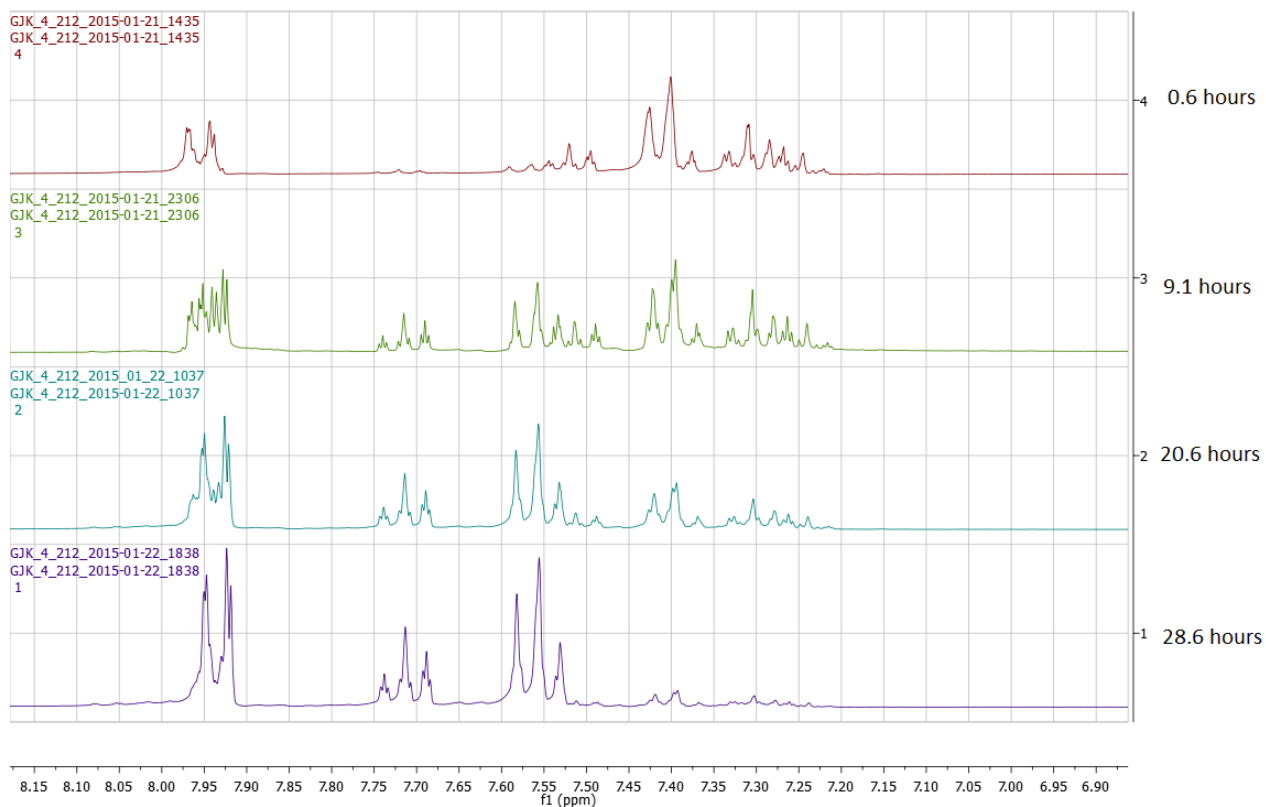


**Figure S9.** Decomposition of complex **3** in methanol with benzoin as monitored by UV-Vis (Top – full spectra; bottom – pseudo first-order decay plot). Shown are representative wavelengths from full spectra taken every 30 minutes. The sample was made in the following manner: Complex **3** (0.01550g, 14.7 μmol, 1 equiv) and benzoin (0.03184g, 150 μmol, 10.2 equiv) were dissolved in methanol (100mL). Then 4 mL of this solution was filtered over celite/cotton into a cuvette. The cuvette was sealed with a septum-topped cap and purged by bubbling a balloon of O<sub>2</sub> gas through the solution with an outlet. Another O<sub>2</sub> balloon was fitted onto the septum for analysis of the sample by UV-Vis.

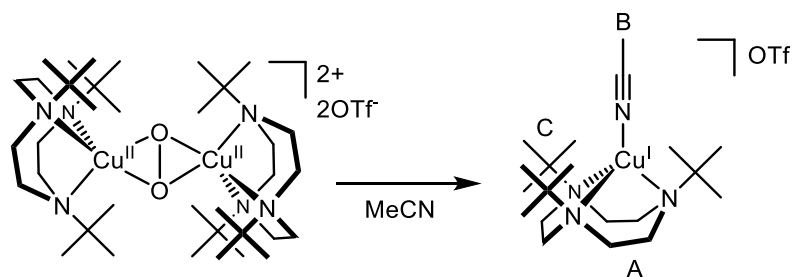


**Figure S10.** Decomposition of complex **3** in methanol with 2,4-di-*tert*-butylphenol as monitored by UV-Vis (Top – full spectra; bottom – pseudo first-order decay plot). Shown are representative wavelengths from full spectra taken every 30 minutes. The sample was made in the following manner: Complex **3** (0.00522g, 4.96 μmol, 1 equiv) and 2,4-di-*tert*-butylphenol (0.00881g, 42.7 μmol, 8.6 equiv) were dissolved in methanol (10mL). Then 4 mL of this solution was filtered over celite/cotton into a cuvette. The cuvette was sealed with a septum-topped cap and purged by bubbling a balloon of O<sub>2</sub> gas through the solution with an outlet. Another O<sub>2</sub> balloon was fitted onto the septum for analysis of the sample by UV-Vis.

## E. NMR Spectra



**Figure S11.** Representative example of conversion of benzoin to benzil at  $50\text{ }^\circ\text{C}$  followed by  $^1\text{H}$  NMR.

Solvent Decomposition of Complex **3** in Acetonitrile

Complex **3** was dissolved in acetonitrile until decomposition was complete (solution becomes clear and colorless). Solvent was removed *in vacuo*, and solid remaining

was dissolved in  $\text{CDCl}_3$ , leading to the  $^1\text{H}$  NMR spectrum shown below. Note: Asterisks (\*) mark the position of solvent peaks (chloroform, acetone, free acetonitrile, water, and tetramethylsilane).

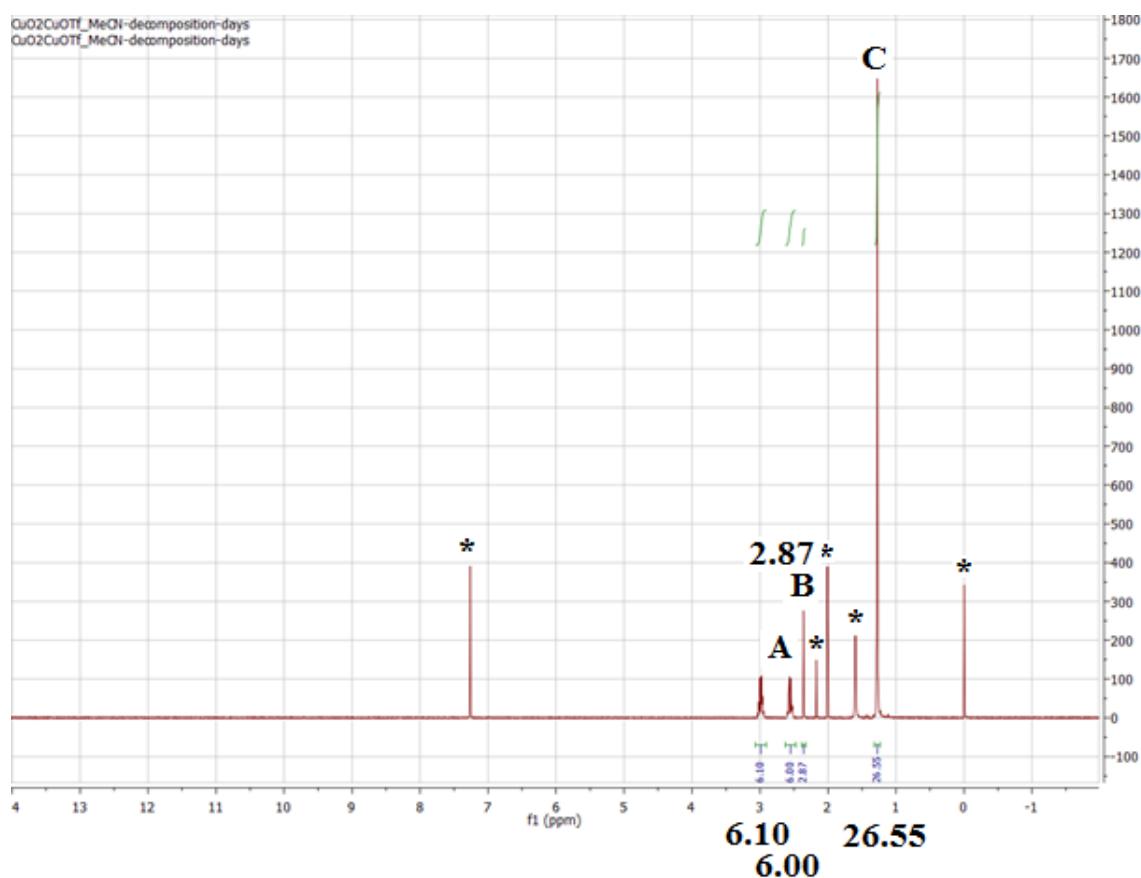
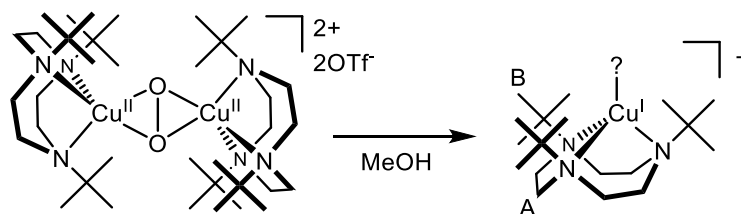


**Figure S12.** NMR of complex **1** generated from decomposition of **3** in acetonitrile.



*Solvent Decomposition of Complex 3 in Methanol.* Complex **3** was dissolved in methanol until decomposition was complete (solution becomes clear and colorless).

Solvent was removed *in vacuo*, and solid remaining was dissolved in  $\text{CDCl}_3$ , leading to



the  $^1\text{H}$  NMR spectrum shown below. Note: Asterisks (\*) mark the position of solvent peaks (chloroform, free methanol, water, and tetramethylsilane).

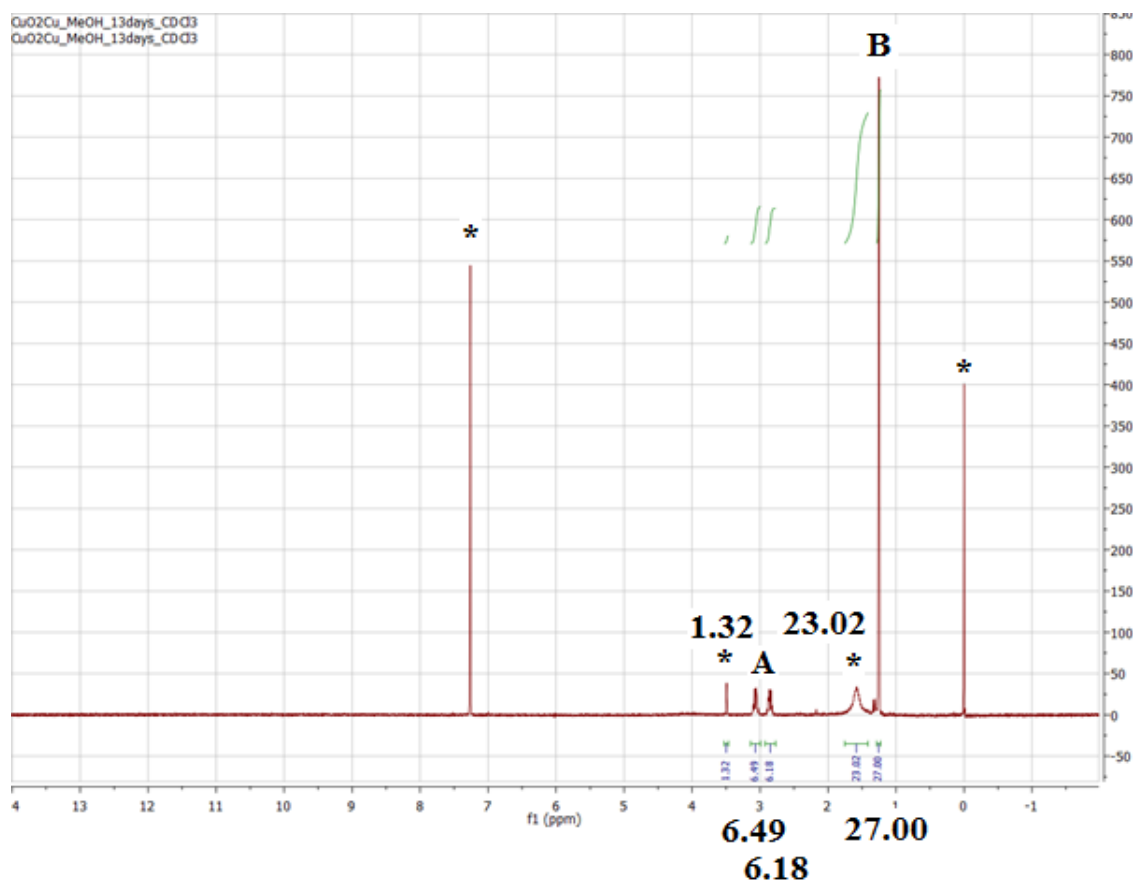
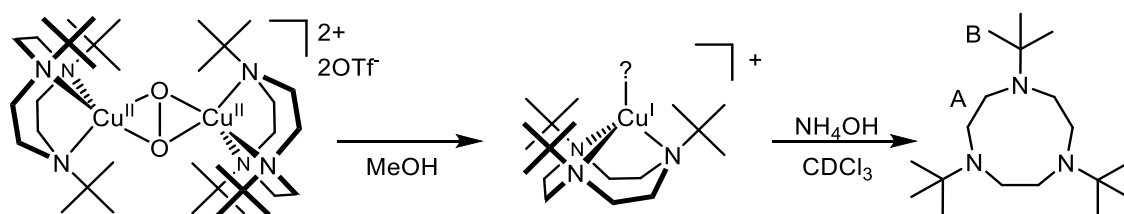
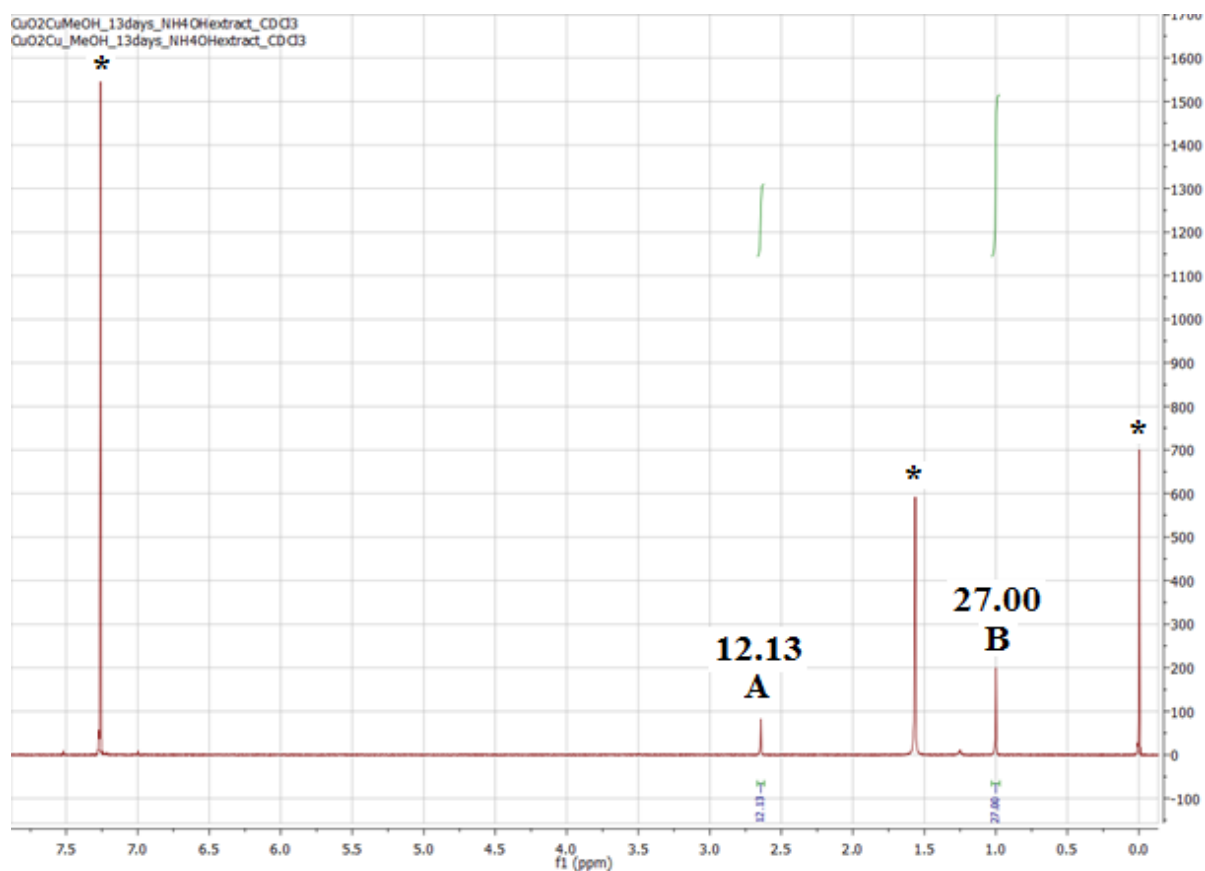


**Figure S13.** Decomposition of **3** in methanol leading to an unknown complex.

### Solvent Decomposition of Complex **3** in Methanol – Ligand Extraction

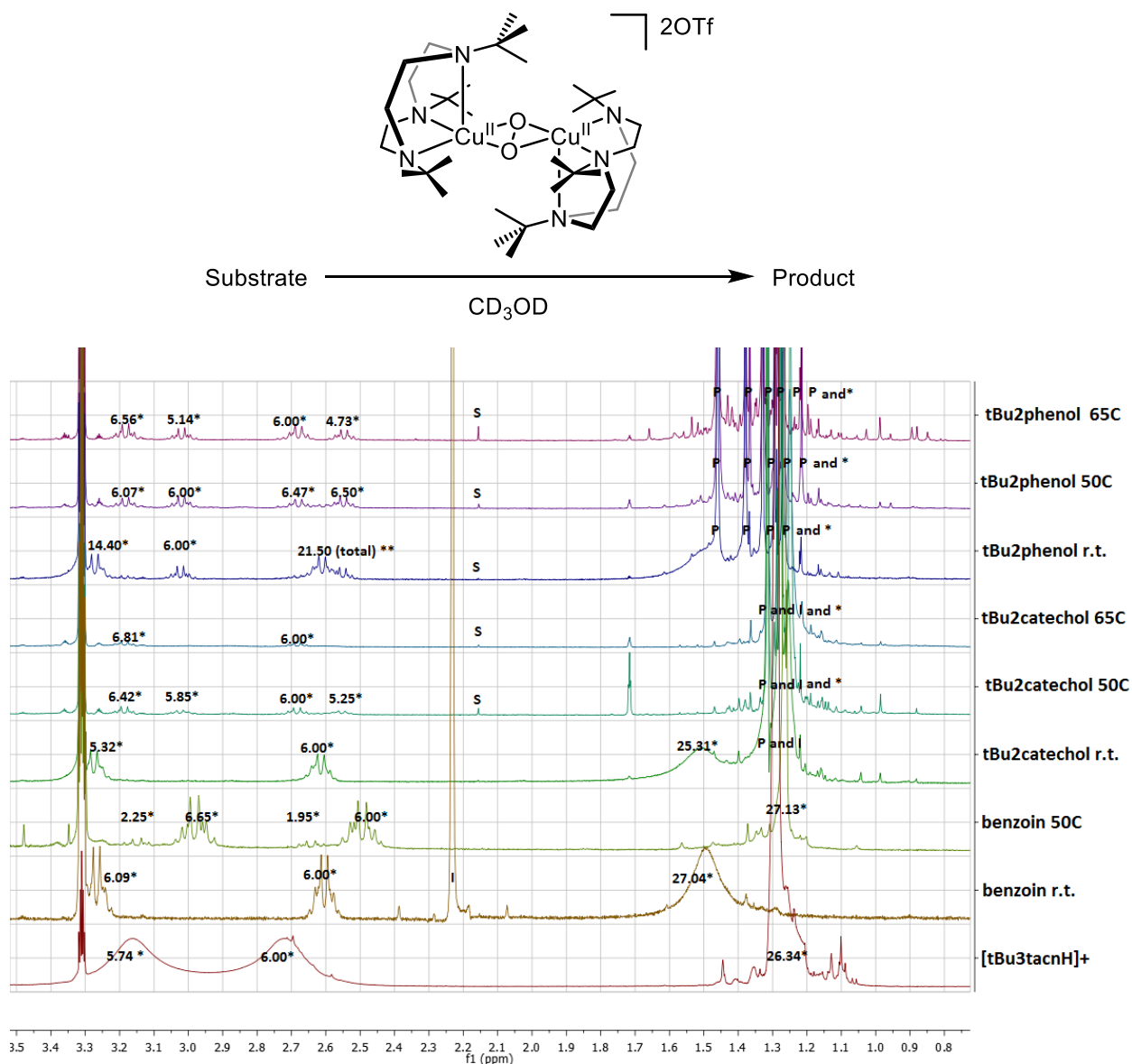


Following the formation of the breakdown product of complex **3** in methanol (*vide supra*), the solid is stirred in aqueous ammonium hydroxide for 15-30 minutes, during which the solution changed from colorless to blue. The organic components were extracted with chloroform. The solvent was removed from the organic layer *in vacuo*, and the solid dissolved in  $\text{CDCl}_3$ , leading to the  $^1\text{H}$  NMR spectrum shown below. Note: Asterisks (\*) mark the position of solvent peaks (chloroform, water, and tetramethylsilane).



**Figure S14.**  $^1\text{H}$  NMR of the extract of  $\text{NH}_4\text{OH}$  demetallation of the complex derived from decomposition of **3** in methanol.





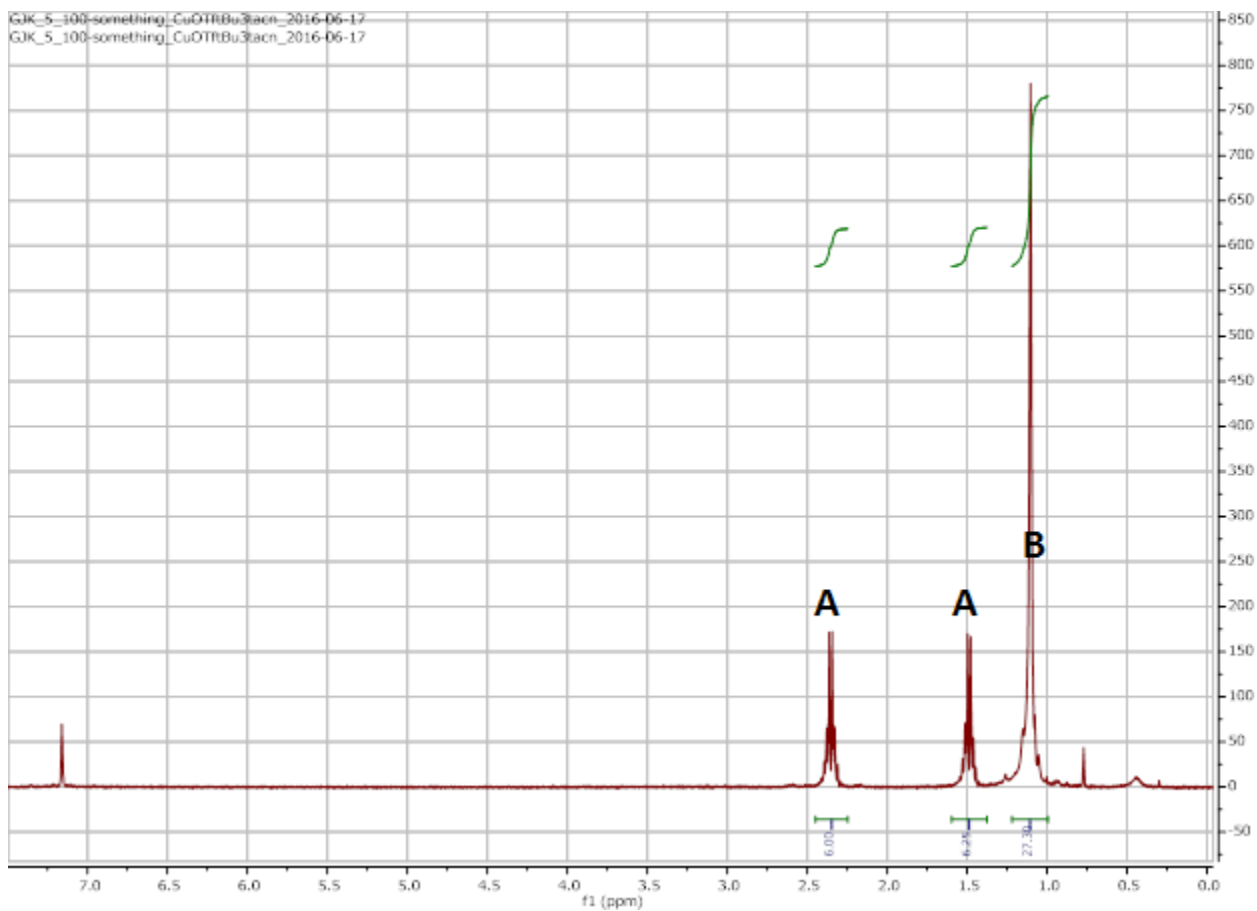
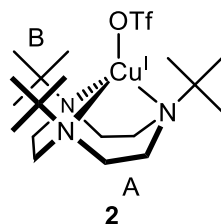


**Figure S16.**  $^1\text{H}$  NMR spectrum of **2** in  $\text{CDCl}_3$  showing the characteristic splitting pattern of ethyl bridge peaks of  $^t\text{Bu}_3\text{tacn}$  bound to copper.

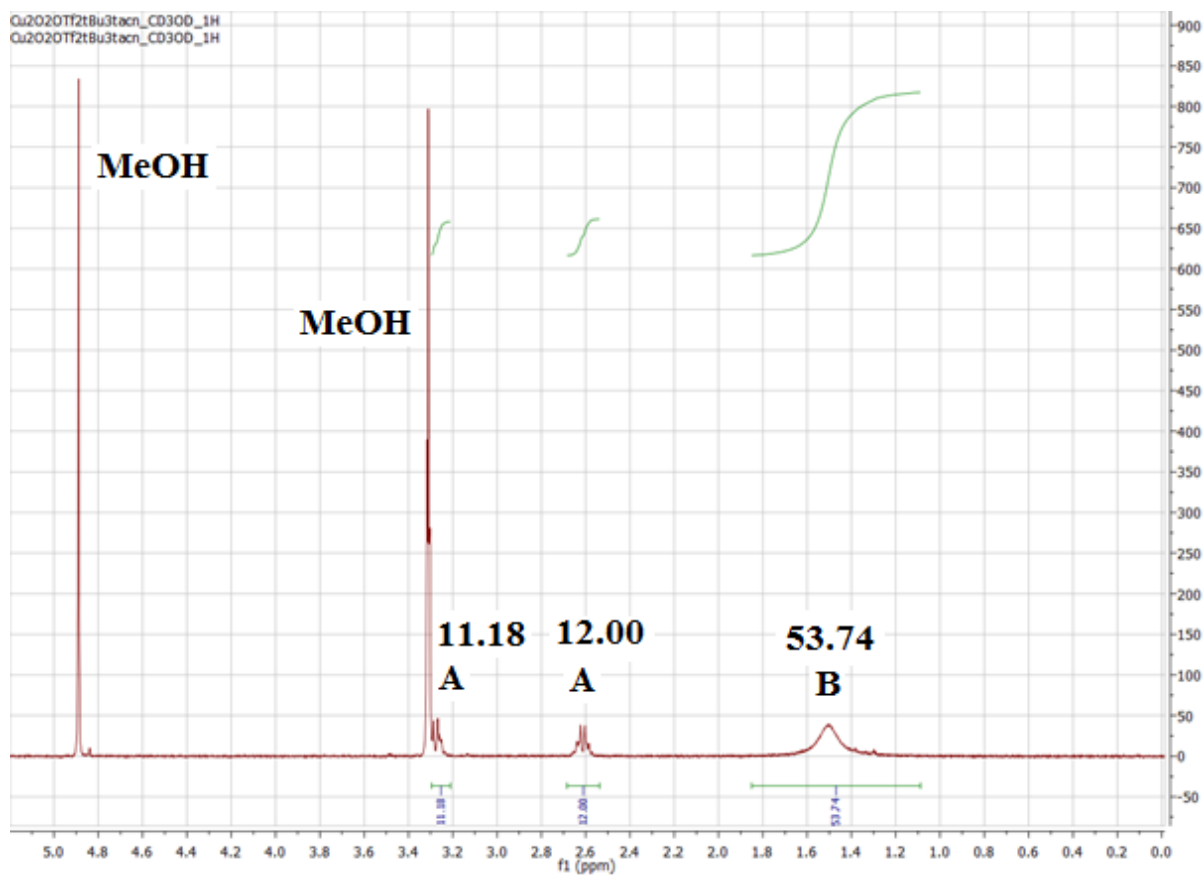
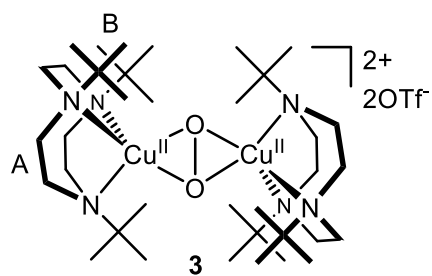
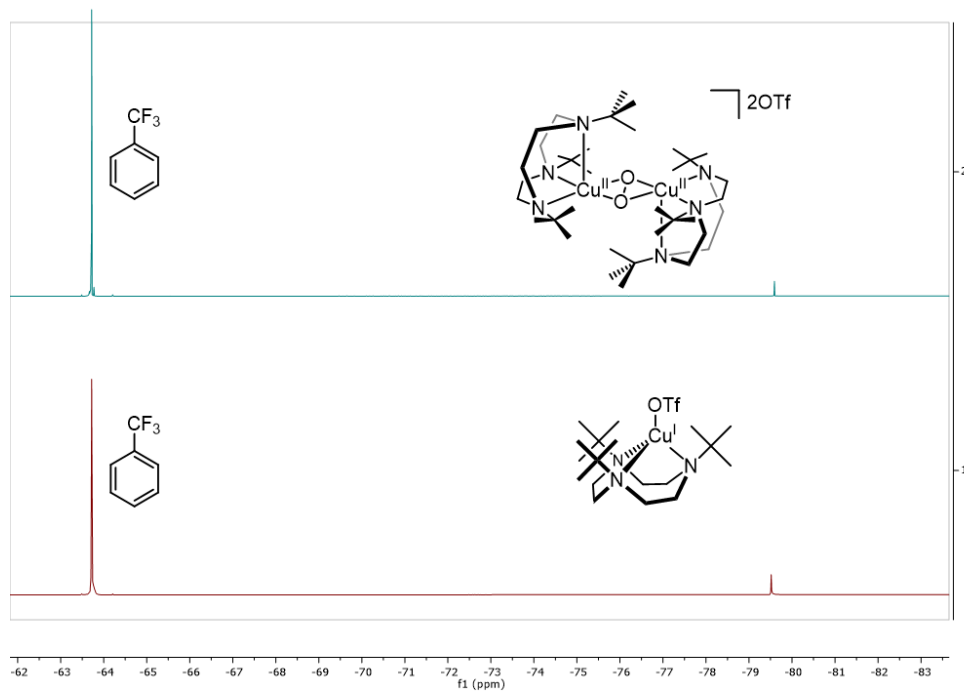
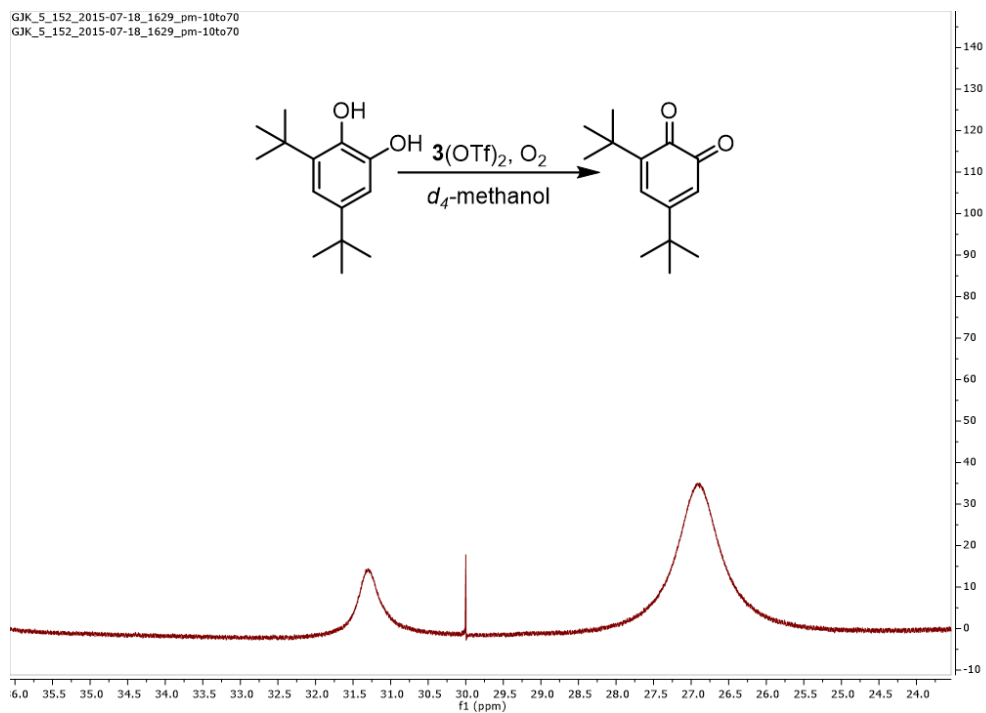


Figure S17.  $^1\text{H}$  NMR of the diamagnetic complex  $3(\text{OTf})_2$  in  $d_4$ -methanol.



**Figure S18.**  $^{19}\text{F}$  NMR spectra of complex **3** (top) and complex **2** (bottom) referenced to  $\text{CF}_3$ toluene (set to -63.72 ppm).



**Figure S19.** Shifted peaks in the paramagnetic spectrum of a reaction converting 3,5-di-*tert*-butylcatechol to 3,5-di-*tert*-butyl-*o*-quinone with  $3(\text{OTf})_2$ .

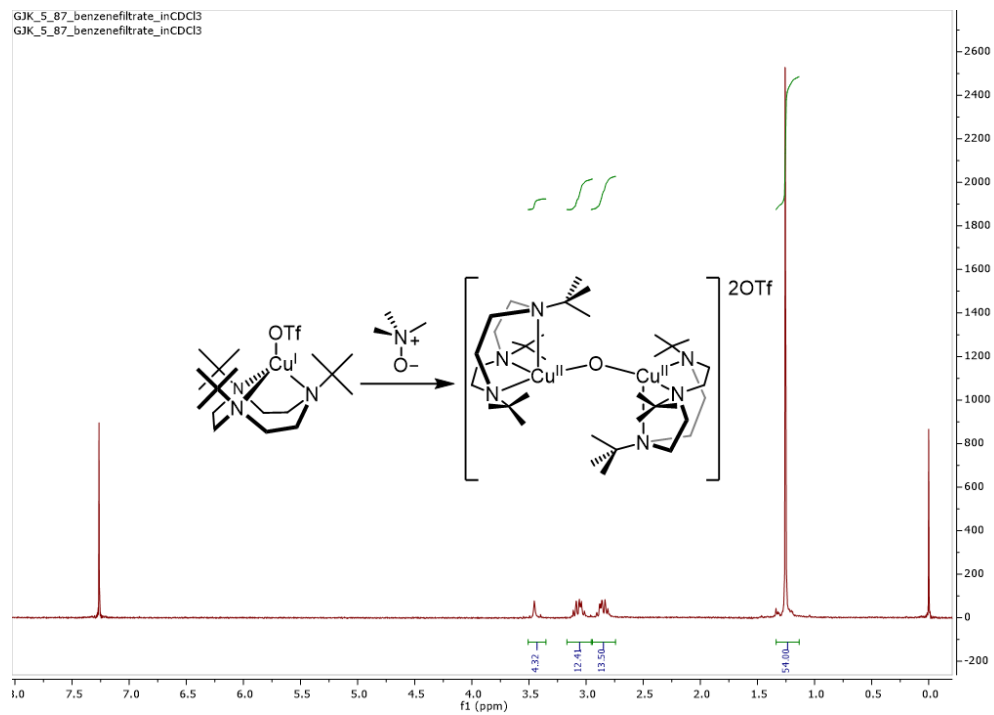


**Figure S20.**  $^1\text{H}$  NMR spectrum in  $\text{CDCl}_3$  of the product of the reaction between **2** and trimethylamine N-oxide.

*Equilibration of Amide Rotamers*

\* Indicates Solvent Peak; # Indicates Internal Standard

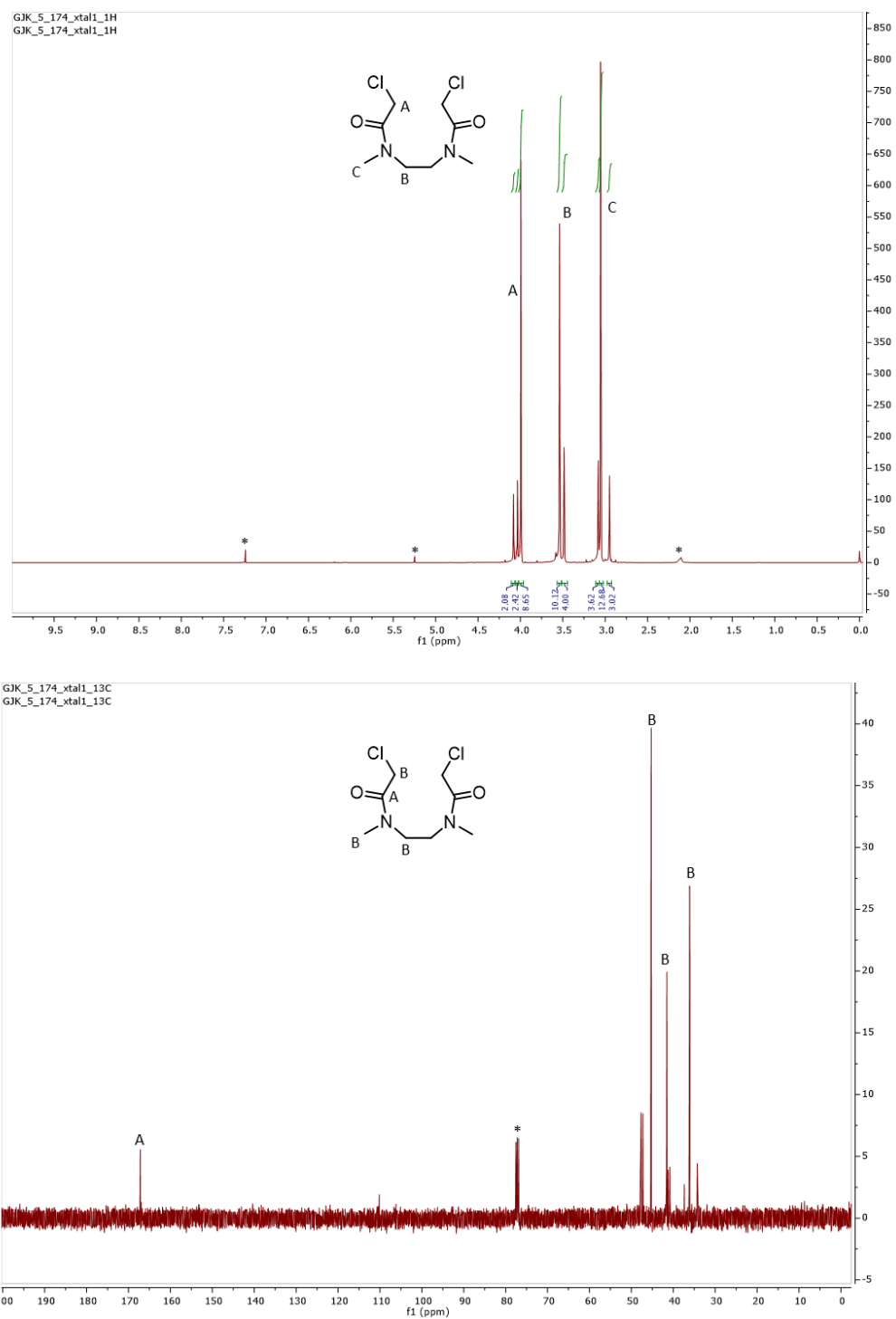


**Figure S21.** <sup>1</sup>H (top) and <sup>13</sup>C (bottom) spectra of Me6 in chloroform at room temperature.

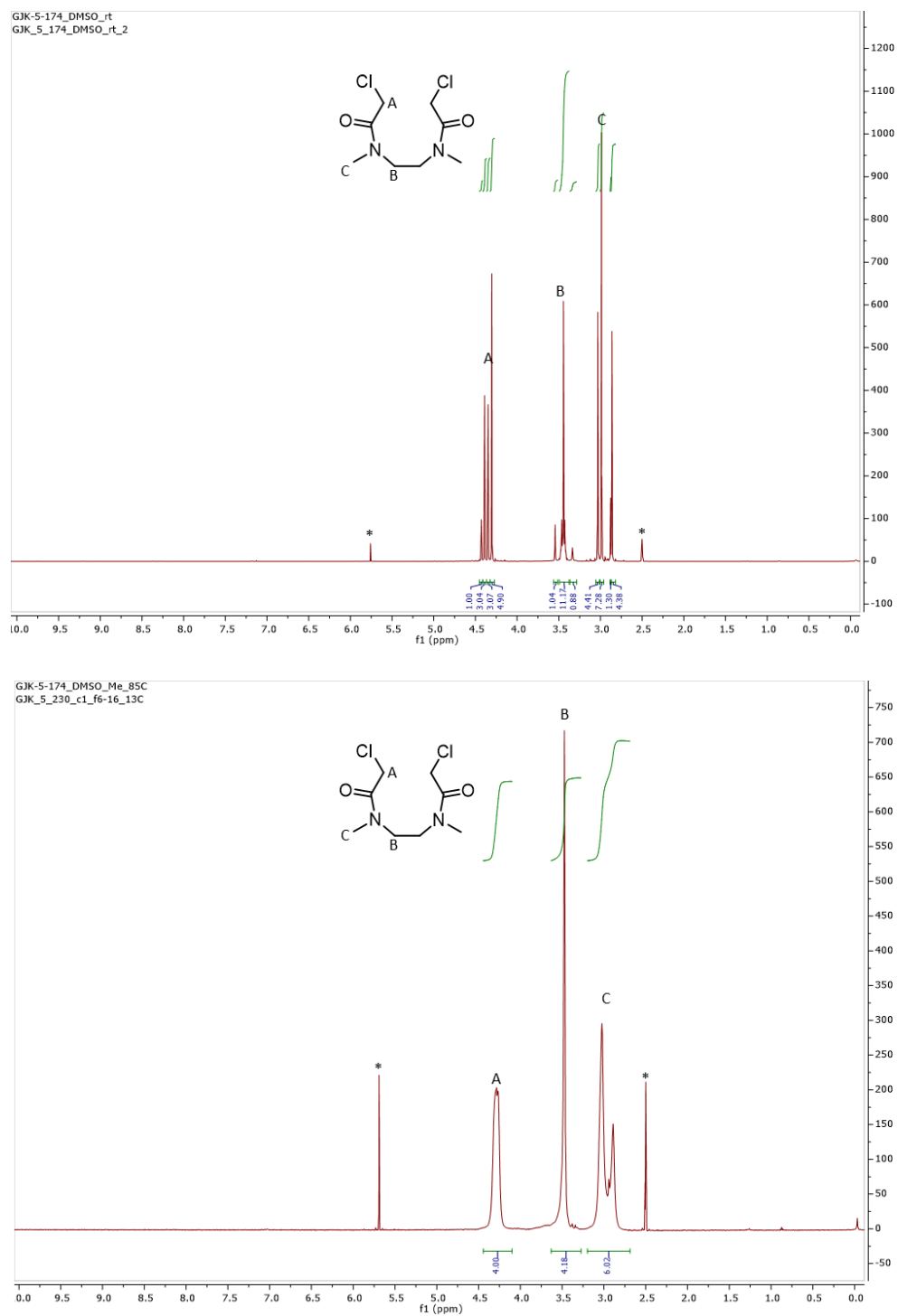


Figure S22.  $^1\text{H}$  NMR of **Me6** in  $d_6$ -DMSO at room temperature (top) and at 85 °C (bottom).

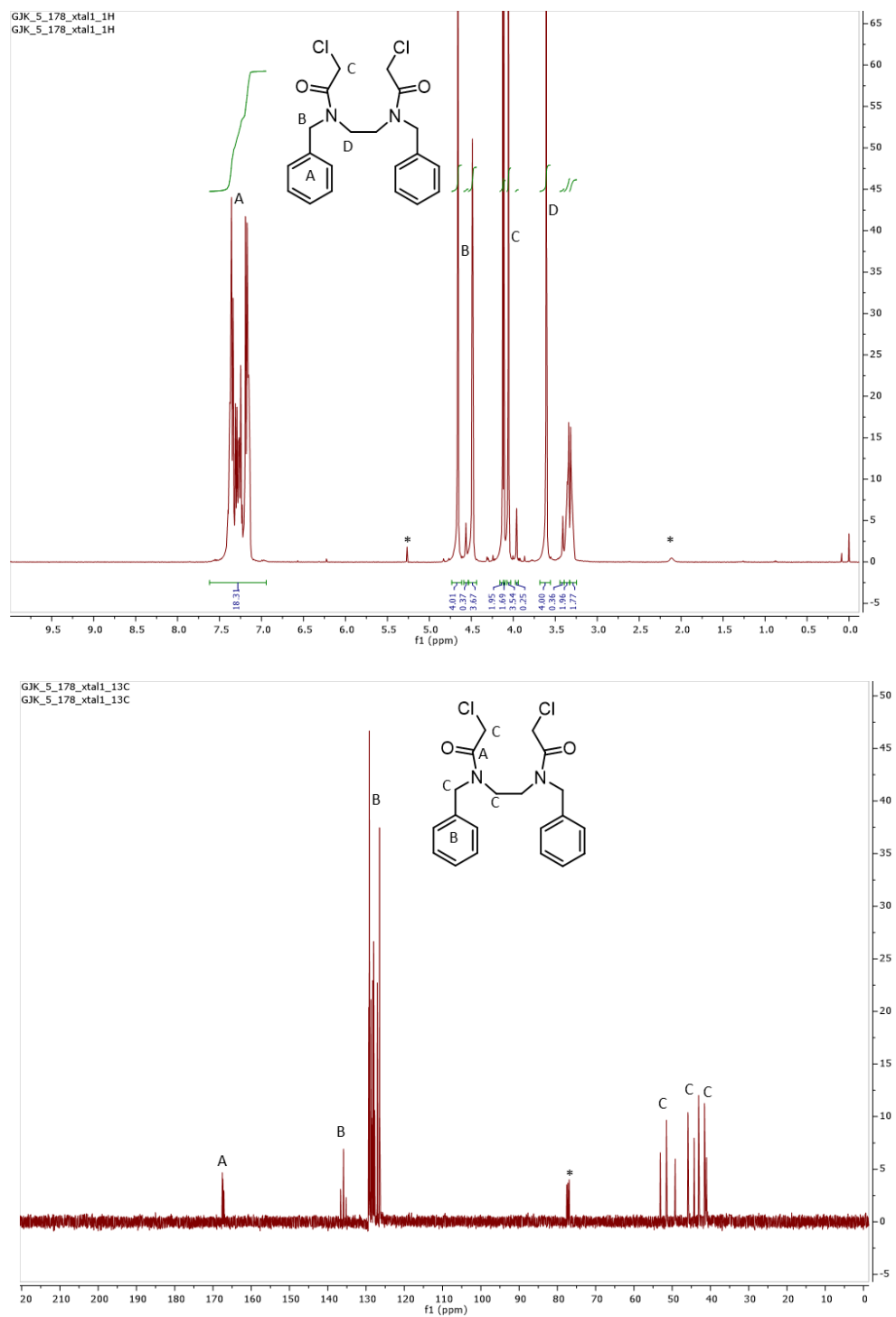


Figure S23.  $^1\text{H}$  (top) and  $^{13}\text{C}$  (bottom) spectra of **Bn6** in chloroform at room temperature.



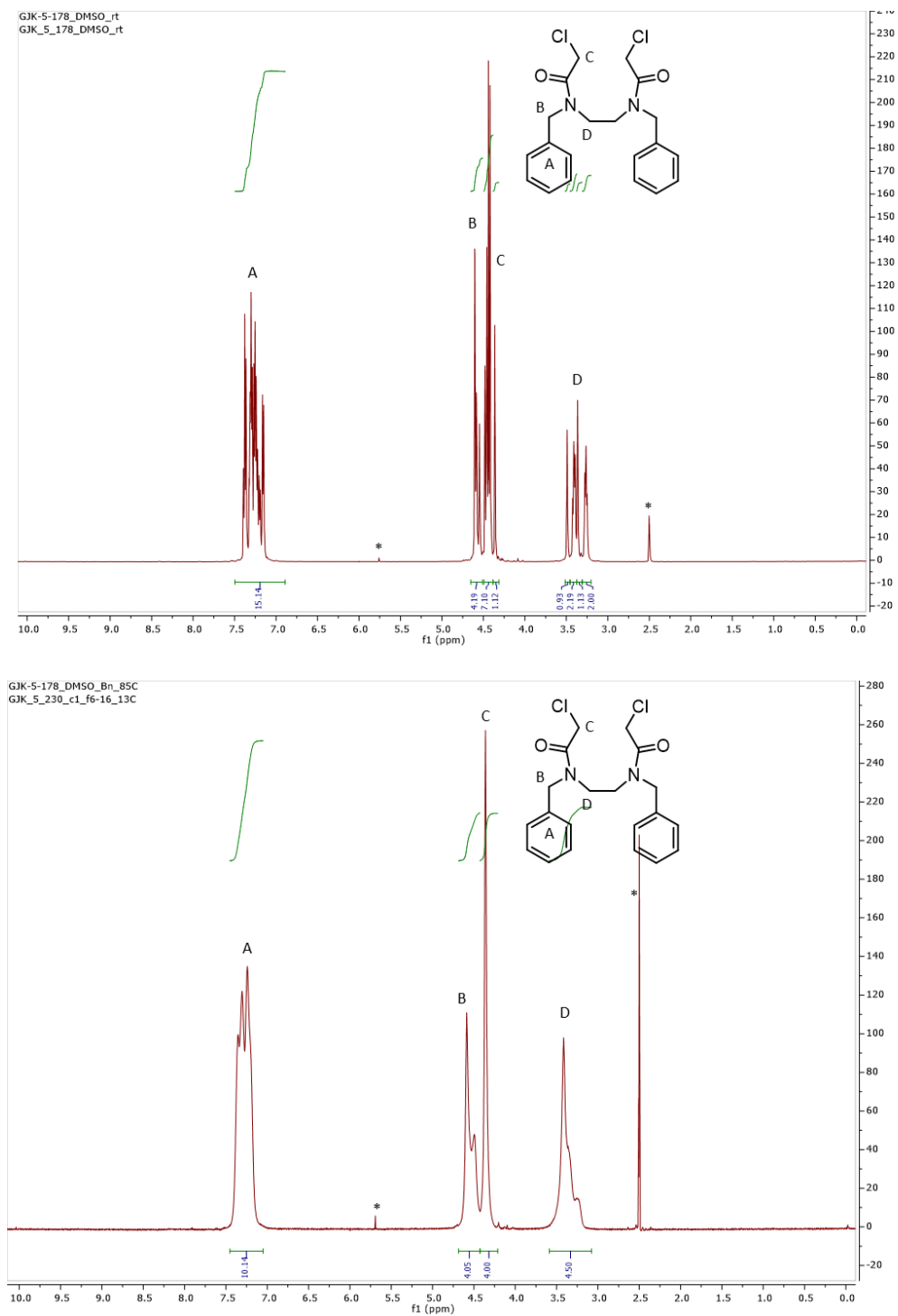


Figure S24.  $^1\text{H}$  NMR of **Bn6** in  $d_6$ -DMSO at room temperature (top) and at  $85\text{ }^\circ\text{C}$  (bottom).

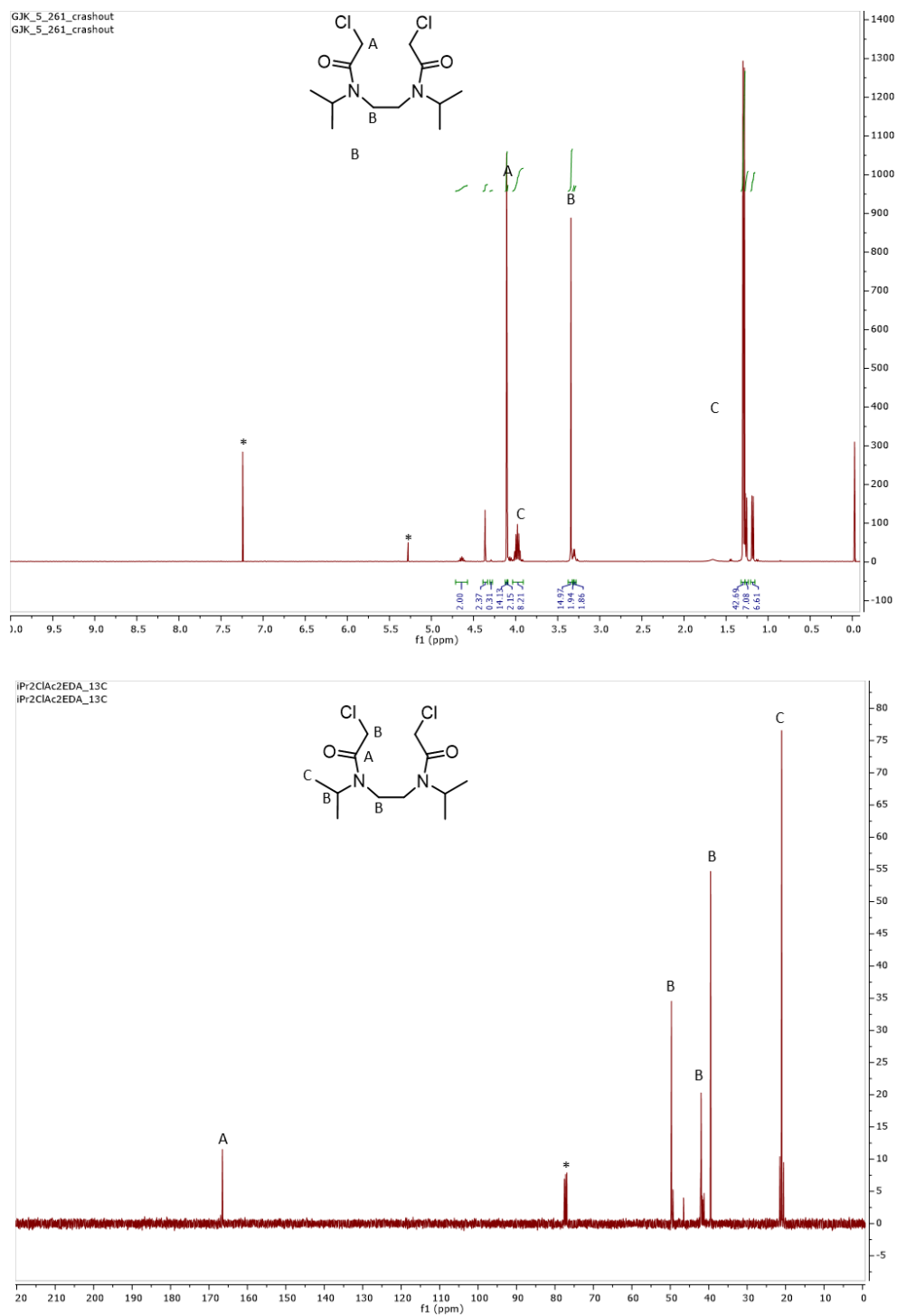


Figure S25.  $^1\text{H}$  (top) and  $^{13}\text{C}$  (bottom) spectra of  $i\text{Pr}_6$  in chloroform at room temperature.

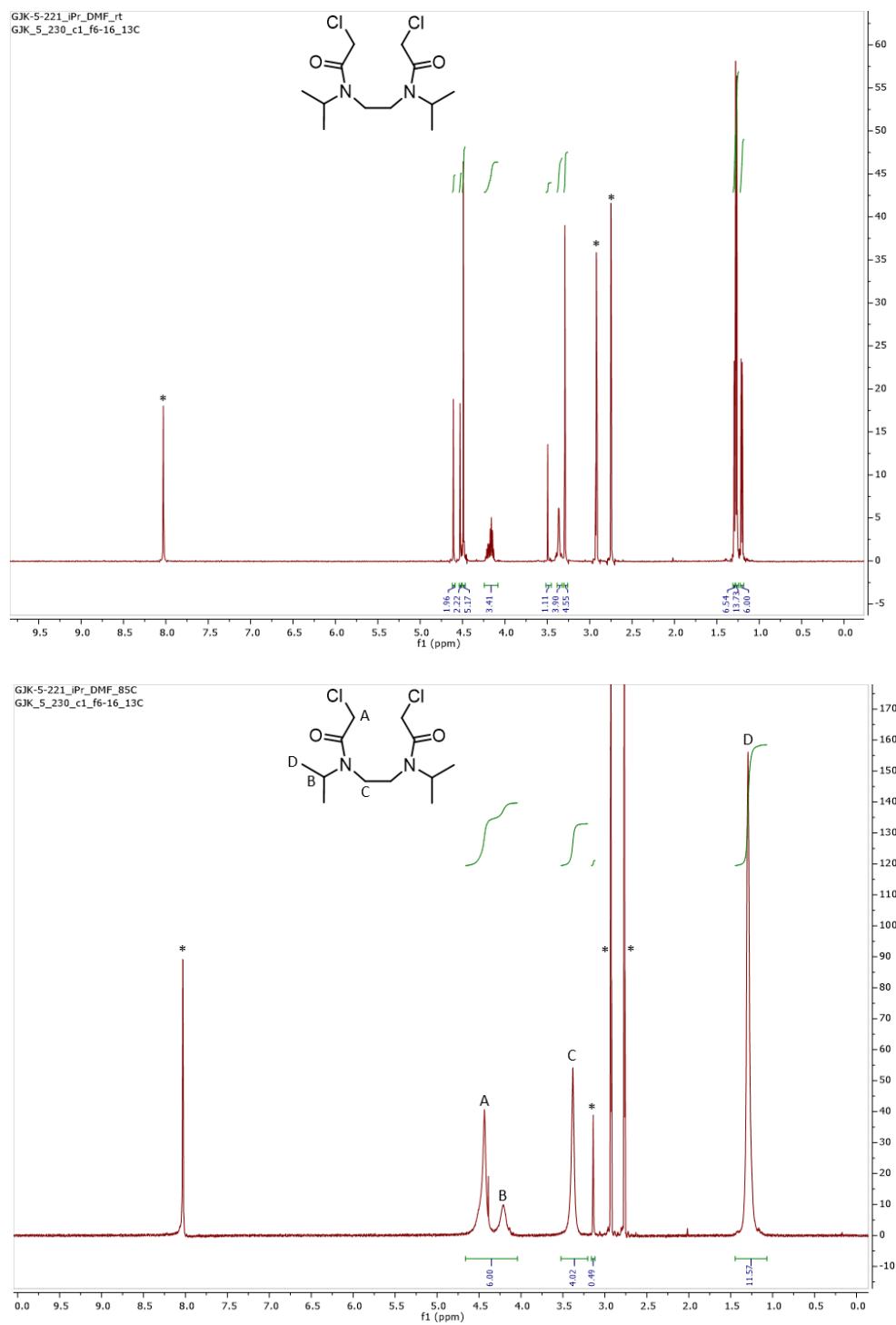
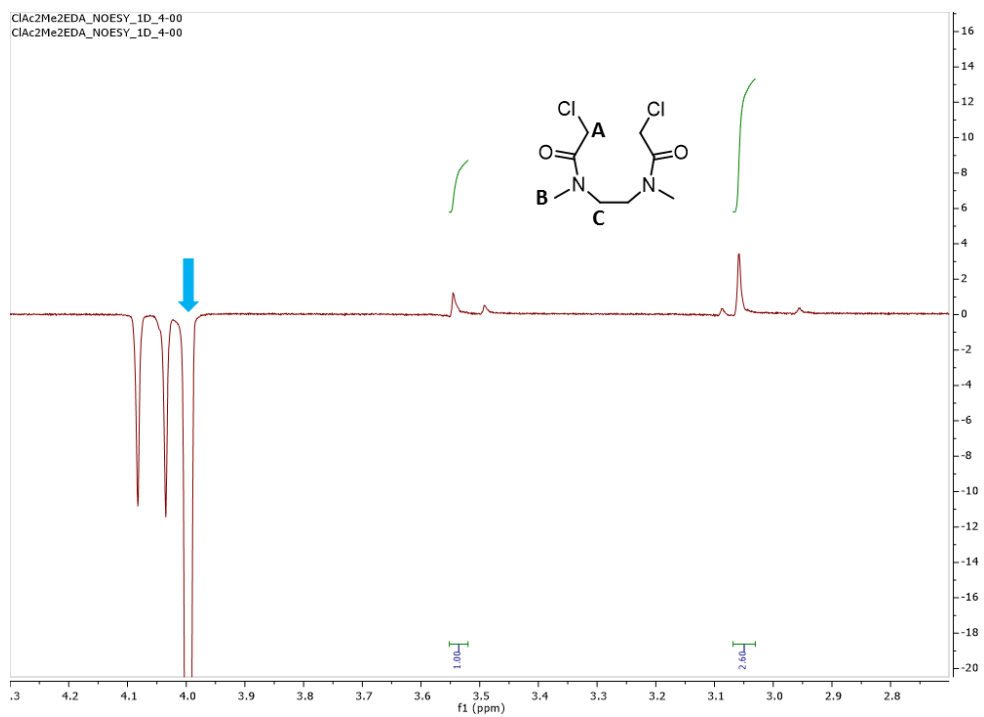
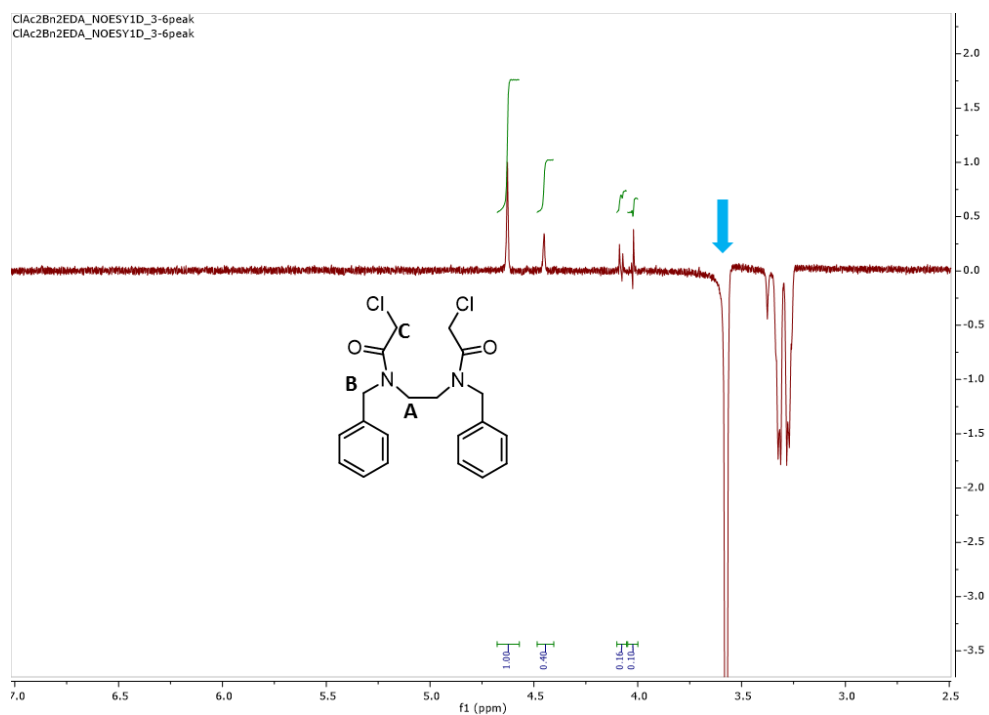


Figure S26.  $^1\text{H}$  NMR of  $^{1}\text{Pr}6$  in  $d_6$ -DMF at room temperature (top) and at  $85\text{ }^\circ\text{C}$  (bottom).



**Figure S27.** NOE spectrum of  $\text{Me}6$  (irradiation indicated by arrow, corresponding to protons labeled A). Though many peaks are enhanced, the peaks corresponding to B (integration 2.60; 0.43 integration/H) has a higher enhanced-integration-per-proton than peaks corresponding to C (integration 1.00; 0.25 integration/H). This may suggest A is closer to B than to C.



**Figure S28.** NOE spectrum of  $\text{Bn}6$  (irradiation indicated by arrow, corresponding to protons labeled A). Though many peaks are enhanced, the peaks corresponding to B (integration 1.00; 0.25 integration/H) has a

higher enhanced-integration-per-proton than peaks corresponding to C (integration 0.10; 0.025 integration/H). This may suggest A is closer to B than to C.

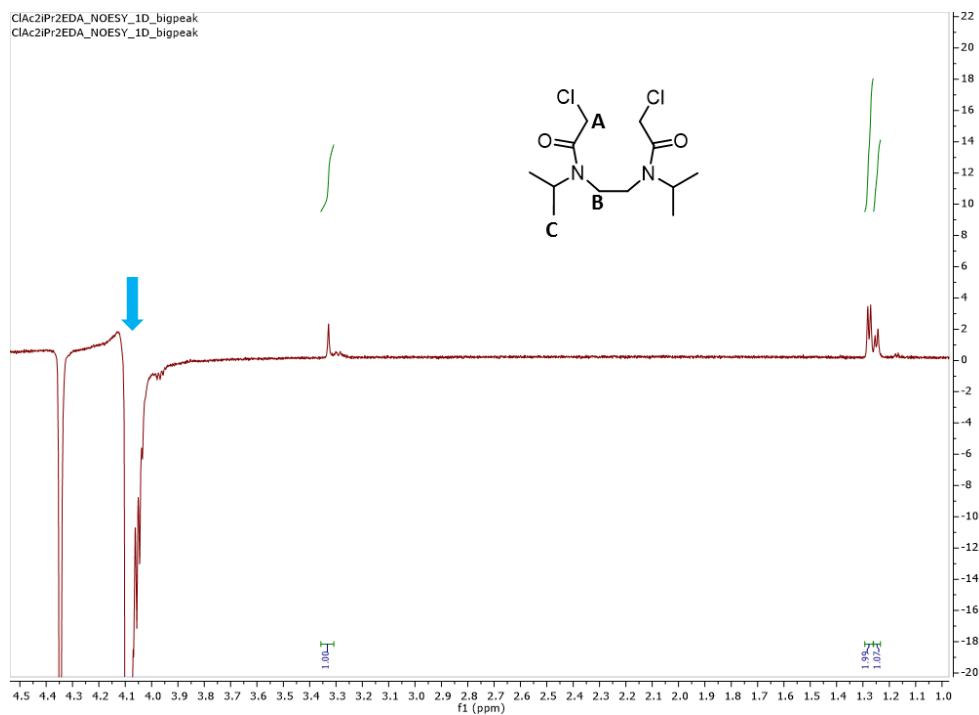


**Figure S29.** NOE spectrum of  $1\text{Pr}6$  (irradiation indicated by arrow, corresponding to protons labeled A). Though many peaks are enhanced, the peaks corresponding to B (integration 1.00; 0.25 integration/H) has a higher enhanced-integration-per-proton than peaks corresponding to C (integration 1.99; 0.17 integration/H). This may suggest A is closer to B than to C.

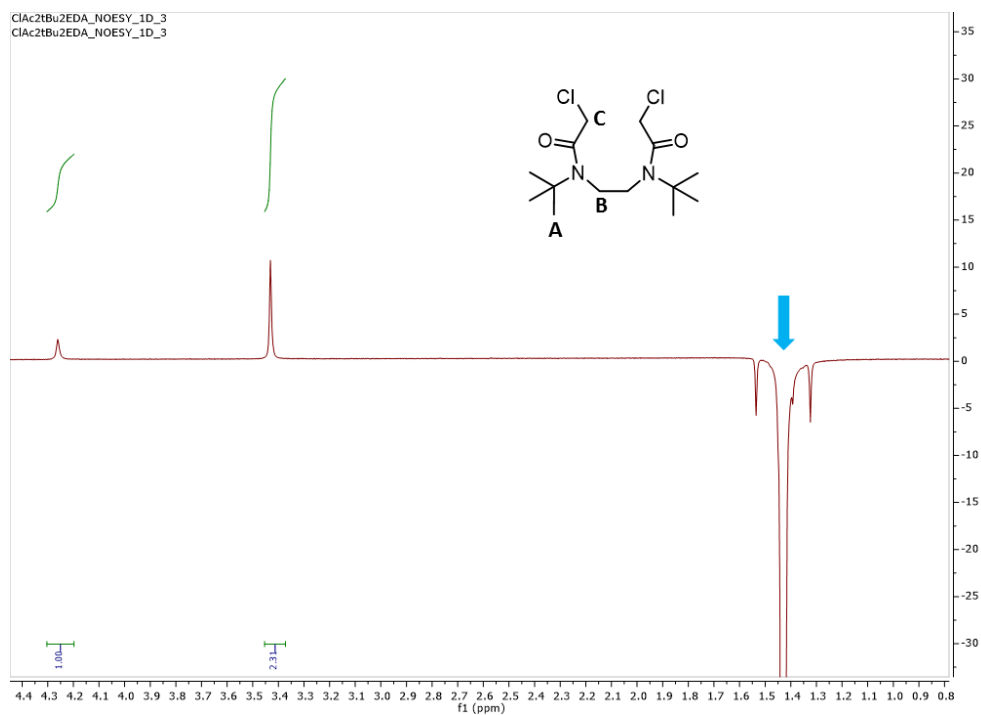


**Figure S30.** NOE spectrum of  $t\text{Bu}6$  (irradiation indicated by arrow, corresponding to protons labeled A). Though many peaks are enhanced, the peaks corresponding to B (integration 2.31; 0.58 integration/H) has a higher enhanced-integration-per-proton than peaks corresponding to C (integration 1.00; 0.25 integration/H). This may suggest A is closer to B than to C.

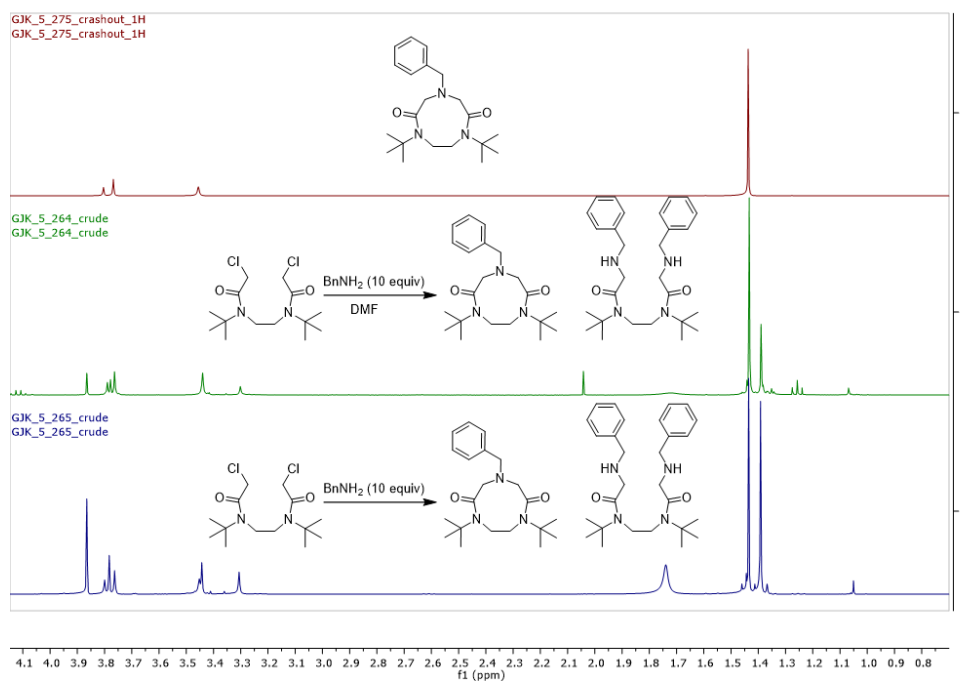


**Figure S31.** Stack plot of  $^1\text{H}$  NMR spectra of **10** (top) compared to the crude solids from reactions of  $t\text{Bu}6$  with 10 equivalents of benzylamine in DMF (middle) and without DMF (bottom).

## Nitrene Reactivity

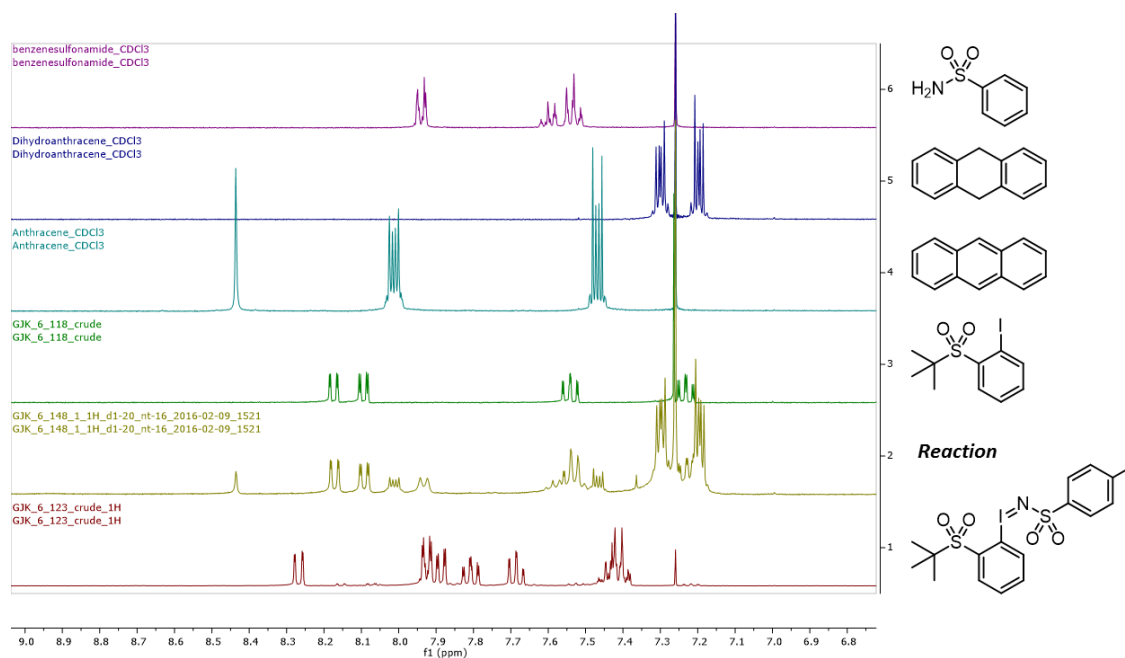


**Figure S32.** Stackplot of  $^1\text{H}$  NMR spectra of the reaction between **2**, **20**, and dihydroanthracene in DCM to various compounds potentially present in the reaction.

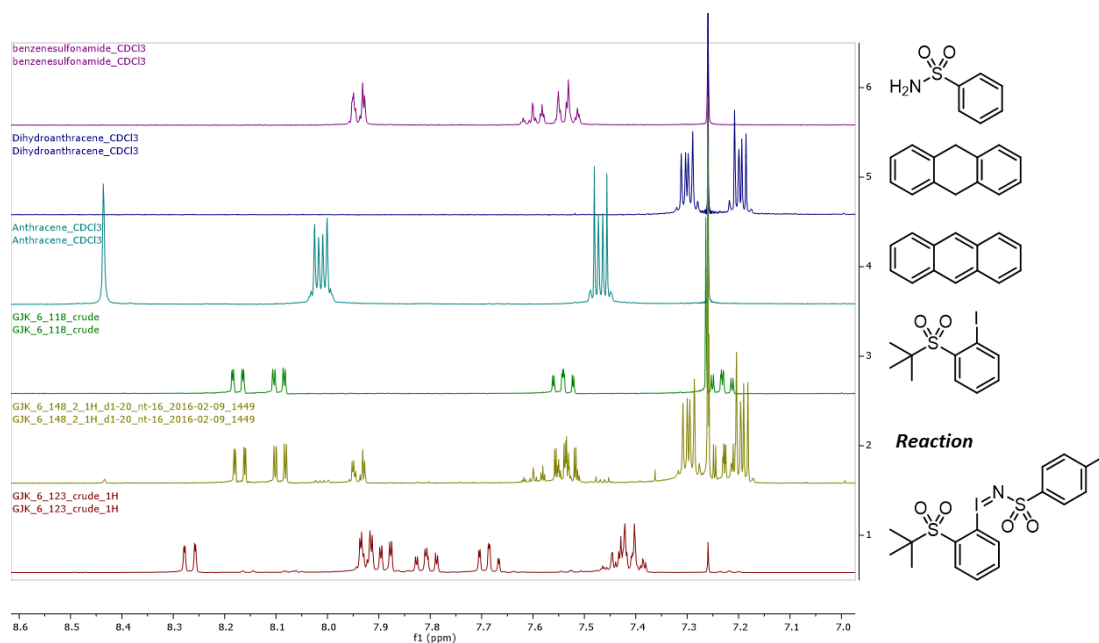


**Figure S33.** Stackplot of  $^1\text{H}$  NMR spectra of the reaction between **2**, **20**, and dihydroanthracene with  $\text{Sc}(\text{OTf})_3$  in DCM to various compounds potentially present in the reaction.

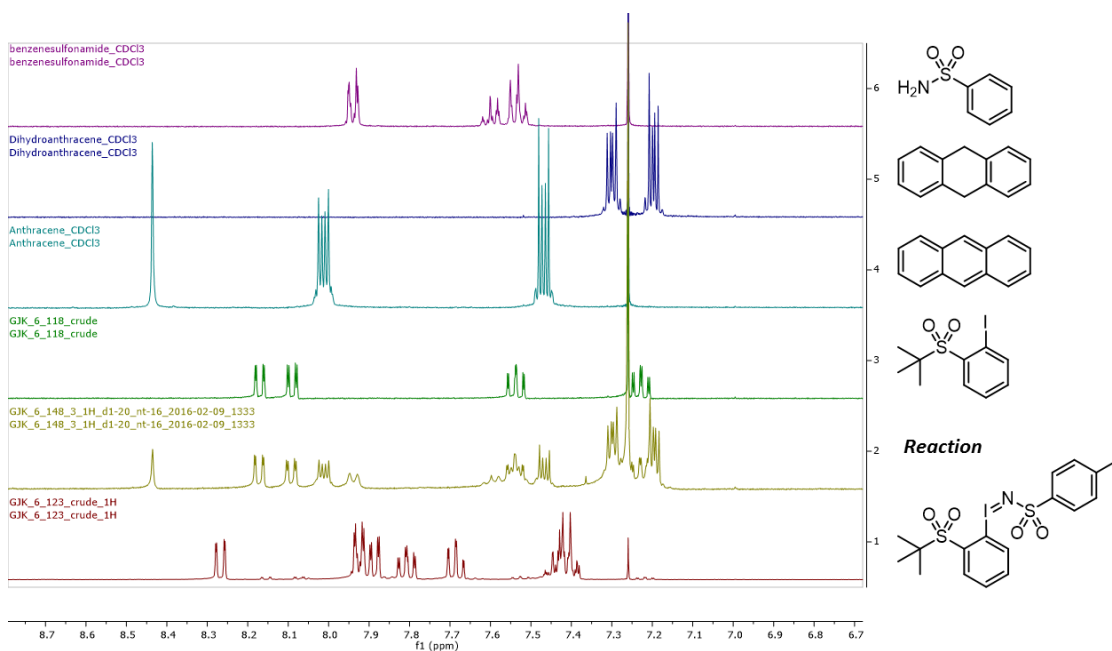


**Figure S34.** Stackplot of  $^1\text{H}$  NMR spectra of the reaction between **21**, **20**, and dihydroanthracene in DCM to various compounds potentially present in the reaction.

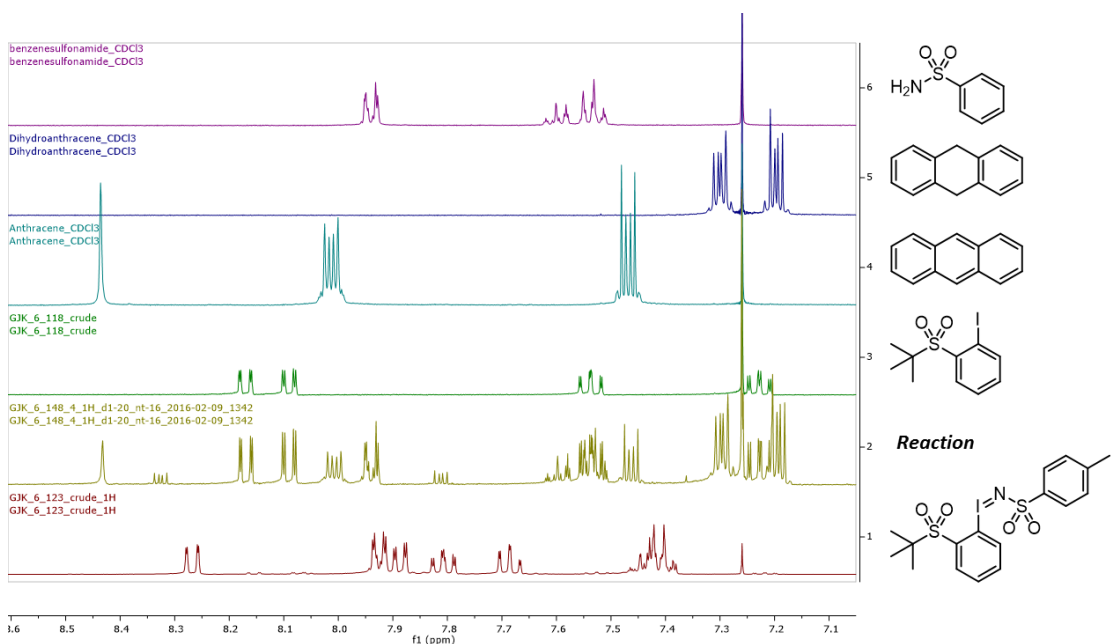


**Figure S35.** Stackplot of  $^1\text{H}$  NMR spectra of the reaction between **21**, **20**, and dihydroanthracene with  $\text{Sc}(\text{OTf})_3$  in DCM to various compounds potentially present in the reaction.



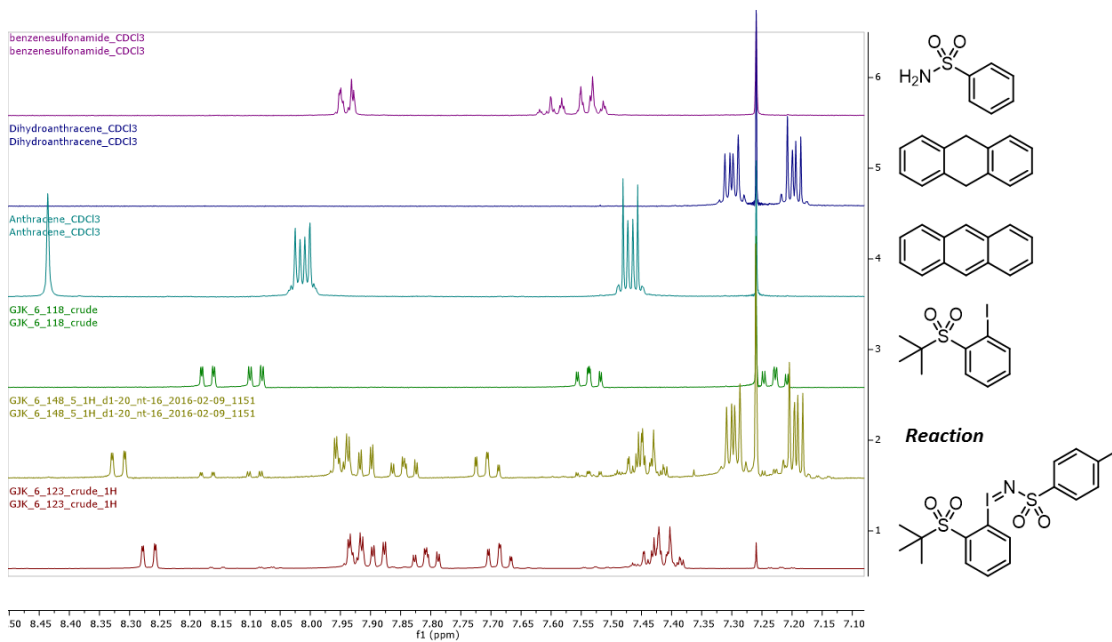


**Figure S36.** Stackplot of  $^1\text{H}$  NMR spectra of the reaction between **20** and dihydroanthracene (no copper) in DCM to various compounds potentially present in the reaction.

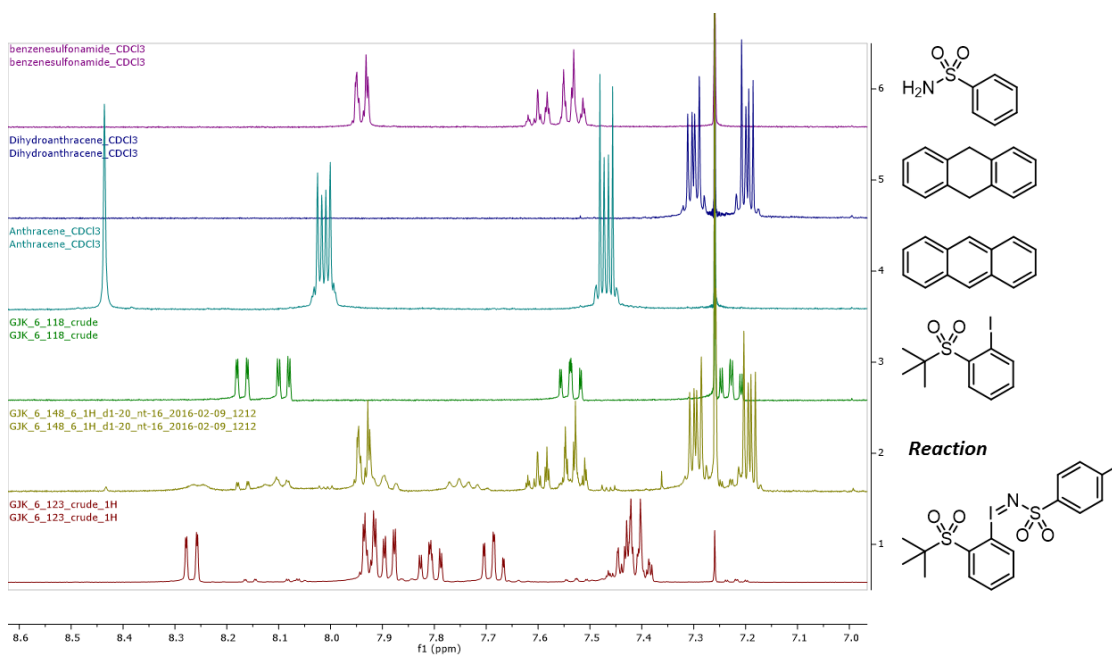


**Figure S37.** Stackplot of  $^1\text{H}$  NMR spectra of the reaction between **20** and dihydroanthracene with  $\text{Sc}(\text{OTf})_3$  (no copper) in DCM to various compounds potentially present in the reaction.

## VI. References

- (1) Shih, C.; Museth, A. K.; Abrahamsson, M.; Blanco-Rodriguez, A. M.; Di Bilio, A. J.; Sudhamsu, J.; Crane, B. R.; Ronayne, K. L.; Towrie, M.; Vlček, A.; Richards, J. H.; Winkler, J. R.; Gray, H. B. *Science* **2008**, *320*, 1760-1762.
- (2) Pauleta, S. R.; Dell'Acqua, S.; Moura, I. *Coordination Chemistry Reviews* **2013**, *257*, 332-349.
- (3) Li, Y.; Hodak, M.; Bernholc, J. *Biochemistry* **2015**, *54*, 1233-1242.
- (4) Solomon, E. I.; Heppner, D. E.; Johnston, E. M.; Ginsbach, J. W.; Cirera, J.; Qayyum, M.; Kieber-Emmons, M. T.; Kjaergaard, C. H.; Hadt, R. G.; Tian, L. *Chemical Reviews* **2014**, *114*, 3659-3853.
- (5) Gordon, R. B.; Bertram, M.; Graedel, T. E. *Proceedings of the National Academy of Sciences* **2006**, *103*, 1209-1214.
- (6) Allen, S. E.; Walvoord, R. R.; Padilla-Salinas, R.; Kozlowski, M. C. *Chemical Reviews* **2013**, *113*, 6234-6458.
- (7) Constable, D. J. C.; Dunn, P. J.; Hayler, J. D.; Humphrey, G. R.; Leazer, J. J. L.; Linderman, R. J.; Lorenz, K.; Manley, J.; Pearlman, B. A.; Wells, A.; Zaks, A.; Zhang, T. *Y. Green Chemistry* **2007**, *9*, 411-420.
- (8) Wang, Y.; DuBois, J. L.; Hedman, B.; Hodgson, K. O.; Stack, T. D. P. *Science* **1998**, *279*, 537-540.
- (9) Klinman, J. P. *Journal of Biological Chemistry* **2006**, *281*, 3013-3016.
- (10) Prigge, S. T.; Eipper, B. A.; Mains, R. E.; Amzel, L. M. *Science* **2004**, *304*, 864-867.
- (11) Mirica, L. M.; Vance, M.; Rudd, D. J.; Hedman, B.; Hodgson, K. O.; Solomon, E. I.; Stack, T. D. P. *Science* **2005**, *308*, 1890-1892.

- (12) Balasubramanian, R.; Rosenzweig, A. C. *Accounts of Chemical Research* **2007**, *40*, 573-580.
- (13) Balasubramanian, R.; Smith, S. M.; Rawat, S.; Yatsunyk, L. A.; Stemmler, T. L.; Rosenzweig, A. C. *Nature* **2010**, *465*, 115-119.
- (14) Culpepper, M. A.; Cutsail, G. E.; Hoffman, B. M.; Rosenzweig, A. C. *Journal of the American Chemical Society* **2012**, *134*, 7640-7643.
- (15) Solomon, E. I.; Ginsbach, J. W.; Heppner, D. E.; Kieber-Emmons, M. T.; Kjaergaard, C. H.; Smeets, P. J.; Tian, L.; Woertink, J. S. *Faraday Discussions* **2011**, *148*, 11-39.
- (16) Lewis, E. A.; Tolman, W. B. *Chemical Reviews* **2004**, *104*, 1047-1076.
- (17) Mirica, L. M.; Ottenwaelder, X.; Stack, T. D. P. *Chemical Reviews* **2004**, *104*, 1013-1046.
- (18) Halfen, J. A.; Mahapatra, S.; Wilkinson, E. C.; Kaderli, S.; Young, V. G.; Que, L.; Zuberbühler, A. D.; Tolman, W. B. *Science* **1996**, *271*, 1397-1400.
- (19) Obias, H. V.; Lin, Y.; Murthy, N. N.; Pidcock, E.; Solomon, E. I.; Ralle, M.; Blackburn, N. J.; Neuhold, Y.-M.; Zuberbühler, A. D.; Karlin, K. D. *Journal of the American Chemical Society* **1998**, *120*, 12960-12961.
- (20) Cahoy, J.; Holland, P. L.; Tolman, W. B. *Inorganic Chemistry* **1999**, *38*, 2161-2168.
- (21) Pidcock, E.; DeBeer, S.; Obias, H. V.; Hedman, B.; Hodgson, K. O.; Karlin, K. D.; Solomon, E. I. *Journal of the American Chemical Society* **1999**, *121*, 1870-1878.
- (22) Mahadevan, V.; Henson, M. J.; Solomon, E. I.; Stack, T. D. P. *Journal of the American Chemical Society* **2000**, *122*, 10249-10250.
- (23) Mirica, L. M.; Vance, M.; Rudd, D. J.; Hedman, B.; Hodgson, K. O.; Solomon, E. I.; Stack, T. D. P. *Journal of the American Chemical Society* **2002**, *124*, 9332-9333.

- (24) Henson, M. J.; Vance, M. A.; Zhang, C. X.; Liang, H.-C.; Karlin, K. D.; Solomon, E. I. *Journal of the American Chemical Society* **2003**, *125*, 5186-5192.
- (25) Stack, T. D. P. *Dalton Transactions* **2003**, 1881-1889.
- (26) Zhang, C. X.; Liang, H.-C.; Kim, E.-i.; Shearer, J.; Helton, M. E.; Kim, E.; Kaderli, S.; Incarvito, C. D.; Zuberbühler, A. D.; Rheingold, A. L.; Karlin, K. D. *Journal of the American Chemical Society* **2003**, *125*, 634-635.
- (27) Liang, H.-C.; Henson, M. J.; Hatcher, L. Q.; Vance, M. A.; Zhang, C. X.; Lahti, D.; Kaderli, S.; Sommer, R. D.; Rheingold, A. L.; Zuberbühler, A. D.; Solomon, E. I.; Karlin, K. D. *Inorganic Chemistry* **2004**, *43*, 4115-4117.
- (28) Hatcher, L. Q.; Vance, M. A.; Narducci Sarjeant, A. A.; Solomon, E. I.; Karlin, K. D. *Inorganic Chemistry* **2006**, *45*, 3004-3013.
- (29) Ottenwaelder, X.; Rudd, D. J.; Corbett, M. C.; Hodgson, K. O.; Hedman, B.; Stack, T. D. P. *Journal of the American Chemical Society* **2006**, *128*, 9268-9269.
- (30) Q. Hatcher, L.; D. Karlin, K., Ligand Influences in Copper-Dioxygen Complex-Formation and Substrate Oxidations. In *Advances in Inorganic Chemistry*, Eldik, R. v.; Reedijk, J., Eds. Academic Press: 2006; Vol. Volume 58, pp 131-184.
- (31) Maiti, D.; Woertink, J. S.; Narducci Sarjeant, A. A.; Solomon, E. I.; Karlin, K. D. *Inorganic Chemistry* **2008**, *47*, 3787-3800.
- (32) Mahapatra, S.; Kaderli, S.; Llobet, A.; Neuhold, Y.-M.; Palanché, T.; Halfen, J. A.; Young, V. G.; Kaden, T. A.; Que, L.; Zuberbühler, A. D.; Tolman, W. B. *Inorganic Chemistry* **1997**, *36*, 6343-6356.
- (33) Karlin, K. D.; Tyeklar, Z.; Farooq, A.; Haka, M. S.; Ghosh, P.; Cruse, R. W.; Gultneh, Y.; Hayes, J. C.; Toscano, P. J.; Zubieta, J. *Inorganic Chemistry* **1992**, *31*, 1436-1451.

- (34) Kodera, M.; Katayama, K.; Tachi, Y.; Kano, K.; Hirota, S.; Fujinami, S.; Suzuki, M. *Journal of the American Chemical Society* **1999**, *121*, 11006-11007.
- (35) Hayashi, H.; Fujinami, S.; Nagatomo, S.; Ogo, S.; Suzuki, M.; Uehara, A.; Watanabe, Y.; Kitagawa, T. *Journal of the American Chemical Society* **2000**, *122*, 2124-2125.
- (36) Kodera, M.; Kajita, Y.; Tachi, Y.; Katayama, K.; Kano, K.; Hirota, S.; Fujinami, S.; Suzuki, M. *Angewandte Chemie International Edition* **2004**, *43*, 334-337.
- (37) Park, G. Y.; Qayyum, M. F.; Woertink, J.; Hodgson, K. O.; Hedman, B.; Narducci Sarjeant, A. A.; Solomon, E. I.; Karlin, K. D. *Journal of the American Chemical Society* **2012**, *134*, 8513-8524.
- (38) Santagostini, L.; Gullotti, M.; Monzani, E.; Casella, L.; Dillinger, R.; Tucek, F. *Chemistry – A European Journal* **2000**, *6*, 519-522.
- (39) Itoh, S.; Kumei, H.; Taki, M.; Nagatomo, S.; Kitagawa, T.; Fukuzumi, S. *Journal of the American Chemical Society* **2001**, *123*, 6708-6709.
- (40) Mirica, L. M.; Rudd, D. J.; Vance, M. A.; Solomon, E. I.; Hodgson, K. O.; Hedman, B.; Stack, T. D. P. *Journal of the American Chemical Society* **2006**, *128*, 2654-2665.
- (41) Citek, C.; Lyons, C. T.; Wasinger, E. C.; Stack, T. D. P. *Nat Chem* **2012**, *4*, 317-322.
- (42) Hoffmann, A.; Citek, C.; Binder, S.; Goos, A.; Rübhausen, M.; Troeppner, O.; Ivanović-Burmazović, I.; Wasinger, E. C.; Stack, T. D. P.; Herres-Pawlis, S. *Angewandte Chemie International Edition* **2013**, *52*, 5398-5401.
- (43) Mahapatra, S.; Halfen, J. A.; Tolman, W. B. *Journal of the American Chemical Society* **1996**, *118*, 11575-11586.
- (44) Groothaert, M. H.; Lievens, K.; Leeman, H.; Weckhuysen, B. M.; Schoonheydt, R. A. *Journal of Catalysis* **2003**, *220*, 500-512.

- (45) Groothaert, M. H.; van Bokhoven, J. A.; Battiston, A. A.; Weckhuysen, B. M.; Schoonheydt, R. A. *Journal of the American Chemical Society* **2003**, *125*, 7629-7640.
- (46) Smeets, P. J.; Groothaert, M. H.; van Teeffelen, R. M.; Leeman, H.; Hensen, E. J. M.; Schoonheydt, R. A. *Journal of Catalysis* **2007**, *245*, 358-368.
- (47) Groothaert, M. H.; Smeets, P. J.; Sels, B. F.; Jacobs, P. A.; Schoonheydt, R. A. *Journal of the American Chemical Society* **2005**, *127*, 1394-1395.
- (48) Smeets, P. J.; Groothaert, M. H.; Schoonheydt, R. A. *Catalysis Today* **2005**, *110*, 303-309.
- (49) Smeets, P. J.; Hadt, R. G.; Woertink, J. S.; Vanelderren, P.; Schoonheydt, R. A.; Sels, B. F.; Solomon, E. I. *Journal of the American Chemical Society* **2010**, *132*, 14736-14738.
- (50) Vanelderren, P.; Hadt, R. G.; Smeets, P. J.; Solomon, E. I.; Schoonheydt, R. A.; Sels, B. F. *Journal of Catalysis* **2011**, *284*, 157-164.
- (51) Woertink, J. S.; Smeets, P. J.; Groothaert, M. H.; Vance, M. A.; Sels, B. F.; Schoonheydt, R. A.; Solomon, E. I. *Proceedings of the National Academy of Sciences* **2009**, *106*, 18908-18913.
- (52) Solomon, E. I.; Smeets, P. J. R.; Woertink, J. S.; Schoonheydt, R. A.; Sels, B. F., Low temperature direct selective methane to methanol conversion. Google Patents: 2011.
- (53) Tsai, M.-L.; Hadt, R. G.; Vanelderren, P.; Sels, B. F.; Schoonheydt, R. A.; Solomon, E. I. *Journal of the American Chemical Society* **2014**, *136*, 3522-3529.
- (54) Vanelderren, P.; Snyder, B. E. R.; Tsai, M.-L.; Hadt, R. G.; Vancauwenbergh, J.; Coussens, O.; Schoonheydt, R. A.; Sels, B. F.; Solomon, E. I. *Journal of the American Chemical Society* **2015**, *137*, 6383-6392.

- (55) Culpepper, M. A.; Rosenzweig, A. C. *Critical Reviews in Biochemistry and Molecular Biology* **2012**, *47*, 483-492.
- (56) Walters, K. J.; Gassner, G. T.; Lippard, S. J.; Wagner, G. *Proceedings of the National Academy of Sciences* **1999**, *96*, 7877-7882.
- (57) Shiota, Y.; Juhász, G.; Yoshizawa, K. *Inorganic Chemistry* **2013**, *52*, 7907-7917.
- (58) Shiota, Y.; Yoshizawa, K. *Inorganic Chemistry* **2009**, *48*, 838-845.
- (59) Kitajima, N.; Koda, T.; Iwata, Y.; Morooka, Y. *Journal of the American Chemical Society* **1990**, *112*, 8833-8839.
- (60) Kitajima, N.; Fujisawa, K.; Morooka, Y.; Toriumi, K. *Journal of the American Chemical Society* **1989**, *111*, 8975-8976.
- (61) Cramer, C. J.; Kinsinger, C. R.; Pak, Y. *Journal of Molecular Structure: THEOCHEM* **2003**, *632*, 111-120.
- (62) Wieghardt, K.; Tolksdorf, I.; Herrmann, W. *Inorganic Chemistry* **1985**, *24*, 1230-1235.
- (63) Chaudhuri, P.; Wieghardt, K. *Prog. Inorg. Chem.* **1987**, *35*, 329-436.
- (64) Haselhorst, G.; Stoetzel, S.; Strassburger, A.; Walz, W.; Wieghardt, K.; Nuber, B. *Journal of the Chemical Society, Dalton Transactions* **1993**, 83-90.
- (65) Company, A.; Gómez, L.; Fontrodona, X.; Ribas, X.; Costas, M. *Chemistry – A European Journal* **2008**, *14*, 5727-5731.
- (66) Weisman, G. R.; Vachon, D. J.; Johnson, V. B.; Gronbeck, D. A. *Journal of the Chemical Society, Chemical Communications* **1987**, 886-887.

- (67) Schäfer, K.-O.; Bittl, R.; Zweggart, W.; Lenzian, F.; Haselhorst, G.; Weyhermüller, T.; Wieghardt, K.; Lubitz, W. *Journal of the American Chemical Society* **1998**, *120*, 13104-13120.
- (68) Koek, J. H.; Kohlen, E. W. J. M. *Tetrahedron Letters* **2006**, *47*, 3673-3675.
- (69) Gros, G.; Hasserodt, J. *Eur. J. Org. Chem.* **2015**, *2015*, 183-187.
- (70) Hasserodt, J.; Gros, G. New method of preparation of unsym. 1,4,7-triazacyclononane and related intermediates thereof. FR3017386A1, 2015.
- (71) Krakowiak, K. E.; Bradshaw, J. S.; Izatt, R. M. *The Journal of Organic Chemistry* **1990**, *55*, 3364-3368.
- (72) Grenz, A.; Ceccarelli, S.; Bolm, C. *Chemical Communications* **2001**, 1726-1727.
- (73) Belousoff, M. J.; Duriska, M. B.; Graham, B.; Batten, S. R.; Moubaraki, B.; Murray, K. S.; Spiccia, L. *Inorganic Chemistry* **2006**, *45*, 3746-3755.
- (74) Thangavel, A.; Wieliczko, M.; Bacsa, J.; Scarborough, C. C. *Inorganic Chemistry* **2013**, *52*, 13282-13287.
- (75) Poater, A.; Cosenza, B.; Correa, A.; Giudice, S.; Ragone, F.; Scarano, V.; Cavallo, L. *European Journal of Inorganic Chemistry* **2009**, *2009*, 1759-1766.
- (76) Fillol, J. L.; Codola, Z.; Garcia-Bosch, I.; Gomez, L.; Pla, J. J.; Costas, M. *Nat. Chem.* **2011**, *3*, 807-813.
- (77) Prat, I.; Mathieson, J. S.; Guell, M.; Ribas, X.; Luis, J. M.; Cronin, L.; Costas, M. *Nat. Chem.* **2011**, *3*, 788-793.
- (78) Garcia-Bosch, I.; Company, A.; Cady, C. W.; Styring, S.; Browne, W. R.; Ribas, X.; Costas, M. *Angewandte Chemie International Edition* **2011**, *50*, 5648-5653.



- (79) Draksharapu, A.; Codolà, Z.; Gómez, L.; Lloret-Fillol, J.; Browne, W. R.; Costas, M. *Inorganic Chemistry* **2015**, *54*, 10656-10666.
- (80) Nagashima, H.; Sunada, Y.; Watanabe, M.; Noda, D.; Kawamura, M.; Kai, H.; Hamada, A.; Hayakawa, H.; Koike, N. Manufacture of triazacyclononane iron complex for radical polymerization catalyst. WO2008114864A1, 2008.
- (81) Kawamura, M.; Sunada, Y.; Kai, H.; Koike, N.; Hamada, A.; Hayakawa, H.; Jin, R.-H.; Nagashima, H. *Advanced Synthesis & Catalysis* **2009**, *351*, 2086-2090.
- (82) Nagashima, H.; Sunada, Y.; Kai, H. Regeneration of iron complexes employed as reverse atom-transfer radical polymerization (ATRP) catalysts. JP2010095623A, 2010.
- (83) Nakanishi, S.-i.; Kawamura, M.; Kai, H.; Jin, R.-H.; Sunada, Y.; Nagashima, H. *Chemistry – A European Journal* **2014**, *20*, 5802-5814.
- (84) Hage, R.; Iburg, J. E.; Kerschner, J.; Koek, J. H.; Lempers, E. L. M.; Martens, R. J.; Racherla, U. S.; Russell, S. W.; Swarthoff, T.; van Vliet, M. R. P.; Warnaar, J. B.; Wolf, L. v. d.; Krijnen, B. *Nature* **1994**, *369*, 637-639.
- (85) Marcus, R. A.; Sutin, N. *Biochimica et Biophysica Acta (BBA) - Reviews on Bioenergetics* **1985**, *811*, 265-322.
- (86) Rizvi, M. A.; Akhoun, S. A.; Maqsood, S. R.; Peerzada, G. M. *J. Anal. Chem.* **2015**, *70*, 633-638.
- (87) Poropudas, M. J.; Vigo, L.; Oilunkaniemi, R.; Laitinen, R. S. *Dalton Transactions* **2013**, *42*, 16868-16877.
- (88) Nakajima, K.; Shibata, M.; Nishibayashi, Y. *Journal of the American Chemical Society* **2015**, *137*, 2472-2475.

- (89) Salomon, R. G.; Kochi, J. K. *Journal of the American Chemical Society* **1973**, *95*, 3300-3310.
- (90) Karahalidis, G. J.; Thangavel, A.; Chica, B.; Bacsa, J.; Dyer, R. B.; Scarborough, C. C. *Inorganic Chemistry* **2016**, *55*, 1102-1107.
- (91) Lam, B. M. T.; Halfen, J. A.; Young, V. G.; Hagadorn, J. R.; Holland, P. L.; Lledós, A.; Cucurull-Sánchez, L.; Novoa, J. J.; Alvarez, S.; Tolman, W. B. *Inorganic Chemistry* **2000**, *39*, 4059-4072.
- (92) Funahashi, Y.; Nishikawa, T.; Wasada-Tsutsui, Y.; Kajita, Y.; Yamaguchi, S.; Arii, H.; Ozawa, T.; Jitsukawa, K.; Tosha, T.; Hirota, S.; Kitagawa, T.; Masuda, H. *Journal of the American Chemical Society* **2008**, *130*, 16444-16445.
- (93) Decker, H.; Dillinger, R.; Tucek, F. *Angewandte Chemie International Edition* **2000**, *39*, 1591-1595.
- (94) Battaini, G.; Carolis, M. D.; Monzani, E.; Tucek, F.; Casella, L. *Chemical Communications* **2003**, 726-727.
- (95) Askari, M. S.; Esguerra, K. V. N.; Lumb, J.-P.; Ottenwaelder, X. *Inorganic Chemistry* **2015**, *54*, 8665-8672.
- (96) Berreau, L. M.; Mahapatra, S.; Halfen, J. A.; Houser, R. P.; Young, J. V. G.; Tolman, W. B. *Angewandte Chemie International Edition* **1999**, *38*, 207-210.
- (97) Verma, P.; Weir, J.; Mirica, L.; Stack, T. D. P. *Inorganic Chemistry* **2011**, *50*, 9816-9825.
- (98) Swift, T. J., 2 - The Paramagnetic Linewidth A2 - Holm, G.N. La Mar W. DeW. Horrocks R.H. In *NMR of Paramagnetic Molecules*, Academic Press: 1973; pp 53-83.

- (99) Vila, A. J.; Ramirez, B. E.; Di Bilio, A. J.; Mizoguchi, T. J.; Richards, J. H.; Gray, H. B. *Inorganic Chemistry* **1997**, *36*, 4567-4570.
- (100) Salvato, B.; Santamaria, M.; Beltramini, M.; Alzuet, G.; Casella, L. *Biochemistry* **1998**, *37*, 14065-14077.
- (101) Esguerra, K. V. N.; Fall, Y.; Petitjean, L.; Lumb, J.-P. *J. Am. Chem. Soc.* **2014**, *136*, 7662-7668.
- (102) Hay, A. S.; Becker, H. D., Coupling of phenols with quinol ethers. Google Patents: 1970.
- (103) Kushioka, K. *The Journal of Organic Chemistry* **1983**, *48*, 4948-4950.
- (104) Kushioka, K.; Tanimoto, I.; Maruyama, K. *Journal of the Chemical Society, Perkin Transactions 2* **1989**, 1303-1308.
- (105) Haack, P.; Kärigel, A.; Greco, C.; Dokic, J.; Braun, B.; Pfaff, F. F.; Mebs, S.; Ray, K.; Limberg, C. *Journal of the American Chemical Society* **2013**, *135*, 16148-16160.
- (106) Halfen, J. A.; Young, V. G.; Tolman, W. B. *Inorganic Chemistry* **1998**, *37*, 2102-2103.
- (107) Itoh, S.; Nakao, H.; Berreau, L. M.; Kondo, T.; Komatsu, M.; Fukuzumi, S. *Journal of the American Chemical Society* **1998**, *120*, 2890-2899.
- (108) Parmeggiani, C.; Cardona, F. *Green Chemistry* **2012**, *14*, 547-564.
- (109) Ryland, B. L.; Stahl, S. S. *Angewandte Chemie International Edition* **2014**, *53*, 8824-8838.
- (110) Miles, K. C. S., Shannon S. *Aldrichimica Acta* **2015**, *48*, 8-10.
- (111) Xu, B.; Lumb, J.-P.; Arndtsen, B. A. *Angewandte Chemie International Edition* **2015**, *54*, 4208-4211.

- (112) Armand, P.; Kirshenbaum, K.; Falicov, A.; Dunbrack Jr, R. L.; Dill, K. A.; Zuckermann, R. N.; Cohen, F. E. *Folding and Design* **1997**, *2*, 369-375.
- (113) Gorske, B. C.; Stringer, J. R.; Bastian, B. L.; Fowler, S. A.; Blackwell, H. E. *Journal of the American Chemical Society* **2009**, *131*, 16555-16567.
- (114) Kanady, J. S.; Tsui, E. Y.; Day, M. W.; Agapie, T. *Science* **2011**, *333*, 733-736.
- (115) Stack, T. D. P.; Holm, R. H. *Journal of the American Chemical Society* **1988**, *110*, 2484-2494.
- (116) Lee, S. C.; Lo, W.; Holm, R. H. *Chemical Reviews* **2014**, *114*, 3579-3600.
- (117) Zhang, Y.; Holm, R. H. *Journal of the American Chemical Society* **2003**, *125*, 3910-3920.
- (118) Lancaster, K. M.; Roemelt, M.; Ettenhuber, P.; Hu, Y.; Ribbe, M. W.; Neese, F.; Bergmann, U.; DeBeer, S. *Science (Washington, DC, U. S.)* **2011**, *334*, 974-977.
- (119) Coric, I.; Mercado, B. Q.; Bill, E.; Vinyard, D. J.; Holland, P. L. *Nature (London, U. K.)* **2015**, *526*, 96-99.
- (120) Lavie-Cambot, A.; Cantuel, M.; Leydet, Y.; Jonusauskas, G.; Bassani, D. M.; McClenaghan, N. D. *Coordination Chemistry Reviews* **2008**, *252*, 2572-2584.
- (121) Saracini, C.; Ohkubo, K.; Suenobu, T.; Meyer, G. J.; Karlin, K. D.; Fukuzumi, S. *Journal of the American Chemical Society* **2015**, *137*, 15865-15874.
- (122) Kundu, S.; Miceli, E.; Farquhar, E.; Pfaff, F. F.; Kuhlmann, U.; Hildebrandt, P.; Braun, B.; Greco, C.; Ray, K. *Journal of the American Chemical Society* **2012**, *134*, 14710-14713.

(123) Wiese, S.; Badiei, Y. M.; Gephart, R. T.; Mossin, S.; Varonka, M. S.; Melzer, M. M.; Meyer, K.; Cundari, T. R.; Warren, T. H. *Angewandte Chemie International Edition* **2010**, *49*, 8850-8855.

#### Additional References

(A) Buru, Cassantra T. (2015) *Modular Synthesis of Asymmetric Triazacyclononane Derivatives and Potential Aerobic Copper Oxidation Catalyst Supported by a Bridging Bulky Triazacyclononane* (Master's Thesis). Stored in Emory ETD.

(B) Pickel, Thomas; Karahalil, Gregory J; Buru, Cassandra T; Bacsa, John; Scarborough, Christopher C. *Manuscript in Progress*.

(C) Pickel, Thomas; *Unpublished Work*.